Durham E-Theses

Semileptonic decays of heavy mesons and the standard model

Michael Fairbairn Wade

How to cite:

Wade, Michael Fairbairn (1990) Semileptonic decays of heavy mesons and the standard model. Doctoral thesis, Durham University.

Semileptonic Decays of Heavy Mesons

and the Standard Model

A thesis presented for the degree of

Doctor of Philosophy

by

Michael Fairbairn Wade

University of Durham

Department of Physics

October 1990

1 7 OCT 1991

Abstract

The formalism for a helicity amplitude analysis of the exclusive semileptonic decays of B mesons ($\overline{B} \to Dl\overline{\nu}$ and $\overline{B} \to D^*l\overline{\nu}$ for $l = e$, μ and τ) is introduced. In particular it is shown how measurements of the angular distribution of the subsequent decay $D^* \to D\pi$ can fully determine the theoretically uncertain hadronic ($\overline{B} \to D, D^*$) matrix elements.

A spectator quark based model for the hadronic amplitudes is introduced, and then compared to other existing models and with the presently available experimental data, to extract the quark mixing matrix element $|V_{cb}|$. The extraction of $|V_{ub}|$, using exclusive models for $b \to u$ decays, is also discussed.

The predictions of the free-quark model of inclusive semileptonic B decays are compared with those of the exclusive models, in an attempt to test the reliability of the inclusive model's predictions for $|V_{cb}|$ and $|V_{ub}|$.

A phenomenological analysis of experimental measurements of $K^0 - \overline{K^0}$ and $B^0 - \overline{B^0}$ mixing is made, incorporating the above determinations of the mixing matrix elements, with a view to constraining the parameters of the standard model, such as the mass of the top-quark.

Acknowledgements

To Mum, Dad and Rick

I may not understand, but I am willing to admire.

Sir Anthony Hope Hawkins, 1863-1933

Declaration

I declare that no material in this thesis has previously been submitted for a degree at this or any other University.

The research described in chapters 4, 5, and 6 was carried out in collaboration with Prof. A.D. Martin and Dr. K. Hagiwara, and has been published in the following articles:

i) 'Helicity Amplitude Analysis of $B \to D^* l \nu$ decays'

K.Hagiwara, A.D. Martin and M.F. Wade, *Phys. Lett.* **B228**, 144 (1989)

ii) 'Exclusive Semileptonic B Meson Decays'

K.Hagiwara, A.D. Martin and M.F. Wade, *Nucl. Phys.* **B327**, 569 (1989)

iii) 'The Semileptonic Decays $B \to M \tau \nu$ as a probe of Hadron Dynamics'

K.Hagiwara, A.D. Martin and M.F. Wade, *Z. Phys.* **C46**, 299 (1989)

The work described in chapter 7 was done in collaboration with Prof. A.D. Martin and Dr. J.-R. Cudell, with advice from Dr. K. Hagiwara and Dr. K. Teshima.

Other work by the author:

iv) 'Thrust in $e^+ e^-$-Annihilation'

K. Teshima and M.F. Wade, Durham preprint DTP/90/32.

Statement of Copyright

Unless otherwise stated, the particle masses, lifetimes, decay constants and other parameters used in this thesis are are taken from the 1990 Particle Data Group Tables, published in *Phys. Lett.* **B239** (1990).

Contents

1 Introduction

I don't pretend to understand the Universe – it's a great
deal bigger than I am... People ought to be modester.
Thomas Carlyle, 1795-1881

1.1 The Standard Model

Elementary particle physics research is the study of the fundamental particles and interactions of nature. The wealth of experimental data so far available is all compatible with the so-called 'Minimal Standard Model' of Glashow [1], Salam [2] and Weinberg [3]. Current experiments are designed to measure even more accurately the parameters of the model in an effort to discover 'new' physics which it cannot explain.

The fundamental matter particles of nature are believed to be fermions. Their various interactions are predicted by combining the formalism of Lagrangian densities with the theory of Lie groups. For each type of interaction the fermions are assigned to representations of a Lie algebra, and the Lagrangian density is then made invariant under local (i.e. position-dependent) Lie group transformations, called gauge transformations. This procedure requires the introduction of one 'gauge field' for each group generator, and these fields describe the vector bosons which mediate the force.

More explicitly, the standard model itself is based upon the Lie group

$$SU(3)_C \times SU(2)_L \times U(1)_Y, \tag{1.1}$$

where the three symmetries are known as Colour, Weak Isospin and Hypercharge respectively. The strengths of the interactions are determined by three coupling constants g_s, g and g' associated with the three Lie groups of (1.1) respectively. As it stands, the above theory describes only massless particles, because fermion mass terms are not invariant under $SU(2)_L$ symmetry transformations, and gauge boson mass terms are not invariant under their respective gauge transformations. However, in nature most of the fermions are massive, as are the gauge bosons associated with the weak interactions. For a long time this severe problem remained unsolved, until it was discovered that it could be overcome by the introduction of

1

scalar fields (called 'Higgs' fields, after their originator), which acquire a non-zero vacuum expectation value and so break the $SU(2)_L \times U(1)_Y$ part of the symmetry group, allowing mass terms to appear. The simplest (or 'minimal') possibility is the introduction of one complex scalar $SU(2)_L$ doublet Higgs field, which breaks the symmetry

$$SU(3)_C \times SU(2)_L \times U(1)_Y \rightarrow SU(3)_C \times U(1)_{EM}, \qquad (1.2)$$

so that the eight gluons of Quantum Chromodynamics (QCD) and the photon of Quantum Electrodynamics (QED) remain massless. Amazingly, the Higgs doublet is also able to generate masses for the fermions, although the actual values are not predicted. Furthermore, three linear combinations of the original four generators of $SU(2)_L \times U(1)_Y$ become just the massive gauge bosons $W^{\pm}$ and Z^0 that are required by weak interaction phenomenology.

The matter fields, which, as we have mentioned, are fermions, are of two types, quarks and leptons. Originally only one 'family' of fermions was known, made up of two quarks, called up (u) and down (d), and two leptons, the electron (e) and neutrino (ν_e). However, two further copies (or 'generations') of this family have since been discovered, seeming to differ only in the particle masses. Each fermion is described mathematically by a four-component Dirac spinor ψ, which can be split into two parts, called left- and right-handed, defined by

$$\psi_{L,R} \equiv \frac{1}{2}(1 \mp \gamma_5)\psi. \qquad (1.3)$$

If the particles being described have zero mass, then left- and right-handed fermions have negative and positive helicity respectively. It is important to note here that the fermion mass terms in the Lagrangian are of the form

$$m\overline{\psi}\psi = m(\overline{\psi}_L \psi_R + \overline{\psi}_R \psi_L), \qquad (1.4)$$

and so require the existence of both left- and right-handed fields.

Of the four quarks of the second and third generations introduced above only three 'flavours', strange (s), charm (c) and bottom (b), have so far been discovered. These all short-lived and have to be manufactured in accelerators (or generated

2

by cosmic ray collisions). A sixth flavour, top (t), has yet to be detected, but for many reasons is believed to exist. No evidence has yet been found for the existence of any more flavours. Indeed, recent experiments with the new LEP collider at CERN indicate that there may well be no more than three generations of fermions. The three generations of quarks and their group representations can be summarised by

$$
\begin{pmatrix} u \\ d' \end{pmatrix}_L \quad \begin{pmatrix} c \\ s' \end{pmatrix}_L \quad \begin{pmatrix} t \\ b' \end{pmatrix}_L \quad (3,2)
$$
$$
u_R, d'_R \qquad c_R, s'_R \qquad t_R, b'_R \qquad (3,1)
$$
(1.5)

The numbers in brackets at the end of each line are the dimensions of the representations of the particles under $SU(3)_C$ and $SU(2)_L$ transformations respectively. Under $SU(3)_C$ transformations each quark is a triplet, but the relevant colour index has been suppressed. Under $SU(2)_L$ the left-handed fermions all transform as doublets, while the right-handed fermions are singlets. The primes on the d, s, b quarks refers to the fact that the mass and weak interaction eigenstates are not necessarily the same, as will be explained in section 1.3.

The three generations of leptons, all of which have been detected, are

$$
\begin{pmatrix} \nu_e \\ e \end{pmatrix}_L \quad \begin{pmatrix} \nu_\mu \\ \mu \end{pmatrix}_L \quad \begin{pmatrix} \nu_\tau \\ \tau \end{pmatrix}_L \quad (1,2)
$$
$$
e_R \qquad \mu_R \qquad \tau_R \qquad (1,1)
$$
(1.6)

where again the numbers in brackets are the dimensions of the $SU(3)_C$ and $SU(2)_L$ representations. That the leptons are $SU(3)_C$ singlets simply reflects the fact that they do not have strong interactions. Note that the minimal standard model contains no right-handed neutrino fields, with the result that all the neutrinos are massless (see (1.4)).

The Lagrangian of the standard model is not completely determined by the symmetry group, but includes 17 *a priori* free parameters (or 18 if one includes the strong CP-violating parameter θ_{QCD}). It is hoped that the discovery of an underlying theory (of which the standard model might be just a part), or of some other symmetry principles, will reduce this number, or maybe even determine them all. However, at present, the following parameters all need to be determined experimentally:

3

a) The 6 quark masses m_d, m_s, m_b, m_u, m_c & m_t.

b) The 3 charged lepton masses m_e, m_μ & m_τ.

c) The 3 symmetry group couplings g_s, g & g'.

d) The 4 Kobayashi-Maskawa (KM) matrix parameters.

e) The Higgs mass m_H.

This thesis is primarily concerned with the determination of some of the parameters that appear in the KM matrix, the origin and meaning of which is discussed in section 1.3 below.

1.2 Quarks, the Strong Interaction and Hadrons

While leptons are detected as discrete particles in nature, no experiment has yet managed to find an isolated quark. Most people now believe that it is impossible to do so, because the strong interactions of Quantum Chromodynamics (QCD), as predicted by the $SU(3)_C$ gauge group, predict that the coupling, g_s, between the quarks and gluons, increases rapidly with increasing distance (or equivalently with decreasing energy). Thus quarks are 'confined' and form $SU(3)_C$-singlet bound-states with other quarks, from which they cannot be isolated. These bound-states, called hadrons, are found in two types; baryons, which contain three quarks (or three anti-quarks) and mesons, which contain a quark and an antiquark.

Particle physics calculations are usually either based upon perturbative expansions in the coupling constants (in those cases where such series are believed to be reliable), or on 'lattice' QCD computations (although such methods are still in their infancy). Unfortunately, the above increase in the QCD coupling constant means that hadronic physics is not well described by perturbation theory at low energies, (i.e. the behaviour of quarks is dominated by 'non-perturbative' physics). Some non-lattice techniques have been found to give fairly good results at low energies, such as chiral perturbation theory and current algebra, but in contrast to perturbative QCD these only work well at low energies. It is hoped that improvements in the techniques of lattice calculations, and in the computers used to do them, will eventually give reliable results at these low energies. As the masses of the quarks and hadrons being studied increase, it is expected that

perturbative QCD will begin to give more reliable answers, and thus the behaviour of such particles should be more easily understood.

In any calculations involving quarks, these non-perturbative effects produce great uncertainty in the final results and even after many years of studying hadrons, physicists have not been able to probe very deeply into their internal stucture and behaviour.

1.3 The Fermion Eigenstates and the Kobayashi-Maskawa Matrix

The following discussion is carried out for the quarks, but all the arguments can be used for the leptons also, with some simplifications, as will be discussed at the end of the section. For notational simplicity it is convenient to divide the quarks into two three-component column vectors in 'generation' space,

$$U \equiv \begin{pmatrix} u \\ c \\ t \end{pmatrix} \qquad D \equiv \begin{pmatrix} d \\ s \\ b \end{pmatrix}, \tag{1.7}$$

for the 'up-type' and 'down-type' quarks of (1.5) respectively, where each individual quark field is understood to be a four-component Dirac spinor.

In order to describe the origin of the KM matrix, it is necessary to extract certain terms from the full standard-model Lagrangian. The first of these are the quark mass terms, which arise from the Higgs mechanism, as briefly outlined above. The result, which is a generalisation of (1.4), is a mass term of the form

$$\mathcal{L}_{mass} = \overline{U''_L} M^u U''_R + \overline{D''_L} M^d D''_R + \text{h.c.}, \tag{1.8}$$

where the mass matrices M^u and M^d are, in general, non-diagonal, non-hermitian 3×3 matrices in generation space, and the double primes allow for the fact that the eigenstates in the original Lagrangian may not coincide with the physically useful ones.

The other term in the standard model Lagrangian which we need to discuss in some detail is that responsible for the charged-current weak interactions. It

describes the interactions of the charged $W^\pm$ bosons with the matter fields, and is

$$\mathcal{L}_{cc} = -\frac{g}{2\sqrt{2}}(W_\mu^+ J_{cc}^\mu + W_\mu^- J_{cc}^{\mu\dagger}), \qquad (1.9)$$

where g is the coupling associated with the original $SU(2)_L$ gauge group. The charged current of (1.9), which involves only left-handed fields, is

$$\begin{aligned} J_{cc}^\mu &= \overline{U''}\gamma^\mu(1-\gamma_5)D'' \\ &= 2\overline{U''_L}\gamma^\mu D''_L. \end{aligned} \qquad (1.10)$$

This interaction is responsible for processes such as nuclear β-decay, via the reaction $d \to uW^{*-} \to ul^-\overline{\nu}$ (where W^{*-} is a virtual (off-mass-shell) W^- boson), and for the semileptonic decays that are the main focus of this thesis.

In order to find the mass (or propagation) eigenstates, we must diagonalise the two mass matrices M^u and M^d of (1.8). This can be accomplished by means of a biunitary transformation [4]. There exist unitary matrices S^u and T^u such that

$$S^{u\dagger}M^uT^u \equiv m^u = \text{diag}(m_u, m_c, m_t) \qquad (1.11)$$

is a real diagonal matrix with non-negative elements. Similar matrices S^d and T^d can be found for M^d. We can then define

$$\begin{aligned} U_L &\equiv S^{u\dagger}U''_L \\ U_R &\equiv T^{u\dagger}U''_R \end{aligned} \qquad (1.12)$$

and similarly for the down-type quarks.

The quark mass terms then become

$$\begin{aligned} \mathcal{L}_{mass} &= \overline{U_L}S^{u\dagger}M^uT^uU_R + \overline{D_L}S^{d\dagger}M^dT^dD_R + \text{h.c.} \\ &= \overline{U_L}m^uU_R + \overline{D_L}m^dD_R + \text{h.c.} \\ &= \overline{U}m^uU + \overline{D}m^dD. \end{aligned} \qquad (1.13)$$

Under the same transformation the charged current becomes

$$\begin{aligned} J_{cc}^\mu &= 2\overline{U_L}S^{u\dagger}\gamma^\mu S^d D_L \\ &= 2\overline{U_L}\gamma^\mu V D_L \\ &= \overline{U}\gamma^\mu(1-\gamma_5)VD \\ &\equiv \overline{U}\gamma^\mu(1-\gamma_5)D', \end{aligned} \qquad (1.14)$$

where

$$D' = \begin{pmatrix} d' \\ s' \\ b' \end{pmatrix} \equiv VD \qquad (1.15)$$

are the weak interaction eigenstates originally given in (1.5), and where

$$V \equiv S^{u\dagger}S^d \qquad (1.16)$$

is a 3×3 unitary matrix known as the Kobayashi-Maskawa mixing matrix, after its originators (the 2×2 version of the above theory was originally proposed by Cabibbo, so the matrix V is sometimes known as the Cabibbo-Kobayashi-Maskawa matrix). In the last line of (1.14) it is conventional to define the up-type mass and weak interaction eigenstates to be the same, and the down-type to be different. The result of the mass and weak interaction eigenstates being different is to allow flavour-changing quark decays of the type $b \to cW^-$, $c \to sW^+$, with rates proportional to $|V_{cb}|^2$, $|V_{cs}|^2$ respectively.

Note that it is possible to redefine the phases of the quark fields by the transformations

$$\begin{aligned} U &\to P^u U \\ D &\to P^d D, \end{aligned} \qquad (1.17)$$

where $P^{u,d}$ are diagonal matrices of phases, without affecting any terms except the charged current. The KM matrix is transformed according to

$$V \to P^u V P^{d\dagger} \qquad \text{or, equivalently,} \qquad V_{ij} \to \sum_{\alpha,\beta} P^u_{i\alpha} V_{\alpha\beta} (P^d_{j\beta})^*. \qquad (1.18)$$

All observables of the KM matrix must, of course, be unchanged by such phase transformations.

The same calculations can also be made in the leptonic sector. The addition of right-handed neutrinos to the minimal standard model can give rise to neutrino oscillations, where neutrinos, like quarks, can change from generation to generation. However, if neutrinos are massless (as must be the case if the ν_R do not exist), one can define the mass eigenstates to coincide with the weak interaction eigenstates.

7

1.4 The Kobayashi-Maskawa Matrix

As explained in the previous section, the mass and weak interaction eigenstates are related by the 3×3 unitary KM quark mixing matrix V. In general a 3×3 unitary matrix can be written in terms of 3 real parameters and 6 complex phases. However, using the phase transformations (1.17) we can absorb 5 of these phases into the definitions of the quark fields (1 phase remains, since an overall phase change of all the quark fields leaves V unaffected). All possible parametrisations of the KM matrix are related by phase transformations of the form (1.18). One parametrisation, which is widely accepted now, is that of Chau and Keung [5], based on work by Maiani [6] and Wolfenstein [7];

$$
\begin{aligned}
V &\equiv \begin{pmatrix} V_{ud} & V_{us} & V_{ub} \\ V_{cd} & V_{cs} & V_{cb} \\ V_{td} & V_{ts} & V_{tb} \end{pmatrix} \\
&= \begin{pmatrix} 1 & 0 & 0 \\ 0 & c_{23} & s_{23} \\ 0 & -s_{23} & c_{23} \end{pmatrix} \begin{pmatrix} c_{13} & 0 & s_{13}e^{-i\delta} \\ 0 & 1 & 0 \\ -s_{13}e^{i\delta} & 0 & c_{13} \end{pmatrix} \begin{pmatrix} c_{12} & s_{12} & 0 \\ -s_{12} & c_{12} & 0 \\ 1 & 0 & 0 \end{pmatrix} \qquad (1.19) \\
&= \begin{pmatrix} c_{12}c_{13} & c_{13}s_{12} & s_{13}e^{-i\delta} \\ -c_{23}s_{12} - c_{12}s_{23}s_{13}e^{i\delta} & c_{12}c_{23} - s_{12}s_{23}s_{13}e^{i\delta} & c_{13}s_{23} \\ s_{12}s_{23} - c_{12}c_{23}s_{13}e^{i\delta} & -c_{12}s_{23} - c_{23}s_{12}s_{13}e^{i\delta} & c_{13}c_{23} \end{pmatrix},
\end{aligned}
$$

where

$$
\begin{aligned}
s_{ij} &\equiv \sin\theta_{ij} \\
c_{ij} &\equiv \cos\theta_{ij},
\end{aligned}
\qquad (1.20)
$$

with θ_{ij} being the mixing angle between the ith and j^{th} generations. By suitable redefinitions of the phases of the quark fields (this time by factors ± 1), the parameters may be made to lie in the ranges

$$
\begin{aligned}
0 &\leq \theta_{ij} < \pi/2 \\
0 &\leq \delta < 2\pi.
\end{aligned}
\qquad (1.21)
$$

The moduli of all 9 matrix elements of the KM matrix are, in principle, observable, for example from semileptonic decays. Although the phase δ is observable, one cannot actually measure $Im(V_{ij})$ directly, because it depends upon the

parametrisation used. The observable J, defined by the relation [8]

$$J \sum_k \epsilon_{ijk}\epsilon_{klm} \equiv Im(V_{il}V_{jm}V_{im}^*V_{jl}^*), \qquad (1.22)$$

is, however, a function of the phase δ. J is an observable because changing the quark phases has no effect, as can be shown by using (1.18). Any observable of the KM matrix can thus be written as a function of the moduli of the matrix elements and J. In the parametrisation (1.19) we find

$$J = c_{12}c_{23}c_{13}^2 s_{12}s_{23}s_{13}\sin\delta. \qquad (1.23)$$

1.5 The Discrete Symmetries C, P and T

Charge conjugation (C), Parity (P) and Time-Reversal (T) are discrete symmetries that play an important role in particle physics. Charge conjugation interchanges particles and antiparticles, Parity (space reflection) reverses all momenta, but leaves spins unchanged, while Time-Reversal reverses both spins and momenta.

The famous CPT theorem tells us that the standard model is invariant under the product of the three symmetries, taken in any order, but the transformation properties under the three transformations separately depend upon the particular terms in the Lagrangian. For instance the electromagnetic interaction is invariant under all three transformations separately, but weak interactions are not.

Parity violation was first observed in the decay of the Cobalt-60 nucleus [9], and is due to the fact that the weak interaction treats left-and right-handed fermions differently, as is shown by the explicit forms of the charged current (1.10).

For many years it was thought that physics was invariant under the combined operator CP, until the observation of the CP-violating decay $K_L^0 \to \pi^+\pi^-$ [10] in 1964. The origin of this very small violation of CP is not fully understood, but one explanation could be the existence of a complex phase in the KM matrix. In fact, in 1973 Kobayashi and Maskawa [11] originally introduced the third generation of quarks in (1.5) (even though only three quarks had been discovered) in order to account for this phenomenon. With only two generations the mixing matrix can be made real by redefinition of the quark phases, but with a third generation this is no longer possible in general, and CP violation results.

In fact, for the KM matrix to describe CP-violation the following conditions must be met:

1) The up-type quarks must have different masses,

2) The down-type quarks must have different masses

3) The parameter J of (1.22) must be non-zero.

A discussion of current attempts to determine the CP-violating angle δ will be given in Chapter 2.

1.6 Experimental Determination of the KM Matrix Elements

Recent reviews of the KM matrix can be found in [12] and [13]. The most recent experimental determinations of the KM matrix elements are given in brief below.

1) $|V_{ud}|$

Our knowledge of $|V_{ud}|$ comes from two sources. The most accurate determination is from a comparison of nuclear β-decay and muon decay [14], which was greatly improved theoretically in 1987 [15], when more accurate calculations of the radiative corrections brought predictions from the eight most commonly studied nuclei into very good agreement. The value calculated from this method is

$$|V_{ud}| = 0.9744 \pm 0.0010. \tag{1.24}$$

A less accurate determination comes from the comparison of the experimentally measured decay rate $\pi^+ \rightarrow \pi^0 e^+ \nu$ [16] with the theoretical rate calculated using current algebra [17], updated by using a more recent measurement of the $\pi^+-\pi^0$ mass difference [18], yielding

$$|V_{ud}| = 0.970 \pm 0.020. \tag{1.25}$$

The larger error here is predominantly the experimental error, which is an order of magnitude larger than the theoretical error.

2) $|V_{us}|$

Here again there are two main sources for the determination of the matrix element. The first is the semileptonic K_{e3} decay ($K \rightarrow \pi e \nu$), analysed using chiral perturbation theory in order to take into account flavour $SU(3)$ breaking [19]. The value extracted from the data is

$$|V_{us}| = 0.2196 \pm 0.0023 \qquad (1.26)$$

The second source is from hyperon β-decays. Originally these were analysed assuming $SU(3)$ flavour symmetry [20], leading to the value $|V_{us}| = 0.231 \pm 0.003$, but a more recent analysis, using the quark model to include the flavour symmetry breaking effects [21], and including the most recent data, gives [12]

$$|V_{us}| = 0.222 \pm 0.003. \qquad (1.27)$$

Averaging these two values gives a combined value

$$|V_{us}| = 0.2205 \pm 0.0018. \qquad (1.28)$$

3) $|V_{cd}|$

The matrix element $|V_{cd}|$ can be derived from neutrino and antineutrino pro-duction of c quarks from d quarks in nucleons, followed by semileptonic decay of the charmed quark, resulting in the production of oppositely charged muons

$$\begin{array}{ll} \nu + d \rightarrow \mu^- c & c \rightarrow s \mu^+ \nu \\ \overline{\nu} + \overline{d} \rightarrow \mu^+ \overline{c} \quad \text{with} \quad & \overline{c} \rightarrow \overline{s} \mu^- \overline{\nu}. \end{array} \qquad (1.29)$$

These experiments have been performed by the CDHS group at the CERN SPS collider [22] and at a recent Tevatron experiment at Fermilab [23]. Combining the measurements of these two experiments, and using recent determinations of the semileptonic branching fractions of charmed mesons [24], yields

$$|V_{cd}| = 0.204 \pm 0.017. \qquad (1.30)$$

11

4) $|V_{cs}|$

Again there are two main experimental sources for this matrix element. The first is from the same experiments as in (1.29), but where the charmed quark is produced from strange quarks in the parton sea, instead of valence d quarks. This calculation is not very accurate, on account of the lack of knowledge of the strange quark density, and the most conservative assumptions lead to a lower bound of [12,22]

$$|V_{cs}| > 0.66. \tag{1.31}$$

The matrix element may also be extracted from an analysis of semileptonic D-meson decays, analogously to the extraction of $|V_{us}|$ from K_{e3} decays above, which leads to the result [12]

$$|V_{cs}| = 1.02 \pm 0.18. \tag{1.32}$$

5) $|V_{cb}|$

This matrix element is extracted from analyses of semileptonic decays of bottom mesons, and is the main topic of the analysis of Chapters 3 to 7. Taking into account various models used for the hadronic interactions, the exclusive analysis of chapter 6 gives

$$|V_{cb}| = 0.039 \pm 0.005. \tag{1.33}$$

6) $|V_{ub}|$

The matrix element $|V_{ub}|$ is just recently coming within the reach of experiments analysing charmless B-meson decays. Using the exclusive analysis described in chapter 6 we find

$$|\frac{V_{ub}}{V_{cb}}| = 0.07^{+0.14}_{-0.04}. \tag{1.34}$$

7) $|V_{td}|$, $|V_{ts}|$, $|V_{tb}|$

Since the top-quark has yet to be detected experimentally, there is no direct measurement of any of the KM matrix elements related to it.

1.7 Using Unitarity to Determine the KM Matrix Elements

Unitarity of the KM matrix is equivalent to the conditions

$$\delta_{ij} = \sum_k V_{ik} V_{jk}^* \tag{1.35}$$

$$= \sum_k V_{ki} V_{kj}^* \tag{1.36}$$

By assuming that there are only three generations of quarks, there are two ways to use these conditions.

a) To check that the conditions are satisfied if all the relevent elements are known.

b) To calculate the matrix elements that we either know with poor accuracy, or cannot measure at all.

1) $|V_{cs}|$

As mentioned above, the determination of $|V_{cs}|$ can be improved. Using the unitarity condition (1.35), with $i = j = c$, we can write

$$|V_{cs}| = \sqrt{1 - |V_{cd}|^2 - |V_{cb}|^2}$$
$$= 0.978 \pm 0.004. \tag{1.37}$$

We are now in a position to deduce the allowed ranges of the KM elements $|V_{ti}|$, associated with the top quark.

2) $|V_{tb}|$

Using (1.36), with $i = j = b$, we find

$$|V_{tb}| = \sqrt{1 - |V_{cb}|^2 - |V_{ub}|^2}$$
$$= 0.9992 \pm 0.0002, \tag{1.38}$$

so, ironically, the most accurately determined element is one that we cannot yet measure experimentally.

13

3) $|V_{ts}|$

Using condition (1.36), with $i = s, j = b$, we have

$$V_{ts} = -\frac{V_{us}V_{ub}^* + V_{cs}V_{cb}^*}{V_{tb}^*}.$$ (1.39)

Now, using the results above, the first term in the numerator is negligible compared to the second, so

$$|V_{ts}| \approx \left|\frac{V_{cs}V_{cb}}{V_{tb}}\right| = 0.038 \pm 0.005.$$ (1.40)

4) $|V_{td}|$

This element can be determined using (1.36) with $i = d, j = b$, which implies that

$$V_{td} = -\frac{V_{cd}V_{cb}^* + V_{ud}V_{ub}^*}{V_{tb}^*}.$$ (1.41)

To a good approximation we may set $|V_{tb}| = 1$ and use the fact that $Re(V_{cd}) \gg Im(V_{cd})$ in the parametrisation (1.19), so

$$|V_{td}| \approx |V_{cb}| \; |V_{cd} + V_{ud}\frac{V_{ub}^*}{V_{cb}}|,$$ (1.42)

resulting in

$$0.003 \lesssim |V_{td}| \lesssim 0.02.$$ (1.43)

Finally the results for the moduli of the matrix elements, using both direct experimental measurements and unitarity can be summarised as

$$|V_{ij}| = \begin{pmatrix} 0.9749 - 0.9758 & 0.2187 - 0.2223 & 0.001 - 0.009 \\ 0.2180 - 0.2225 & 0.9739 - 0.9753 & 0.034 - 0.044 \\ 0.0005 - 0.019 & 0.032 - 0.045 & 0.9990 - 0.9994 \end{pmatrix},$$ (1.44)

corresponding to the following range of the mixing angles of (1.19)

$$s_{12} = 0.2205 \pm 0.0018 \qquad c_{12} = 0.9754 \pm 0.0004$$

$$s_{23} = 0.039 \pm 0.005 \qquad c_{23} = 0.9992 \pm 0.0002$$ (1.45)

$$s_{13}/s_{23} = 0.07^{+0.14}_{-0.04} \qquad c_{13} \geq 0.9999.$$

Efforts to determine δ, which are all by indirect methods, will be discussed in Chapter 2.
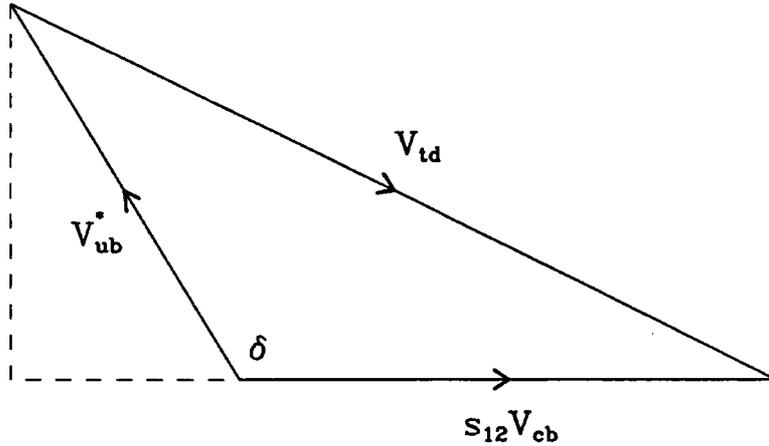
Figure 1.1 The KM triangle, which represents the less accurately known KM matrix parameters of (1.47) graphically.

The less well-known parameters of the KM matrix can be summarised in the following way: using (1.36) with $i = d, j = b$ leads to

$$V_{ub}^* V_{ud} + V_{cb}^* V_{cd} + V_{tb}^* V_{td} = 0, \qquad (1.46)$$

which can be rewritten, to a good approximation, in the form

$$V_{cb} \sin \theta_{12} = V_{ub}^* + V_{td}, \qquad (1.47)$$

using (1.45) and the reality of V_{cb} in this parametrisation. This relationship is represented digramatically in fig.1.1.

1.8 Thesis Outline

Chapter 2 decribes how experimental measurements of $K^0 - \overline{K^0}$ and $B^0 - \overline{B^0}$ mixing can be used to give indirect evidence of the values of the KM matrix parameters (at present these give the best means of measuring δ).

Chapter 3 reviews the experimental results on B meson decays, and the problems associated with their extraction from the raw data.

Chapters 4 to 6 describe theoretical studies of exclusive semileptonic meson decays, which can be used both to measure the moduli of the KM matrix elements

and to probe non-perturbative effects. The formalism is introduced in chapter 4, the models of hadronic matrix elements are explained in chapter 5 and the comparison with experimental data is presented in chapter 6.

Finally, chapter 7 gives a description of the inclusive study of semileptonic B meson decays, including comparisons with the exclusive models of the preceding chapters.

References

1. S.L. Glashow, *Nucl. Phys.* **22**, 579 (1961).

2. A. Salam, in *Elementary Particle Physics (Nobel Symposium no. 8)*, Ed. N. Svartholm, (Almqvist and Wilsell, Stockholm, 1968).

3. S. Weinberg, *Phys. Rev. Lett.* **19**, 1264 (1967).

4. T.-P. Cheng and L.-F. Li, in *Gauge Theory of Elementary Particle Physics* pp. 357-362 (Oxford University Press, New York, 1984).

5. L.-L. Chau and W.-Y. Keung, *Phys. Rev. Lett.* **53**, 1802 (1984).

6. L. Maiani, *Phys. Lett.* **62B**, 183 (1976).

7. L. Wolfenstein, *Phys. Rev. Lett.* **51**, 1945 (1983).

8. C. Jarlskog, in *Proceedings of the International Symposium on Production and Decay of Heavy Hadrons* p. 331, Ed. K.R. Schubert and R. Waldi, (H.B. Druck, Hamburg, 1986).

9. C.S. Wu, E. Ambler, R. Hayward, D. Hoppes and R. Hudson, *Phys. Rev* **105**, 1413 (1957).

   C.S. Wu, E. Ambler, R. Hayward, D. Hoppes and R. Hudson, *Phys. Rev* **106**, 1361 (1957).

10. J.H. Christenson, J.W. Cronin, V.L. Fitch and R. Turlay, *Phys. Rev. Lett.* **13**, 138 (1964).

11. M. Kobayashi and M. Maskawa, *Progr. Theor. Phys.* **49**, 652 (1973).

12. F.J. Gilman, K. Kleinknecht and B. Renk, SLAC-PUB-5155 (Dec 1989).

    Particle Data Group: Review of Particle Properties, *Phys. Lett.* **B239**, 1 (1990).

13. K.R. Schubert, in *Proc. of Int. Europhysics Conf. on H.E. Physics* p.790, Ed. O. Botner, (1987).

14. W.J. Marciano and A. Sirlin, *Phys. Rev. Lett.* **56**, 22 (1986).

15. A. Sirlin and R. Zucchini, *Phys. Rev. Lett.* **57**, 1994 (1986).

    W. Jaus and G. Rasche, *Phys. Rev.* **D35**, 3420 (1987).

A. Sirlin, *Phys. Rev.* **D35**, 3423 (1987).

16. W.K. MacFarlane et al., *Phys. Rev.* **D32**, 547 (1985).

17. A. Sirlin, *Rev. Mod. Phys.* **50**, 573 (1978).

18. J.F. Crawford et al., *Phys. Rev. Lett.* **56**, 1043 (1986).

19. H. Leutwyler and M. Roos, *Z. Phys.* **C25**, 91 (1984).

20. M. Bourquin et al., *Z. Phys.* **C21**, 27 (1983).

21. J.F. Donoghue, B.R. Holstein and S.W. Klimt, *Phys.Rev.* **D35**, 934 (1987).

22. H. Abramowicz et al., *Z. Phys.* **C15**, 19 (1982).

23. M. Schaevitz, talk to the Twelfth International Workshop on Weak Interactions and Neutrinos, Ginosar, Israel, April 9-14, 1989, and Nevis report no. 1415 1989 (unpublished).

24. D. Hitlin, in *Proceedings of the 1987 International Symposium on Lepton and Photon Interactions at High Energies, Hamburg, July 27-31, 1987* p. 179, Ed. W. Bartel and R. Rückl, (North Holland, Amsterdam, 1988).

2 K^0-$\overline{K^0}$, B^0-$\overline{B^0}$ Mixing and CP Violation

By indirections find directions out.

William Shakespeare, 1564-1616

2.1 Introduction

In the previous chapter we discussed briefly the determination of the KM matrix from 'direct' measurements, where the observed rates of processes are, to a good approximation, calculable from Feynman diagrams that are tree-level in the weak interactions. Such measurements therefore determine the square of the moduli of KM matrix elements.

In this chapter we will discuss some 'indirect' measurements, where the quark mixing effects come about from loop diagrams, and so the KM matrix elements appear in the formulae in a more complicated way. By studying such processes one can attempt to determine the CP-violating phase δ, and also to try to improve our knowledge of other less well-known Standard Model parameters, such as the top-quark mass m_t and $|V_{ub}|$.

2.2 Particle-Antiparticle Mixing

It has been known for many years that the mass eigenstates of the neutral Kaons exist in the form K_L^0 and K_S^0, which have unequal masses and lifetimes, rather than the strong interaction eigenstates K^0 and $\overline{K^0}$, which would not. This occurs because of $\Delta S = 2$ interactions, such as the box-diagrams of fig.2.1, which allow K^0-$\overline{K^0}$ mixing. Such mixing has also been observed for neutral B mesons. Although theoretically possible for D mesons, the mixing is expected to be highly suppressed due to the internal quarks in the box diagrams being down-type rather than up-type, coupled with fact that the KM matrix is dominantly diagonal.

Consider the general case of P^0-$\overline{P^0}$ mixing, where P^0 is a $J^P = 0^-$ meson, with CP transformation properties (in the meson rest-frame) defined to be

$$CP|P^0\rangle = -|\overline{P^0}\rangle$$
$$CP|\overline{P^0}\rangle = -|P^0\rangle.$$

(2.1)

19
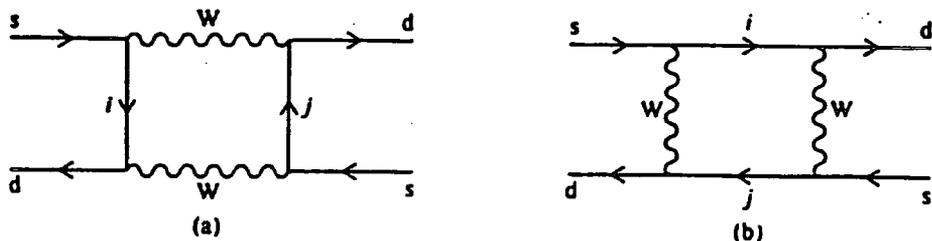
Figure 2.1 The box diagrams relevant to $K^0 - \overline{K^0}$ mixing.

This corresponds to a quark basis

$$|P^0\rangle \equiv |q_L \bar{q}_H\rangle \quad \text{and} \quad |\overline{P^0}\rangle \equiv |q_H \bar{q}_L\rangle, \qquad (2.2)$$

where q_H and q_L mean heavy and light quarks respectively, and has the advantage that all phases appearing in matrix elements arise from the phase $e^{i\delta}$ in the KM matrix (1.19).

The time evolution of a general linear combination of the two states

$$|\psi(t)\rangle \equiv A(t)|P^0\rangle + B(t)|\overline{P^0}\rangle \qquad (2.3)$$

is described by the Schrödinger equation

$$i\frac{\partial}{\partial t}|\psi(t)\rangle = H_{eff}|\psi(t)\rangle, \qquad (2.4)$$

where H_{eff} is the effective Hamiltonian for the process. This gives the following matrix equation for the coefficients A and B,

$$i\begin{pmatrix} \dot{A} \\ \dot{B} \end{pmatrix} = \begin{pmatrix} H_{11} & H_{12} \\ H_{21} & H_{22} \end{pmatrix} \begin{pmatrix} A \\ B \end{pmatrix}, \qquad (2.5)$$

where

$$H_{ij} = \langle i|H_{eff}|j\rangle, \qquad (2.6)$$

with $|1\rangle \equiv |P^0\rangle$ and $|2\rangle \equiv |\overline{P^0}\rangle$, and where the state normalisation is given by

$$\langle i|j\rangle \equiv \delta_{ij}. \qquad (2.7)$$

Second-order perturbation theory enables us to express the matrix elements

20

in the form [1]

$$H_{ij} \equiv M_{ij} - \frac{1}{2} i \Gamma_{ij}.$$ (2.8)

The first term in (2.8) is given by

$$M_{ij} = \delta_{ij} m_{P^0} + \langle i|H_W|j\rangle + \sum_n \frac{\langle i|H_W|n\rangle\langle n|H_W|j\rangle}{m_{P^0} - m_n},$$ (2.9)

where the sum is over all possible intermediate states, and m_{P^0} is the 'strong interaction mass' $(H_S|P^0\rangle = m_{P^0}|P^0\rangle)$. The second term of (2.8) is

$$\Gamma_{ij} = \sum_f \rho_f \langle i|H_W|f\rangle\langle f|H_W|j\rangle,$$ (2.10)

where the sum is over all physical states into which the states i and j can both decay, and ρ_f is the phase-space density. By considering (2.9) and (2.10) it can be seen that the matrices M_{ij} and Γ_{ij} are hermitian, on account of the hermiticity of the strong and weak interaction Hamiltonians [1]. Furthermore CPT invariance implies that

$$M_{11} = M_{22} \qquad \text{and} \qquad \Gamma_{11} = \Gamma_{22}.$$ (2.11)

As a result H_{ij} can be written in the form

$$(H_{ij}) = \begin{pmatrix} M_{11} - \frac{1}{2}i\Gamma_{11} & M_{12} - \frac{1}{2}i\Gamma_{12} \\ M_{12}^* - \frac{1}{2}i\Gamma_{12}^* & M_{11} - \frac{1}{2}i\Gamma_{11} \end{pmatrix},$$ (2.12)

where M_{11} and Γ_{11} are real. If CP were not violated then the off-diagonal elements would be equal

$$M_{12} = M_{21} = M_{12}^* \qquad \text{and} \qquad \Gamma_{12} = \Gamma_{21} = \Gamma_{12}^*.$$ (2.13)

Diagonalising the matrix H_{ij} gives the eigenvalues

$$\lambda_{1,2} = H_{11} \pm \sqrt{H_{12}H_{21}} \equiv m_{1,2} - \frac{1}{2}i\Gamma_{1,2}.$$ (2.14)

21

The masses and decay rates of the two eigenstates are thus given by

$$m_{1,2} \equiv m \pm \frac{1}{2}\Delta m = \text{Re}\left\{H_{11} \pm \sqrt{H_{12}H_{21}}\right\}$$
$$\Gamma_{1,2} \equiv \Gamma \pm \frac{1}{2}\Delta\Gamma = \text{Im}\left\{H_{11} \pm \sqrt{H_{12}H_{21}}\right\}. \qquad (2.15)$$

It is convenient to define the two dimensionless parameters

$$x \equiv \frac{\Delta m}{\Gamma} \qquad \text{and} \qquad y \equiv \frac{\Delta\Gamma}{2\Gamma} \qquad (2.16)$$

for later use. The eigenstates of the effective Hamiltonian are

$$|P^0_{1,2}\rangle = \frac{1}{\sqrt{2(1+|\eta|^2)}}\left\{(1+\eta)|P^0\rangle \pm (1-\eta)|\overline{P^0}\rangle\right\}$$
$$= \frac{1}{\sqrt{1+|\eta|^2}}\left\{|P^0_{\mp}\rangle + \eta|P^0_{\pm}\rangle\right\}, \qquad (2.17)$$

where

$$\eta \equiv \frac{\sqrt{H_{12}} - \sqrt{H_{21}}}{\sqrt{H_{12}} + \sqrt{H_{21}}}, \qquad (2.18)$$

and

$$|P^0_{\pm}\rangle \equiv \frac{1}{\sqrt{2}}\left\{|P^0\rangle \mp |\overline{P^0}\rangle\right\} \qquad (2.19)$$

are CP eigenstates

$$CP|P^0_{\pm}\rangle = \pm|P^0_{\pm}\rangle. \qquad (2.20)$$

If CP were conserved then $H_{12} = H_{21}$, giving $\eta = 0$ from (2.18), and so $|P^0_1\rangle$ would be CP odd and $|P^0_2\rangle$ would be CP even, using (2.17). Also the masses and decay widths would be given by

$$m_{1,2} = M_{11} \pm M_{12}$$
$$\Gamma_{1,2} = \Gamma_{11} \pm \Gamma_{12}. \qquad (2.21)$$

2.3 K^0-$\overline{K^0}$ Mixing

In the neutral Kaon system the two strong interaction eigenstates are defined,

as in (2.2), to be

$$|K^0\rangle \equiv |d\bar{s}\rangle \qquad \text{and} \qquad |\overline{K^0}\rangle \equiv |s\bar{d}\rangle. \qquad (2.22)$$

The two observed mass eigenstates for the K^0-$\overline{K^0}$ system are

$$|K^0_{L,S}\rangle = \frac{1}{\sqrt{2(1+|\eta_K|^2)}} \left\{ (1+\eta_K)|K^0\rangle \pm (1-\eta_K)|\overline{K^0}\rangle \right\} \qquad (2.23)$$

from (2.17), since we know that K^0_S is very nearly CP even (since $\Gamma(K^0_S \to 2\pi) \gg \Gamma(K^0_S \to 3\pi)$) and that K^0_L is very nearly CP odd (since $\Gamma(K^0_L \to 3\pi) \gg \Gamma(K^0_L \to 2\pi)$). From the latter we also know, since the $K^0_L \to 3\pi$ phase space is much smaller that the $K^0_L \to 2\pi$ phase space, that, in the above phase convention, $|\eta_K| \ll 1$ from (2.23).

2.3.1 Asymmetry in the Semileptonic Decay $K^0_L \to \pi^+ l^- \bar{\nu}$

One experimental measurement of CP violation in the neutral Kaon system that has been performed is a measurement of the decay asymmetry in a beam of K^0_L. From the definitions of (2.22) it can be seen that the semileptonic decay of K^0 produces l^+, while that of $\overline{K^0}$ produces l^-, so that

$$\begin{aligned}
\delta_K &\equiv \frac{\Gamma(K^0_L \to l^+) - \Gamma(K^0_L \to l^-)}{\Gamma(K^0_L \to l^+) + \Gamma(K^0_L \to l^-)} \\
&= \frac{|1+\eta_K|^2 - |1-\eta_K|^2}{|1+\eta_K|^2 + |1-\eta_K|^2} \\
&= 2\frac{\mathrm{Re}\eta_K}{1+|\eta_K|^2} \\
&\approx 2\mathrm{Re}\eta_K.
\end{aligned} \qquad (2.24)$$

Experimental measurements of the asymmetry give [2]

$$\delta_K = (0.327 \pm 0.012)\%, \qquad (2.25)$$

which yields

$$\mathrm{Re}\eta_K = (1.65 \pm 0.06) \times 10^{-3}. \qquad (2.26)$$

2.3.2 The CP Violation Parameters ϵ and ϵ'

The other common test of CP violation is from the experimental measurement

of the amplitude ratios

$$\eta_{00} \equiv \frac{\langle \pi^0 \pi^0 | H_W | K_L^0 \rangle}{\langle \pi^0 \pi^0 | H_W | K_S^0 \rangle}$$

$$\eta_{+-} \equiv \frac{\langle \pi^+ \pi^- | H_W | K_L^0 \rangle}{\langle \pi^+ \pi^- | H_W | K_S^0 \rangle}.$$

(2.27)

To calculate these we note that the two-pion states may be rewritten in terms of states of definite strong isospin $I = 0, 2$ via [3]

$$\langle \pi^0 \pi^0 | = -\frac{1}{\sqrt{3}} \langle 2\pi(I = 0)| + \frac{\sqrt{2}}{\sqrt{3}} \langle 2\pi(I = 2)|$$

$$\langle \pi^+ \pi^- | = \frac{\sqrt{2}}{\sqrt{3}} \langle 2\pi(I = 0)| + \frac{1}{\sqrt{3}} \langle 2\pi(I = 2)|,$$

(2.28)

using Clebsch-Gordan decomposition. We define the isospin amplitudes, A_I, using

$$\langle 2\pi(I) | H_W | K^0 \rangle = A_I e^{i\delta_I}$$

$$\langle 2\pi(I) | H_W | \overline{K^0} \rangle = -A_I^* e^{i\delta_I},$$

(2.29)

where δ_I are the strong interaction phase-shifts due to strong interactions between the final-state pions, and the second amplitude is derived from the first using CPT invariance.

It is convenient to define the three quantities

$$\epsilon \equiv \frac{\langle 2\pi(I = 0) | H_W | K_L^0 \rangle}{\langle 2\pi(I = 0) | H_W | K_S^0 \rangle}$$

(2.30)

$$\epsilon_2 \equiv \frac{\langle 2\pi(I = 2) | H_W | K_L^0 \rangle}{\langle 2\pi(I = 0) | H_W | K_S^0 \rangle}$$

(2.31)

$$\omega \equiv \frac{\langle 2\pi(I = 2) | H_W | K_S^0 \rangle}{\langle 2\pi(I = 0) | H_W | K_S^0 \rangle}.$$

(2.32)

Expanding the numerators and denominators, using (2.23) for the $K_{L,S}^0$ states, and (2.29) for the resulting weak matrix elements, yields

$$\epsilon = \frac{\eta_K + it_0}{1 + i\eta_K t_0}$$

(2.33)

$$\epsilon_2 = \frac{\eta_K + it_2}{1 + i\eta_K t_0} \frac{\mathrm{Re} A_2}{\mathrm{Re} A_0} e^{i(\delta_2 - \delta_0)}$$

(2.34)

$$\omega = \frac{1 + i\eta_K t_2}{1 + i\eta_K t_0} \frac{\mathrm{Re} A_2}{\mathrm{Re} A_0} e^{i(\delta_2 - \delta_0)},$$

(2.35)

where

$$t_I \equiv \frac{\mathrm{Im}A_I}{\mathrm{Re}A_I}. \tag{2.36}$$

Experimental measurements of the $\pi\pi$ phase-shifts give [4]

$$\delta_2 - \delta_0 + \frac{\pi}{2} = (48 \pm 8)^\circ. \tag{2.37}$$

Then, using the definitions of the experimentally measured quantities η_{00} and η_{+-} in (2.27), the Clebsh-Gordan decomposition of the $\pi^0\pi^0$ and $\pi^+\pi^-$ states in (2.28), and the definitions of (2.30)-(2.32), we find

$$\eta_{00} = \frac{\epsilon - \sqrt{2}\epsilon_2}{1 - \sqrt{2}\omega} = \epsilon - 2\frac{\epsilon'}{1 - \sqrt{2}\omega}$$

$$\eta_{+-} = \frac{\epsilon + \epsilon_2/\sqrt{2}}{1 + \omega/\sqrt{2}} = \epsilon + \frac{\epsilon'}{1 + \omega/\sqrt{2}} \tag{2.38}$$

where we have defined the new parameter

$$\begin{aligned}
\epsilon' &\equiv \frac{1}{\sqrt{2}}(\epsilon_2 - \epsilon\omega) \\
&= \frac{\omega}{\sqrt{2}}\left(\frac{\eta_K + it_2}{1 + i\eta_K t_2} - \frac{\eta_K + it_0}{1 + i\eta_K t_0}\right)e^{i(\delta_2 - \delta_0)} \\
&= \frac{i\omega}{\sqrt{2}}\frac{(1 - \eta_K^2)(t_2 - t_0)}{(1 + i\eta_K t_2)(1 + i\eta_K t_0)}e^{i(\delta_2 - \delta_0)}.
\end{aligned} \tag{2.39}$$

Experimental measurements of the $K \to 2\pi$-amplitudes give [4]

$$|\omega| \approx 0.045, \tag{2.40}$$

so that, anticipating that $|\epsilon'| \ll |\epsilon|$, we may write

$$\begin{aligned}
\eta_{00} &\approx \epsilon - 2\epsilon' \\
\eta_{+-} &\approx \epsilon + \epsilon'.
\end{aligned} \tag{2.41}$$

The experimental measurements of the ratios η_{00} and η_{+-} of (2.27) are [2]

$$\begin{aligned}
|\eta_{00}| &= (2.253 \pm 0.024) \times 10^{-3} \\
|\eta_{+-}| &= (2.268 \pm 0.023) \times 10^{-3},
\end{aligned} \tag{2.42}$$

25

with phases

$$\phi_{00} = (48.5 \pm 3.1)^\circ$$
$$\phi_{+-} = (46.0 \pm 1.2)^\circ. \tag{2.43}$$

These give

$$|\epsilon| = (2.263 \pm 0.023) \times 10^{-3} \tag{2.44}$$
$$\text{Re}\left(\frac{\epsilon'}{\epsilon}\right) = (2.2 \pm 1.1) \times 10^{-3}. \tag{2.45}$$

The result for $\text{Re}(\epsilon'/\epsilon)$ is, however, not very reliable, since the two high-precision measurements, by the NA31 [5] and Chicago-Fermilab [6] collaborations, give

$$\text{Re}\left(\frac{\epsilon'}{\epsilon}\right) = (3.3 \pm 1.1) \times 10^{-3} \tag{2.46}$$

and

$$\text{Re}\left(\frac{\epsilon'}{\epsilon}\right) = (-0.4 \pm 1.5) \times 10^{-3} \tag{2.47}$$

respectively, which differ by about 3σ. The measurement of $|\epsilon|$ in (2.44) tells us that $\epsilon \ll 1$ and hence, from (2.33), that $t_0 \ll 1$. Consideration of (2.39) then means that $t_2 \ll 1$ also. Using these approximations we may now write (2.35) as

$$|\omega| \approx \frac{\text{Re}A_2}{\text{Re}A_0}. \tag{2.48}$$

and (2.33) and (2.39) in the more familiar form

$$\epsilon \approx \eta_K + it_0$$
$$\epsilon' \approx \frac{1}{\sqrt{2}}e^{i(\delta_2 - \delta_0 + \pi/2)}|\omega|(t_2 - t_0) \tag{2.49}$$

By considering the matrix elements Γ_{12} and M_{12} for the neutral Kaon system we will be able to make approximations in (2.18) which we will use in the calculation of ϵ of (2.49). In order to calculate the quantity Γ_{12}, it is sufficient to include only 2π states, since the decay rate for $K^0, \overline{K^0} \to 2\pi$ is much larger than for any other decay mode available to both the strong interaction eigenstates. Also, since

$|\omega| \ll 1$, we can further simplify the expression by including only the $I = 0$ state. Thus

$$\Gamma_{12} \propto \langle K^0 | H_W | 2\pi(I=0) \rangle \langle 2\pi(I=0) | H_W | \overline{K^0} \rangle$$
$$= -A_0^{*2}, \tag{2.50}$$

and so

$$\frac{\mathrm{Im}\Gamma_{12}}{\mathrm{Re}\Gamma_{12}} \approx -\frac{2\mathrm{Im}A_0\mathrm{Re}A_0}{(\mathrm{Re}A_0)^2 + (\mathrm{Im}A_0)^2} = \frac{-2t_0}{1+t_0^2} \approx -2t_0, \tag{2.51}$$

which implies that

$$\mathrm{Im}\Gamma_{12} \ll \mathrm{Re}\Gamma_{12}. \tag{2.52}$$

Then, knowing that $|\eta| \ll 1$, (2.18) implies that

$$\mathrm{Im}M_{12} \ll \mathrm{Re}M_{12}. \tag{2.53}$$

Thus the mass and decay rate differences between the long- and short-lived eigenstates are given by

$$\Delta m_K \equiv m_L - m_S = 2\mathrm{Re}\sqrt{H_{12}H_{21}} \approx 2\mathrm{Re}M_{12}$$
$$\Delta\Gamma_K \equiv \Gamma_L - \Gamma_S = \overset{-4}{\underset{\wedge}{\mathrm{Im}}}\sqrt{H_{12}H_{21}} \approx 2\mathrm{Re}\Gamma_{12}. \tag{2.54}$$

The experimental results for the mass difference and decay rates are [2]

$$\Delta m_K = (3.522 \pm 0.016) \times 10^{-12} MeV$$
$$\Gamma_S = (7.374 \pm 0.017) \times 10^{-12} MeV \tag{2.55}$$
$$\Gamma_L = (1.273 \pm 0.010) \times 10^{-14} MeV,$$

which imply that the parameters of (2.16) are

$$x \equiv \frac{\Delta m_K}{\Gamma_K} = 0.954 \pm 0.006 \qquad \text{and} \qquad y \equiv \frac{\Delta\Gamma_K}{2\Gamma_K} = -0.996. \tag{2.56}$$

The mixing parameter η of (2.18) is

$$\eta_K = \frac{\sqrt{H_{12}} - \sqrt{H_{21}}}{\sqrt{H_{12}} + \sqrt{H_{21}}}$$
$$= \frac{H_{12} - H_{21}}{4\sqrt{H_{12}H_{21}} + (\sqrt{H_{12}} - \sqrt{H_{21}})^2} \tag{2.57}$$
$$= \frac{i(\mathrm{Im}M_{12} - \frac{1}{2}i\mathrm{Im}\Gamma_{12})}{\Delta m_K - \frac{1}{2}i\Delta\Gamma_K}\left(1 + O(\eta_K^2)\right)$$

27

which may be rewritten, using (2.56), in the form

$$
\eta_K = \frac{ix}{x - iy} \left(\frac{\mathrm{Im}M_{12}}{\Delta m_K} - \frac{1}{2}i\frac{y}{x}\frac{\mathrm{Im}\Gamma_{12}}{\mathrm{Re}\Gamma_{12}} \right)
$$
$$
= \frac{ix}{x - iy} \left(\frac{\mathrm{Im}M_{12}}{\Delta m_K} + i\frac{y}{x}t_0 \right)
$$

(2.58)

Hence ϵ may be written as

$$
\epsilon = \eta_K + it_0
$$
$$
= \frac{ix}{x - iy} \left(\frac{\mathrm{Im}M_{12}}{\Delta m_K} + t_0 \right).
$$

(2.59)

Using the values of Δm_K, Γ_S and Γ_L given above

$$
\frac{ix}{x - iy} = \frac{x}{\sqrt{x^2 + y^2}}e^{i\phi},
$$

(2.60)

where

$$
\phi = \tan^{-1}(-x/y) = (43.8 \pm 0.2)^\circ.
$$

(2.61)

The angle ϕ is usually approximated to 45°. Using $\mathrm{Re}\epsilon = \mathrm{Re}\eta_K$ from (2.49), we can now see that the measurement of δ_K given in (2.25) is in good agreement with the determination of $|\epsilon|$ given in (2.44).

2.3.3 Theoretical Calculation of η_K and ϵ

In order to predict ϵ we will use a box diagram calculation for $\mathrm{Im}M_{12}$. In such a calculation, intermediate states such as π, 2π and η are not included in the second-order term of (2.9). Denoting the contribution from such intermediate states as 'soft', we get

$$
M_{12} \approx (M_{12})^{box} + (M_{12})^{soft}.
$$

(2.62)

As argued by Hagelin [7], it is expected that, in a phase convention where A_0 is real, $(\mathrm{Im}M_{12})^{soft}$ will be negligible. On converting this back to the usual basis

(2.22), this means that

$$(\mathrm{Im}M_{12})^{soft} \approx -2t_0(\mathrm{Re}M_{12})^{soft}, \tag{2.63}$$

so that

$$\mathrm{Im}M_{12} \approx (\mathrm{Im}M_{12})^{box} - t_0\Delta m_K + 2t_0(\mathrm{Re}M_{12})^{box}, \tag{2.64}$$

using (2.54). Hence we find that

$$\epsilon \approx \frac{ix}{x-iy}\left(\frac{(\mathrm{Im}M_{12})^{box}}{\Delta m_K} + 2t_0\frac{(\mathrm{Re}M_{12})^{box}}{\Delta m_K}\right). \tag{2.65}$$

The calculation of M_{12} is discussed in section 2.5 below. The second term, proportional to t_0, is very much smaller than the first, and so, even though it is included in the phenomenological analysis discussed below, it will not be discussed here. The expressions used for t_0 are from the $1/N$ analysis of [8].

2.3.4 Status of $Re(\epsilon'/\epsilon)$

The theoretical calculation of ϵ' from (2.49) requires the evaluation of t_0 and t_2, defined in (2.36). This is discussed in detail in ref. [8], using the $1/N$ expansion.

Neither the theoretical or experimental analyses are particularly reliable. The evaluation of hadronic matrix elements is extremely difficult, and only in the $1/N$ expansion can all the required matrix elements be evaluated [8]. Unfortunately, the accuracy of the $1/N$ expansion is not well known. Furthermore, even in analyses using other techniques, the results are highly dependent upon the strange quark mass, which is not accurately determined. Finally the experimental results seem to be in some confusion also (see (2.46) and (2.47)), and so we will not include any further analysis of $\mathrm{Re}(\epsilon'/\epsilon)$.

2.4 B^0-$\overline{B^0}$ mixing

The neutral B meson strong interaction eigenstates are defined, using (2.2), to be

$$|B^0\rangle \equiv |d\bar{b}\rangle \qquad \text{and} \qquad |\overline{B^0}\rangle \equiv |b\bar{d}\rangle. \tag{2.66}$$

Evaluation of the box diagrams for the B^0-$\overline{B^0}$ system shows [7] that the dom-

inant terms are

$$M_{12} \propto m_t^2 (V_{tb} V_{td}^*)^2$$

$$\Gamma_{12} \propto m_b^2 (V_{ub} V_{ud}^* + V_{cb} V_{cd}^*)^2 = m_b^2 (V_{tb} V_{td}^*)^2,$$

$$(2.67)$$

so that $\Gamma_{12}/M_{12} \approx O(m_b^2/m_t^2)$ and that Γ_{12} and M_{12} are nearly in-phase. Hence, from (2.12) and (2.15), we can conclude that

$$\Delta \Gamma_B = 2|\Gamma_{12}| \ll \Delta M_B = 2|M_{12}|, \qquad (2.68)$$

and from (2.18) that $|1 + \eta_B|/|1 - \eta_B| \approx 1$ (i.e. $\mathrm{Re}\eta_B \ll \mathrm{Im}\eta_B$).

Experimental studies of B^0-$\overline{B^0}$ mixing have so far concentrated on effects that are related not to CP violation, but just to mixing. Furthermore, the time dependence of the mixing has not been studied, just the effects integrated over time. The time evolution of the two mass eigenstates is given by

$$|B_{1,2}^0(t)\rangle = e^{-i\lambda_{1,2}t}|B_{1,2}^0(0)\rangle, \qquad (2.69)$$

so the time evolution of states originally produced as B^0 or $\overline{B^0}$ is

$$|B^0(t)\rangle = g_+(t)|B^0\rangle + \frac{1 - \eta_B}{1 + \eta_B} g_-(t)|\overline{B^0}\rangle$$

$$|\overline{B^0}(t)\rangle = \frac{1 + \eta_B}{1 - \eta_B} g_-(t)|B^0\rangle + g_+(t)|\overline{B^0}\rangle,$$

$$(2.70)$$

where

$$g_\pm(t) \equiv \frac{1}{2}(e^{-i\lambda_1 t} \pm e^{-i\lambda_2 t})$$

$$= \frac{1}{2}(e^{-im_1 t}e^{-i\frac{1}{2}\Gamma_1 t} \pm e^{-im_2 t}e^{-i\frac{1}{2}\Gamma_2 t}).$$

$$(2.71)$$

Given that

$$\int_0^\infty dt |g_+(t)|^2 = \frac{\Gamma_B}{2(\Gamma_B^2 - \frac{1}{4}\Delta\Gamma_B^2)(\Gamma_B^2 + \Delta m_B^2)}(2\Gamma_B^2 + \Delta m_B^2 - \frac{1}{4}\Delta\Gamma_B^2)$$

$$\int_0^\infty dt |g_-(t)|^2 = \frac{\Gamma_B}{2(\Gamma_B^2 - \frac{1}{4}\Delta\Gamma_B^2)(\Gamma_B^2 + \Delta m_B^2)}(\Delta m_B^2 - \frac{1}{4}\Delta\Gamma_B^2),$$

$$(2.72)$$

we can write the experimentally measureable quantities

$$r_d \equiv \frac{\Gamma(B^0 \to l^-)}{\Gamma(B^0 \to l^+)} = \left|\frac{1 - \eta_B}{1 + \eta_B}\right|^2 \frac{x_d^2 - y_d^2}{2 + x_d^2 - y_d^2}$$

$$\bar{r}_d \equiv \frac{\Gamma(\overline{B^0} \to l^+)}{\Gamma(\overline{B^0} \to l^-)} = \left|\frac{1 + \eta_B}{1 - \eta_B}\right|^2 \frac{x_d^2 - y_d^2}{2 + x_d^2 - y_d^2}, \tag{2.73}$$

with

$$x_d \equiv \frac{\Delta m_B}{\Gamma_B} \qquad \text{and} \qquad y_d \equiv \frac{\Delta \Gamma_B}{2\Gamma_B} \tag{2.74}$$

defined in analogy with (2.16) (the subscript, which refers to the light quark in the meson, is to avoid confusion with the equivalent quantities that occur in the mixing of neutral B_s mesons). Using $|1 - \eta_B|/|1 + \eta_B| \approx 1$ and $\Delta \Gamma_B \ll \Delta m_B$ we can write

$$r_d \approx \bar{r}_d \approx \frac{x_d^2}{2 + x_d^2}, \tag{2.75}$$

or

$$x_d \approx \frac{2 r_d}{1 - r_d}. \tag{2.76}$$

The experimental quantity that is actually measured is the ratio of like-sign to unlike-sign lepton events

$$R \equiv \frac{\Gamma(l^+ l^+) + \Gamma(l^- l^-)}{\Gamma(l^+ l^-)} \tag{2.77}$$

If the $B^0 \overline{B^0}$ pair is produced from the $\Upsilon(4S)$ resonance then the two mesons are in a P-wave state, which is odd under particle interchange, so the two mesons must remain distinct. Once the first one decays the other behaves like a single B meson and thus can change its form. Hence in this case

$$R = r_d. \tag{2.78}$$

Measurements of B^0-$\overline{B^0}$ mixing are available from both ARGUS [9] and CLEO

[10] collaborations, running at the $\Upsilon(4S)$ resonance, giving

$$
\begin{array}{llll}
r_d = 0.21 \pm 0.08 & & x_d = 0.73 \pm 0.18 & \text{ARGUS} \\
& \Rightarrow & & \\
r_d = 0.18 \pm 0.08 & & x_d = 0.66 \pm 0.18 & \text{CLEO,}
\end{array}
\tag{2.79}
$$

which give a combined result of

$$
x_d = 0.70 \pm 0.13.
\tag{2.80}
$$

2.5 Effective Hamiltonians and QCD corrections

The calculation of the quantities η_K, t_I and Δm_B requires the use of effective weak interaction Hamiltonians. This section is devoted to a brief discussion of their origin and derivation (further details can be found in the references mentioned).

An effective weak Hamiltonian, as calculated from lowest order Feynman diagrams, describes the relevant weak interactions at scales $\mu = O(m_W)$. However, matrix elements must be evaluated at a much lower scale, so this effective Hamiltonian must first be transformed into an effective low-energy Hamiltonian. The techniques required to do this are discussed at length in the literature [8,11,12], so we will give only a very brief outline here. The operators of the Hamiltonian are evolved down in energy scale by the use of the Renormalisation Group Equation (RGE) at leading log order, successively removing first the W-boson and top quark (together, since their masses are of the same order), followed by the bottom quark, and then (for Kaon physics) the charmed quark. During this process new operators, not present in the original Hamiltonian, may be introduced (for instance, in the evolution of the $\Delta S = 1$ Hamiltonian, which is relevant for the calculation of t_0 and t_2, the operators that give rise to the penguin diagrams of fig.2.2 are able to mix with the original operators). Finally one obtains an effective low-energy Hamiltonian of the form

$$
\mathcal{H}_{eff} = K \sum_i C_i(\mu) Q_i(\mu),
\tag{2.81}
$$

where K is some known constant, the $Q_i(\mu)$ are the remaining operators at the low-energy scale μ, and $C_i(\mu)$ are known as Wilson coefficient functions, which give the relative strengths of the operators $Q_i(\mu)$, and represent the QCD corrections.
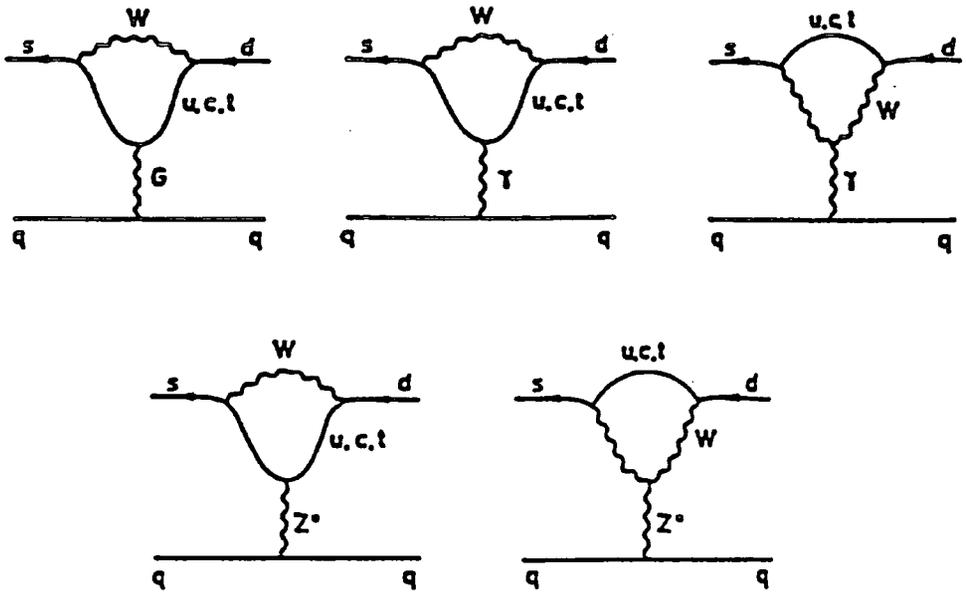
Figure 2.2   The Penguin Diagrams, which occur in the analysis of the $\Delta S = 1$ effective Hamiltonian, used in the evaluation of t_0 and t_2, which are mainly used in the analysis of ϵ'.

For different processes one starts with a different Hamiltonian, so the above procedure must be recalculated each time. In the following discussions we will require

    a) The $\Delta S = 2$ Hamiltonian for $K^0\text{-}\overline{K^0}$ mixing.

    b) The $\Delta B = 2$ Hamiltonian for $B^0\text{-}\overline{B^0}$ mixing.

2.5.1 Evaluation of M_{12}

In order to calculate the CP-violating parameters η_K and ϵ for the K-meson system, and the mixing parameter x_d for the B-meson system, we need to calculate the matrix element M_{12}. To accomplish this we must find the $\Delta S = 2$ (or $\Delta B = 2$) effective Hamiltonian for the process. Since this requires the use of Feynman diagram calculations it is convenient to rewrite H_{12} of (2.6) in terms of states with relativistically covariant normalisation and an effective Hamiltonian density $\mathcal{H}_{eff}$. The off-diagonal elements, which are the only ones that need to be considered, then become

$$H_{12} = M_{12} - \frac{1}{2}i\Gamma_{12} = \frac{1}{2m_p}\langle P^0|\mathcal{H}_{eff}^{\Delta S, B=2}|\overline{P^0}\rangle, \qquad (2.82)$$

33

where the hermitian part of the Hamiltonian density gives M_{12}, and the anti-hermitian part gives Γ_{12}. Calculations of both hermitian and anti-hermitian parts have been performed [7], but we only require M_{12}, so only the hermitian part will actually be included in the discussion below.

The effective Hamiltonian density is initially determined in the box-diagram approximation, by a calculation of the diagrams of fig.2.1, and is then evolved to the low energy scale required, as discussed briefly in the previous section. The final result is of the form

$$\mathcal{H}_{eff}^{\Delta S, B=2} = \frac{G_F^2 M_W^2}{16\pi^2} \left\{ \sum_{i,j=u,c,t} \lambda_i \lambda_j A_{ij} \eta_{ij} \bar{d}\gamma^\mu (1 - \gamma_5) q \bar{d}\gamma_\mu (1 - \gamma_5) q + \text{h.c.}, \right\} \tag{2.83}$$

where $q = s$ or b for the relevant Hamiltonian, and

$$\lambda_i \equiv V_{iq} V_{id}^*. \tag{2.84}$$

The A_{ij} originate from the integral over the internal loop momentum, and the η_{ij} are QCD corrections calculated from the Wilson coefficient functions.

The matrix element (2.82) also requires the evaluation of a hadronic matrix element, which is conventionally defined by

$$\langle P^0 | \bar{d}\gamma^\mu (1 - \gamma_5) q \bar{d}\gamma_\mu (1 - \gamma_5) q | \overline{P^0} \rangle \equiv \frac{8}{3} B_P f_P^2 m_P^2, \tag{2.85}$$

where f_P is the meson decay constant, defined by the matrix element

$$\langle 0 | \bar{d}\gamma^\mu (1 - \gamma_5) q | \overline{P^0}(k) \rangle \equiv i f_P k^\mu, \tag{2.86}$$

and the factor of 8/3 is used so that the normalisation factor $B_P = 1$ in the 'vacuum-insertion' approximation. In this case the factor 8/3 arises from the colour factors associated with the four different ways of contracting the quark operators with the meson states. Discussion of the theoretical values of B_P will be left until sections 2.6 and 2.7.

2.6 Calculation of η_K and ϵ for the K-Meson System

In order to predict ϵ we need to calculate the box-diagram for both $\text{Im}M_{12}$ and $\text{Re}M_{12}$. For the Kaon system, the box-diagrams can be evaluated in the limit

where the masses and momenta of the external quarks are negligible compared to the W boson. The resulting integrals over the loop momentum (as defined in (2.83)) are

$$A_{ij} = x_i x_j \left\{ \left(\frac{4 - 8x_j + x_j^2}{4(1 - x_j)^2} \right) \frac{\log x_j}{x_j - x_i} + (x_j \leftrightarrow x_i) - \frac{3}{4} \frac{1}{(1 - x_i)(1 - x_j)} \right\}$$

$$A_{ii} = \lim_{x_j \to x_i} A_{ij} = x_i \left(\frac{4 - 11x_i + x_i^2}{4(1 - x_i)^2} \right) - \frac{3}{2} \left(\frac{x_i}{1 - x_i} \right)^3 \log x_i, \tag{2.87}$$

where

$$x_i \equiv \frac{m_i^2}{m_W^2}. \tag{2.88}$$

2.6.1 Calculation of $(ImM_{12})^{box}$ for the Kaon System

By considering the magnitude of $Im(\lambda_i \lambda_j) A_{ij}$, using (2.87) and the KM matrix elements given in (1.44), one can see that the terms involving an internal u-quark in the box-diagram are negligible in comparison to those involving c and t quarks. Hence we may write, using (2.83) and (2.85)

$$(ImM_{12})^{box} \approx \frac{G_F^2 m_W^2}{12\pi^2} B_K f_K^2 m_K \sum_{i,j=c,t} Im(\lambda_i \lambda_j) A_{ij} \eta_{ij}. \tag{2.89}$$

2.6.2 Calculation of $(ReM_{12})^{box}$ for the Kaon System

Given that $t_0 \sim 10^{-4}$, a consideration of the product

$$Re(\lambda_i \lambda_j) A_{ij} \tag{2.90}$$

shows that we may neglect all terms in (2.83) except that involving only charmed quarks, and that even that will only give about a 1% correction to ϵ. As a result we may write

$$(ReM_{12})^{box} \approx \frac{G_F^2 m_W^2}{12\pi^2} B_K f_K^2 m_K Re(\lambda_c^2) A_{cc} \eta_{cc}. \tag{2.91}$$

2.6.3 QCD Corrections to $K^0 - \overline{K^0}$ Mixing

The calculation of the QCD corrections, η_{ij}, of (2.83), on the assumption that

35

the quark masses are all much less than the W-boson mass, has been understood for some time, from the formalism introduced by Gilman and Wise [12]. However, we now know that the top-quark mass is of the same order as the W mass and so the above analysis is no longer strictly valid. The calculation has been redone by two groups [13], and their calculations agree well but not exactly. However, it turns out that using the simpler Gilman and Wise technique, but with the top quark integrated out at the same time as the W boson, the results are very similar [8]. Furthermore, over the top-quark mass range that will be considered ($50\,GeV \leq m_t \leq 250\,GeV$), the QCD corrections do not vary significantly with m_t. The values used will be [8]

$$\eta_{cc} = 0.85 \qquad \eta_{ct} = 0.36 \qquad \eta_{tt} = 0.62. \tag{2.92}$$

The formulae for these corrections depend upon Λ_{QCD}, m_c and m_b, and while η_{ct} and η_{tt} are almost independent of these, η_{cc} does vary. However, this term is actually about an order of magnitude smaller than the other terms, so this variation can be neglected.

Evaluations of the factor B_K are numerous, ranging from the MIT bag model calculation of $B_K \approx -0.4$ [14], to the Vacuum-Insertion value $B_K \equiv 1$ given above. More consistent recent values are

$$B_K \approx \begin{cases} 0.84 & \text{QCD sum rules [15]} \\ 0.75 \pm 0.15 & 1/N \text{ expansion [16]} \\ 0.87 \pm 0.20 & \text{Lattice QCD calculation [17].} \end{cases} \tag{2.93}$$

2.7 B^0-$\overline{B^0}$ mixing

For the B-meson system we need to calculate

$$x_d \equiv \frac{\Delta m_B}{\Gamma_B} = 2|M_{12}|\tau_B, \tag{2.94}$$

where the result of (2.68) has been used. In this case the long-distance effects are expected to be small (unlike the K-meson system), so that both real and imaginary parts of M_{12} should be calculable from the box-diagram inspired Hamiltonian.

Unlike the K-meson system, it is no longer automatically justifiable to neglect the masses and momenta of the external quarks, since they are not necessarily negligible compared to the W mass. Calculations including these effects have been done [18], but it actually turns out that, for $m_t \gtrsim 50\,GeV$, the difference is less that 3% for the dominant term, which thus gives

$$x_d = \tau_B \frac{G_F^2 m_W^2}{6\pi^2} B_B f_B^2 m_B |\lambda_t^2| A_{tt} \eta_{tt}, \qquad (2.95)$$

with A_{tt} as in (2.87). The discussion of the QCD correction factor in the presence of high m_t is similar to that given for the K-meson system, and so we shall again use the value calculated using the Gilman and Wise procedure, which gives [8]

$$\eta_{tt} = 0.84, \qquad (2.96)$$

in this case. The main uncertainties in the calculation are in the calculation of the factor $B_B f_B^2$ from the hadronic matrix element (2.85). The usual methods used are QCD sum rules [19] and lattice gauge theory [20]. Both methods yield values that range from $B_B f_B^2 \sim (100 MeV)^2$ to $B_B f_B^2 \sim (200 MeV)^2$ or more.

2.8 Phenomenological Analysis

2.8.1 Parameter Values

The following discussion is based upon the measurements of $|\epsilon|$ and x_d, defined in (2.30) and (2.74) respectively. For the analysis we use the following parameter values:

i) For the less well-known KM matrix angles of (1.19) we use the values obtained from the exlusive B decay analysis of chapter 6

$$|V_{cb}| = s_{23} = 0.039 \pm 0.005 \quad \text{and} \quad \left|\frac{V_{ub}}{V_{cb}}\right| = 0.07^{+0.14}_{-0.04}, \qquad (2.97)$$

although we will also study the effects of changing them to the inclusive B decay values

$$|V_{cb}| = 0.047 \pm 0.004 \quad \text{and} \quad |V_{ub}/V_{cb}| = 0.11 \pm 0.03 \qquad (2.98)$$

discussed in chapter 7 (the ratio is actually taken from ref. [21]).

ii) For the B_K parameter that occurs in the theoretical expression for $|\epsilon|$ we use

$$B_K = 0.80 \pm 0.15, \qquad (2.99)$$

which is between the $1/N$ expansion and lattice values of (2.93).

iii) For the combination $B_B f_B^2$, which is probably the largest theoretical uncertainty, we use two different representative ranges

$$B_B f_B^2 = (175 \pm 50)^2 \, MeV^2 \quad \text{and} \quad B_B f_B^2 = (140 \pm 25)^2 \, MeV^2. \quad (2.100)$$

iv) Finally we use the recent determination of the top-quark mass m_t [22], from measurements of m_Z, m_Z/m_W and $\sin^2 \theta_W(m_Z)$

$$m_t = (137 \pm 40) \, GeV. \qquad (2.101)$$

2.8.2 Analysis of the Measurement of $|\epsilon|$

Since the measurements of the phases ϕ_{00} and ϕ_{+-}, (2.43), of the two $K^0 \to 2\pi$ decay amplitudes η_{00} and η_{+-}, and the theoretical prediction of the phase of ϵ in (2.61) are in good agreement, the angle δ of the KM matrix is restricted to lie in the range $0 < \delta < \pi$.

Fig.2.3 shows the χ^2 contours obtained by fitting to the measured values of $|\epsilon|$ and to the parameters $|V_{cb}|$, $|V_{ub}/V_{cb}|$ and B_K for fixed δ and m_t. The first graph shows the results of Buchalla et al. [8], who use a very restricted range of KM angles:

$$|V_{cb}| = 0.050^{+0.002}_{-0.004} \quad \text{and} \quad \left| \frac{V_{ub}}{V_{cb}} \right| = 0.100^{+0.012}_{-0.013} \qquad (2.102)$$

and the $1/N$ expansion value of $B_K = 0.75 \pm 0.15$. This may be compared to the second graph, which shows the same fit, but to the exclusive B decay values of the KM matrix elements given in (2.97), and the B_K range of (2.99). The excluded region in fig.2.3(a) that does not occur in (b) is caused by the large values of $|V_{cb}|$ and $|V_{ub}|$. However, fig.2.3(a) does show one interesting feature, which will reappear later, that for higher values of m_t there are two distict regions allowed,
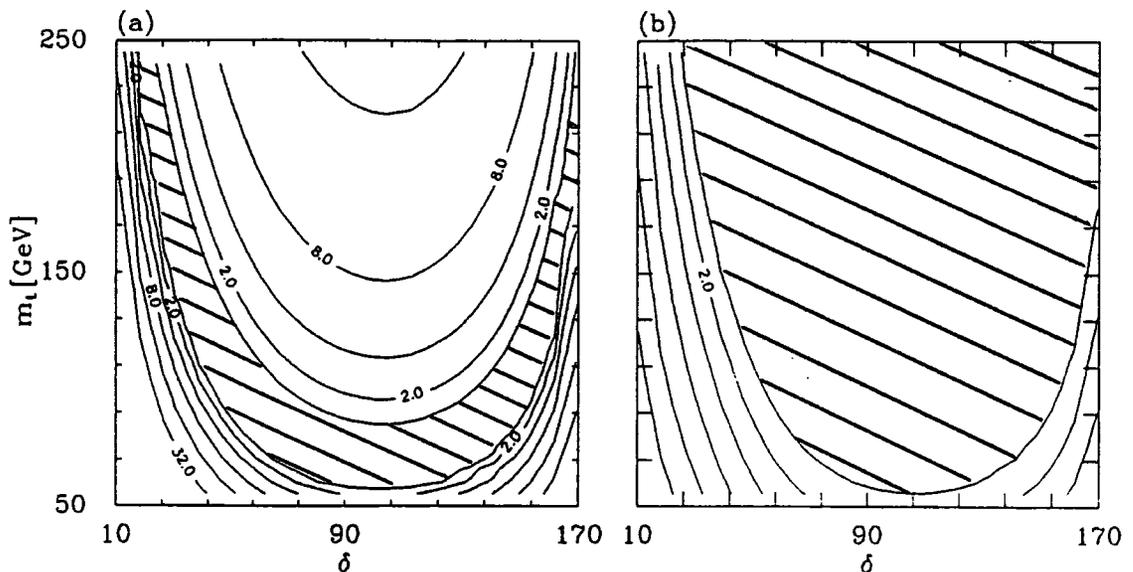
Figure 2.3 χ^2 contour plot for the fit to $|\epsilon|$, for fixed values of δ and m_t. (a) shows the region found by Buchalla et al. [8], using the parameters of (2.102), while (b) shows the results for the parameter ranges given in (2.97) and (2.99). The contours are marked for $\chi^2 = 1, 2, 4, 8, 16, 32$ and the region $\chi^2 \leq 1$ is shaded.

one for $\delta \lesssim 90°$ and the other for $\delta \gtrsim 90°$. Although not visible in fig.2.3(b) this does still occur, but to a much smaller extent.

Neither figure is able to rule out any values of δ except very low and very high ones, even for m_t in the range $(137 \pm 40)\,GeV$. On the other hand, only very low values of m_t are excluded by this analysis.

2.8.3 Combined Analysis of ϵ and x_d

Following the recent indirect estimate of the top-quark mass given in section 2.8.1, and given the uncertainty in the determination of $|V_{ub}|$, as discussed in section 6.7, it is interesting to plot the χ^2 contours for δ vs. $|V_{ub}|$ instead of δ vs. m_t.

Fig.2.4(a) shows the χ^2 contours for the fit to $|\epsilon|$, using the $|V_{cb}|$, m_t and B_K values of (2.97), (2.99) and (2.101) in the δ-$|V_{ub}|$ parameter space. For low $|V_{ub}|$ and extreme values of δ the fit requires large values of all three of the variable parameters. Conversely, the region an high $|V_{ub}|$ and $\delta \sim 90°$ requires all three parameters to be small.
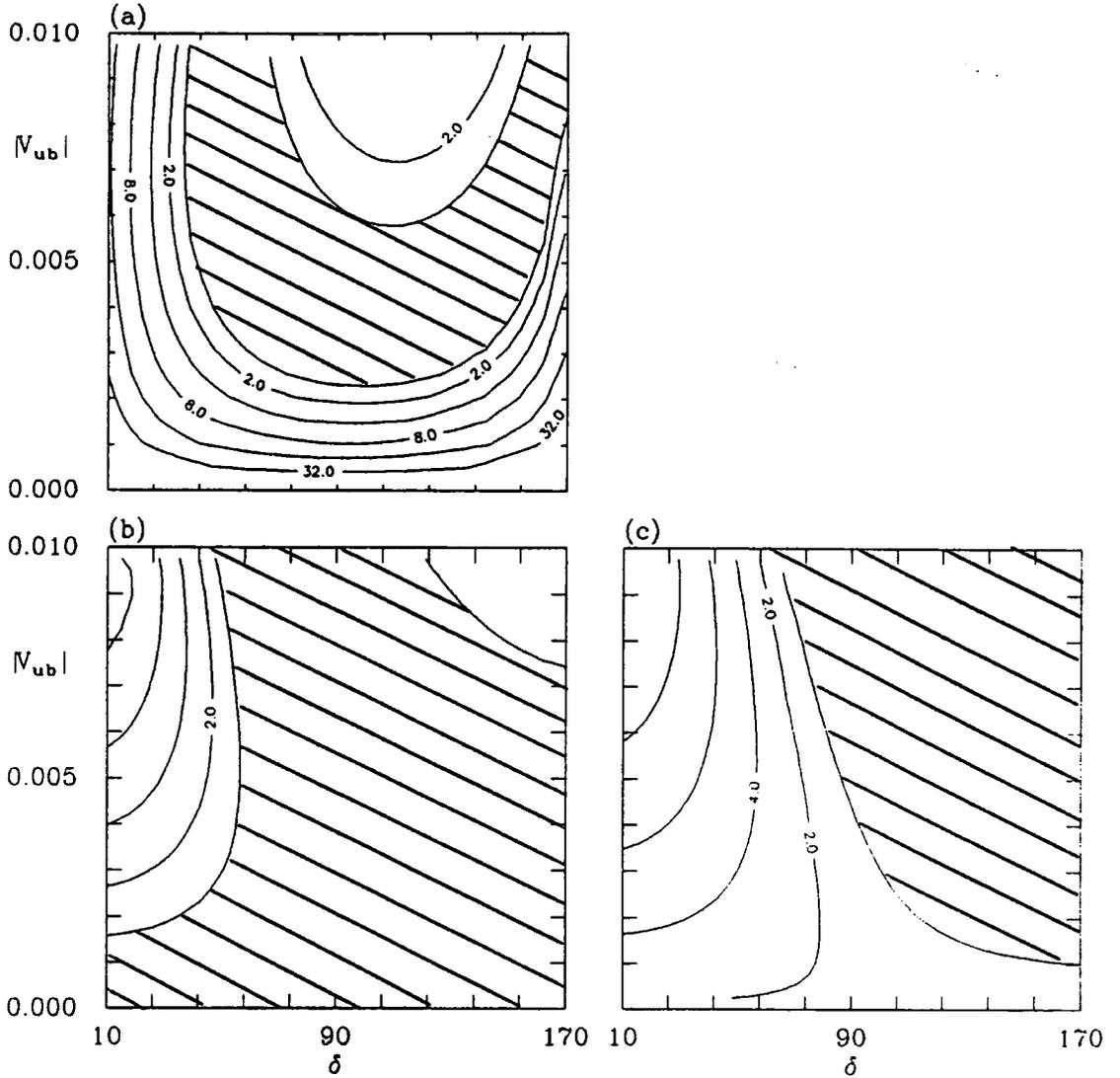
Figure 2.4 χ^2 contour plots, for fixed values of δ and $|V_{ub}|$. Using the parameter ranges of (2.97)-(2.101), (a) shows the fit to $|\epsilon|$, while (b) and (c) show the fits to x_d for $B_B f_B^2 = (175 \pm 50)\,MeV^2$ and $B_B f_B^2 = (140 \pm 25)\,MeV^2$ respectively. The region $\chi^2 \le 1$ is shaded.

Figs.2.4(b) and (c) show the χ^2 contours for fits to x_d, with the parameters $|V_{cb}|$ and m_t as in (2.97) and (2.101) respectively, for the two ranges of $B_B f_B^2$ given in (2.100), again as a function of δ and $|V_{ub}|$. With the larger experimental errors on x_d the allowed region is much larger than in the fit to $|\epsilon|$. Note that x_d increases with δ, m_t and $B_B f_B^2$. The excluded region at the left, with small δ, thus requires large m_t and $B_B f_B^2$, while the region to the top right of (b) requires small m_t and $B_B f_B^2$.
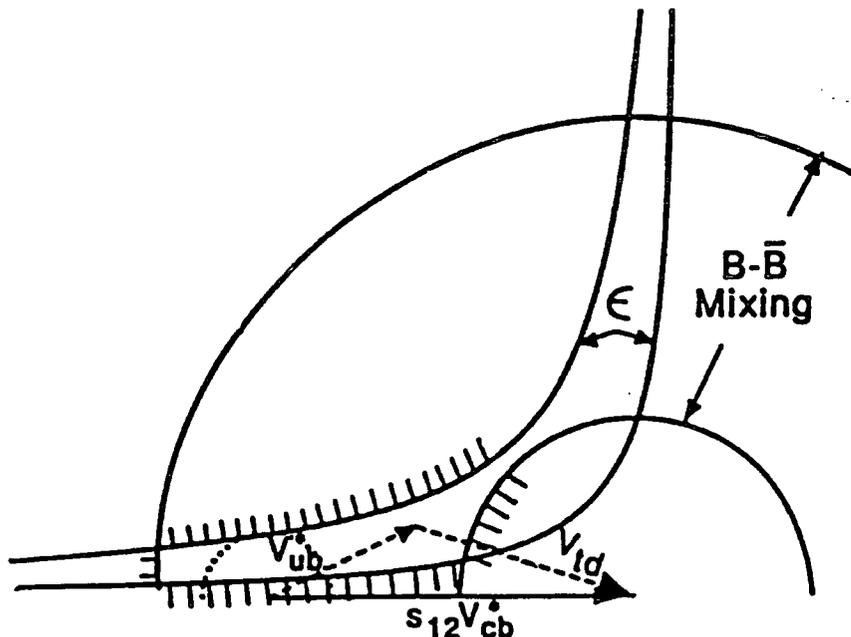
Figure 2.5 How the KM triangle is determined by the measurements of x_d and $|\epsilon|$. The region favoured by the data is indicated by the hatching, although another region, with lower δ and higher $|V_{ub}|$ is also possible.

We now discuss the simultaneous fit to both $|\epsilon|$ and x_d. First we reconsider the KM triangle introduced in section 1.7. The length of the rightmost side, $|V_{td}|$, is determined by $x_d \propto |V_{td}|^2$. Hence for given $|V_{cb}|$, m_t and $B_B f_B^2$ the measurement of x_d defines an annulus, centred on the lower right corner of the triangle, as shown in fig.2.5. Similarly the measurement of $|\epsilon|$ essentially determines the height of the triangle, since the dominant term is $|\epsilon| \propto \mathrm{Im}(V_{td}^{*2}) + \ldots$ Fig.2.5 also shows a typical allowed region from the measurement of $|\epsilon|$. From the diagram we see that, in general, for fixed values of the other parameters, there are two allowed regions, characterised by distinct values of δ and $|V_{ub}|$.

Fig.2.6 shows the χ^2 contours for the combined $|\epsilon|$ and x_d fit, using both the exclusive and inclusive B decay values of $|V_{cb}|$ and the two ranges of $B_B f_B^2$ of (2.100). The two-region structure discussed above is just visible in the top two graphs, but not in the lower two graphs, where the high-$|V_{ub}|$ region is off the top of the scale. We are thus left with the 'higher-δ – lower-$|V_{ub}|$' region, which is indicated on the KM triangle plot of fig.2.5. The four figures also show the best-fits to the data as a star (all four have $\chi^2 < 10^{-15}$).
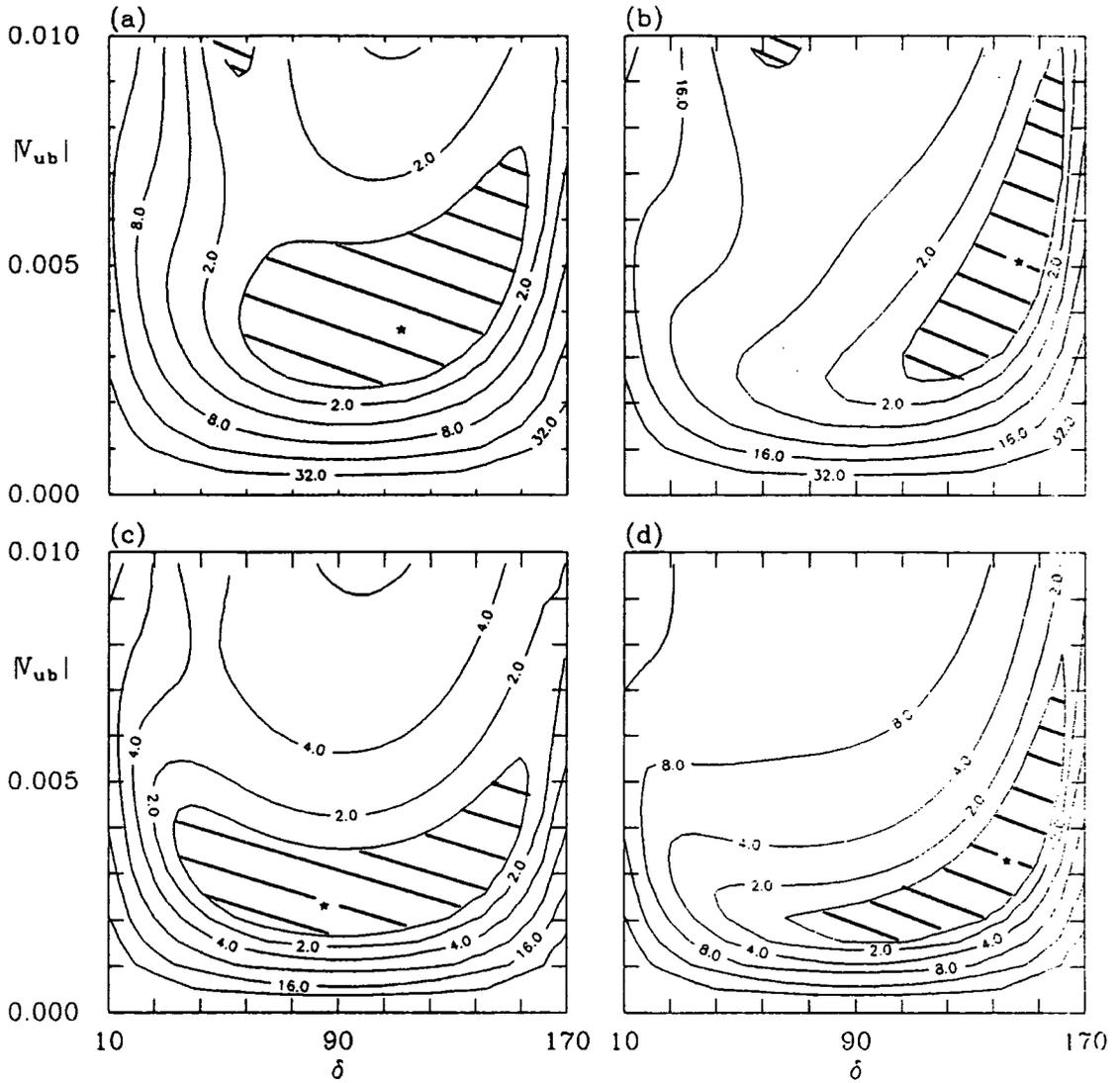
Figure 2.6 χ^2 contour plots for the combined fit to $|\epsilon|$ and x_d, using the parameter values of (2.97)-(2.101). The exclusive B decay value of $|V_{cb}| = 0.039 \pm 0.005$ is used in (a) and (b), while the inclusive value of $|V_{cb}| = 0.047 \pm 0.004$ is used in (c) and (d). Graphs (a) and (c) use $B_B f_B^2 = (175 \pm 50)^2 \, MeV^2$, while (b) and (d) use $B_B f_B^2 = (140 \pm 25)^2 \, MeV^2$. The shaded area shows the $\chi^2 \leq 1$ region, and the stars show the overall best-fit.

In the end none of the contour plots put very strong constraints upon either δ or $|V_{ub}|$ except to exclude extreme values of δ and very low values of $|V_{ub}|$. Values of $|V_{ub}| \gtrsim 0.01$ are possible in the second region, off the plot, but are less likely from the analysis of $b \to u$ decays. Using the value of $|V_{cb}|$ extracted from exclusive B decays the $\chi^2 = 1$ contour for the region shown gives

$$0.0025 \lesssim |V_{ub}| \lesssim 0.0075 \qquad \text{and} \qquad 60° \lesssim \delta \lesssim 155° \qquad (2.103)$$

for $B_B f_B^2 = (175 \pm 50)^2 \, MeV^2$, and

$$0.0025 \lesssim |V_{ub}| \lesssim 0.01 \qquad \text{and} \qquad 105° \lesssim \delta \lesssim 160° \qquad (2.104)$$

for $B_B f_B^2 = (140 \pm 25)^2 \, MeV^2$.

Finally fig.2.7 shows χ^2-m_t profiles for the combined fit to $|\epsilon|$ and x_d, using the two ranges of each of $|V_{cb}|$, $B_B f_B^2$ and $|V_{ub}/V_{cb}|$ given in section 2.8.1. These graphs demonstrate the two-region structure discussed in section 2.8.2. The best-fit follows the high-δ branch of fig.2.3 up to a certain value of m_t and then switches to the low-δ branch, resulting in the sharp local maximum in the value of χ^2. However, only for very tightly-constrained parameters is the m_t region between the minima actually excluded.

2.9 Conclusions

The above analysis still requires both experimental and theoretical improvements. Experimentally we would like more accurate determinations of m_t and x_d, and more data on $b \rightarrow u$ decays for the determination of $|V_{ub}|$. Theoretically we need to improve the analysis of the $b \rightarrow u$ measurements, and to constrain more tightly the hadronic matrix element parameters B_K and $B_B f_B^2$, particularly the latter.
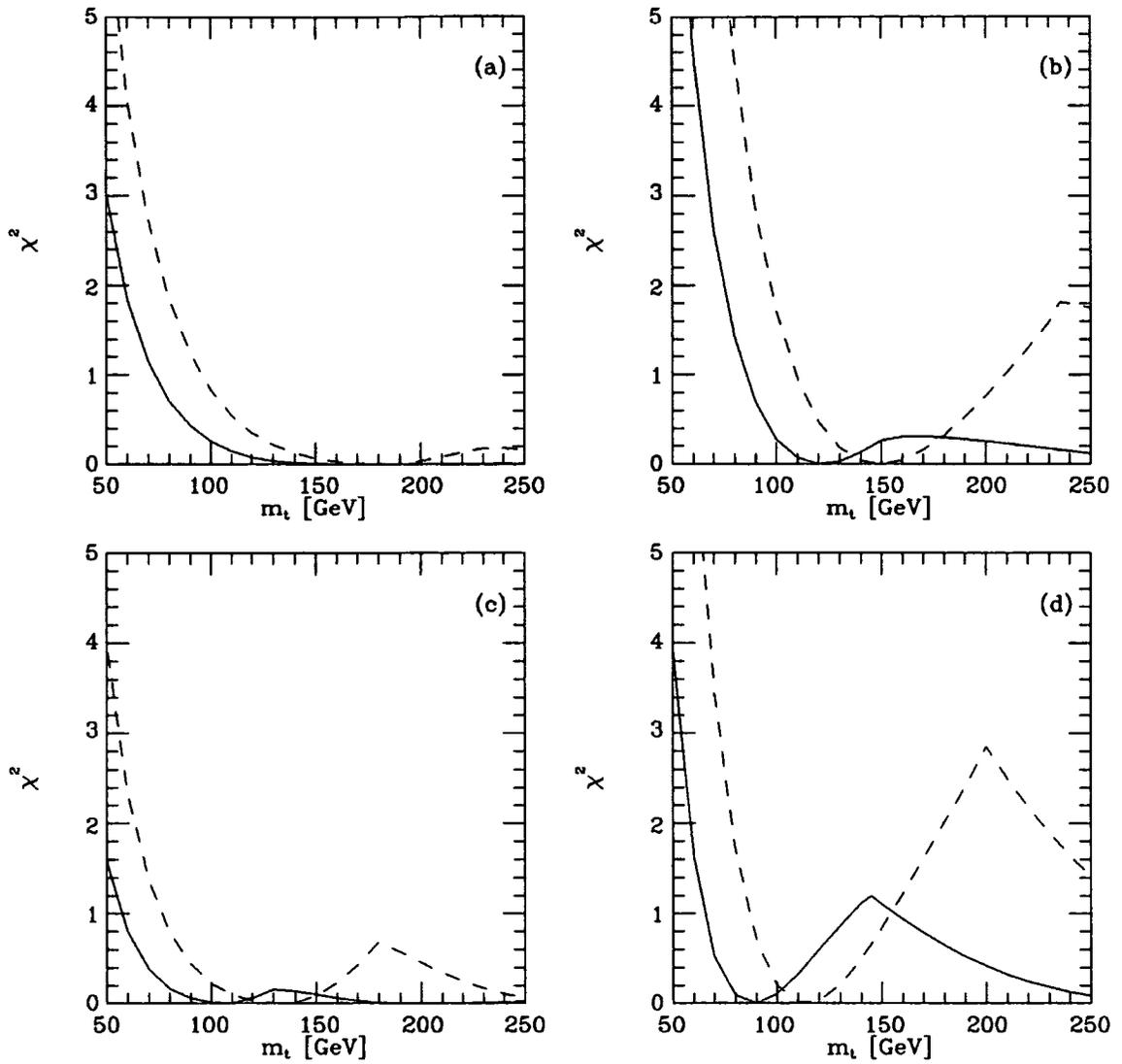
Figure 2.7 χ^2 profiles, as functions of m_t. The solid and dashed lines show the fits with $B_B f_B^2 = (175 \pm 50)^2 MeV^2$ and $B_{\overline{B}} f_B^2 = (140 \pm 25)^2 MeV^2$ respectively. The exclusive B decay value of $|V_{cb}| = 0.039 \pm 0.005$ is used in (a) and (b), while the inclusive value of $|V_{cb}| = 0.047 \pm 0.004$ is used in (c) and (d). Graphs (a) and (c) use $|V_{ub}/V_{cb}| = 0.07^{+0.14}_{-0.04}$, while (b) and (d) use $|V_{ub}/V_{cb}| = 0.11 \pm 0.03$.

References

1. T.-P. Cheng and L.-F. Li, in *Gauge Theory of Elementary Particle Physics* pp.374-378 (Oxford, 1984).

2. Particle Data Group: Review of Particle Properties, *Phys. Lett.* **B239**, 1 (1990).

3. K. Kleinknecht, in *CP Violation*, Ed. C. Jarlskog, (World Scientific, 1989).

4. T. Devlin and J. Dickey, *Rev. Mod. Phys.* **51**, 237 (1979).

5. H. Burckhardt et al., *Phys. Lett.* **B206**, 169 (1988).

6. J.R. Patterson et al., *Phys. Rev. Lett.* **64**, 1491 (1990).

7. J.S. Hagelin, *Nucl. Phys.* **B193**, 123 (1981).

8. G. Buchalla, A.J. Buras and M.K. Harlander, *Nucl. Phys.* **B337**, 313 (1990).

9. H. Albrecht et al., *Phys. Lett.* **209B**, 245 (1988).

10. M. Artuso et al., *Phys. Rev. Lett.* **62**, 2233 (1988).

11. F.J. Gilman and M.B. Wise, *Phys. Rev.* **D20**, 2392 (1979).

12. F.J. Gilman and M.B. Wise, *Phys. Rev.* **D27**, 1128 (1983).

13. W.A. Kaufman, H. Steger and Y.-P. Yao, *Mod. Phys. Lett.* **A3**, 1479 (1988).

    A. Datta, J. Fröhlich and E.A. Paschos, *Z. Phys.* **C46**, 63 (1990).

14. R.E. Schrock and S.B. Treiman, *Phys. Rev.* **D19**, 2148 (1978).

15. L.J. Reinders and S. Yazaki, *Nucl. Phys.* **B288**, 789 (1987).

16. W.A. Bardeen, A.J. Buras and J.-M. Gerard, *Nucl. Phys.* **B293**, 787 (1987).

    W.A. Bardeen, A.J. Buras and J.-M. Gerard, *Phys. Lett.* **B192**, 138 (1987).

    W.A. Bardeen, A.J. Buras and J.-M. Gerard, *Phys. Lett.* **B211**, 343 (1988).

17. M.B. Gavela et al., *Nucl. Phys.* **B306**, 677 (1988).

18. A.J. Buras, W. Slominski and H. Steger, *Nucl. Phys.* **B245**, 369 (1984).

19. E.V. Shuryak, *Nucl. Phys.* **B198**, 83 (1982).

    T.D. Aliev et al., *Sov. J. Nucl. Phys.* **38**, 936 (1983).

    L.J. Reinders et al., *Phys. Rep.* **C127**, 1 (1985).

C.A. Dominguez and N. Paver, *Phys. Lett.* **B197**, 423 (1987).

20. C. Bernard et al., *Phys. Rev.* **D38**, 3540 (1988).

    P. Boucard et al., *Phys. Lett.* **B220**, 219 (1989).

    T. Applequist et al., *Phys. Lett.* **B220**, 233 (1989).

    C.R. Allton et al., SHEP 89/90-11 (1990).

21. B. Gittelman, Invited talk at the 25th Int. Conf. on H.E.P., Singapore, August 1990.

22. F. Dydak, Invited talk at the 25th Int. Conf. on H.E.P., Singapore, August 1990.

3 Semileptonic Decays

Thrice happy he who, not mistook,
Hath read in Nature's mystic book.

Andrew Marvell, 1621-1678

3.1 Introduction

Nearly all hadrons are unstable and can, in general, decay via strong, weak or electromagnetic interactions. Since hadrons are composed of quarks (and gluons) there is considerable theoretical difficulty in calculating precise predictions for these decays, because of the non-perturbative nature of QCD at low energies, as discussed in section 1.2.

In order to allow the most precise tests of the standard model it is necessary to reduce the non-perturbative element of the calculation to a minimum. To this end it is simplest to study semileptonic decays. These are a type of weak decay mediated by virtual W bosons and are described by the charged-current interaction of (1.9). At the quark level the decay is of the form

$$Q \rightarrow ql\nu, \tag{3.1}$$

involving one up-type and one down-type quark. The most well-known example of such a decay is nuclear β-decay, where the underlying process is $d \rightarrow ue\bar{\nu}$.

Such decays are simplest from a theoretical standpoint because the decay $W^* \rightarrow l\nu$ is well understood (since it does not involve QCD). From the experimental side the emitted lepton is easy to detect, but the neutrino momentum must be inferred from the other particles if required, as it cannot be seen.

Following the discussion of the KM matrix in chapter 1, we saw that it is the analysis of such decays that is most often used to determine the moduli of the KM matrix elements.

3.2 Four-Fermion Interactions

The semileptonic decay (3.1) involves two charged-current interactions (dis-

cussed in section 1.3),

$$Q \to qW^* \qquad \text{and} \qquad W^* \to l\nu. \tag{3.2}$$

At energies much less than the W mass, it is possible to combine the two inter-
actions into an effective four-fermion interaction term. For the $b \to c l \bar{\nu}$ case this
effective interaction is

$$\mathcal{L}_{eff} = -\frac{G_F}{\sqrt{2}} V_{cb} \overline{\psi}_c \gamma^\mu (1 - \gamma_5) \psi_b \overline{\psi}_\nu \gamma_\mu (1 - \gamma_5) \psi_l, \tag{3.3}$$

where $G_F/\sqrt{2} = g^2/8m_W^2$ and G_F is the Fermi coupling constant. The corrections
to this interaction are of order $m_b m_l / m_W^2$.

3.3 Quarks and Hadrons

At the quark level the above decays (3.1) seem very simple. However, in nature
quarks are always bound inside hadrons, and it is the description of this that causes
problems.

As explained in section 1.2 it is expected that simple perturbative quark-model
calculations become more reliable as the mass of the quarks increase. For a decay
in which both initial and final quarks are 'heavy', such as those with an underlying
$b \to c$ transition, we expect reasonable results from such a calculation.

For decays where both initial and final quarks are light, such as $s \to u$ and
$d \to u$ decays, we can use the low-energy techniques that have been developed, for
instance in the study of nuclear β-decay.

However, if the decay involves one heavy quark and one light quark, such as
in $b \to u$ and $c \to s$ transitions, it is very hard to predict the hadronic behaviour,
as no reliable techniques have yet been developed for this purpose. It is noticeable
that $D \to K, K^* l \nu$ decays are less well understood than $B \to D, D^* l \nu$ decays for
this reason.

3.4 Methods of Studying Semileptonic Decays

Theoretical studies of semileptonic decays can be divided into two main strate-
gies; either considering all semileptonic decays simultaneously (inclusive), or choos-

ing particular decay channels (exclusive). Since the following chapters are predominantly concerned with B meson decays, we will use them to illustrate the important points. Experimental considerations are discussed in section 3.5 below.

3.4.1 Inclusive Semileptonic Decays

A study of inclusive semileptonic decays includes all processes of the form $B \to X l \nu$, where X can be anything. By detecting the leptons emitted in the decay one can measure the lepton energy spectrum, as shown by the CLEO data in fig.3.1. Unfortunately, the detected leptons are not all produced by semileptonic B decays (called 'primary decays'). Many are from 'secondary' decays, where the B meson decays hadronically, and one of its decay products then decays semileptonically. In order to remove the contribution from such decays, it would be necessary to reconstruct every decay to see how the lepton was produced, so greatly reducing the accuracy of the resulting spectrum. To overcome this problem two strategies are adopted. Firstly, leptons from secondary decays give little contribution above about $1.5\,GeV$ so predictions for the inclusive spectrum can be fitted to the data above this energy. The second method, attempted recently by the CLEO collaboration [1], is to try to predict the secondary decay spectrum by combining the measured D meson momentum spectrum with a theoretical prediction for the D meson's semileptonic decay spectrum, allowing a combined fit of both primary and secondary decays over the whole lepton energy range. Both methods give very similar results. Once a fit has been made, the normalisation of the experimental data gives a prediction for the KM matrix element $|V_{cb}|$, since the $b \to u$ contribution is expected to be very small.

The traditional method used to predict the primary lepton spectrum for inclusive decays is the method introduced by Altarelli et al. [2], based on a perturbative b quark decay calculation, discussed in detail in chapter 7. This technique suffers from some severe drawbacks, as emphasised by Isgur et al. [3]. Semileptonic B decays are dominated by the two exclusive channels $B \to D$ and $B \to D^*$, which means that a purely perturbative calculation, such as that outlined above, cannot possibly reproduce the correct invariant-mass spectrum $d\Gamma/dm_X$, which should exhibit sharp peaks at $m_X = m_D, m_{D^*}$. Furthermore, since the high lepton energy region is dominated by low-mass final states, it is actually the D and D^*
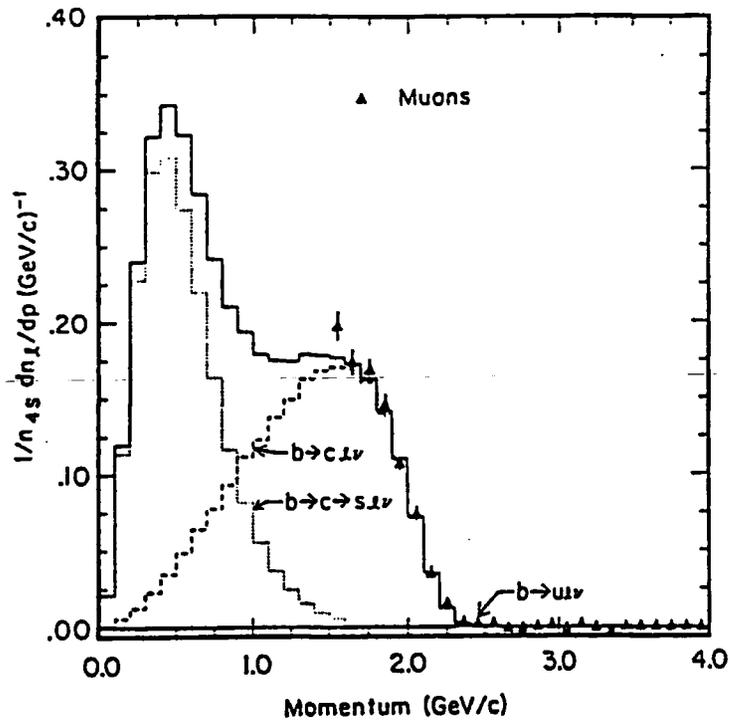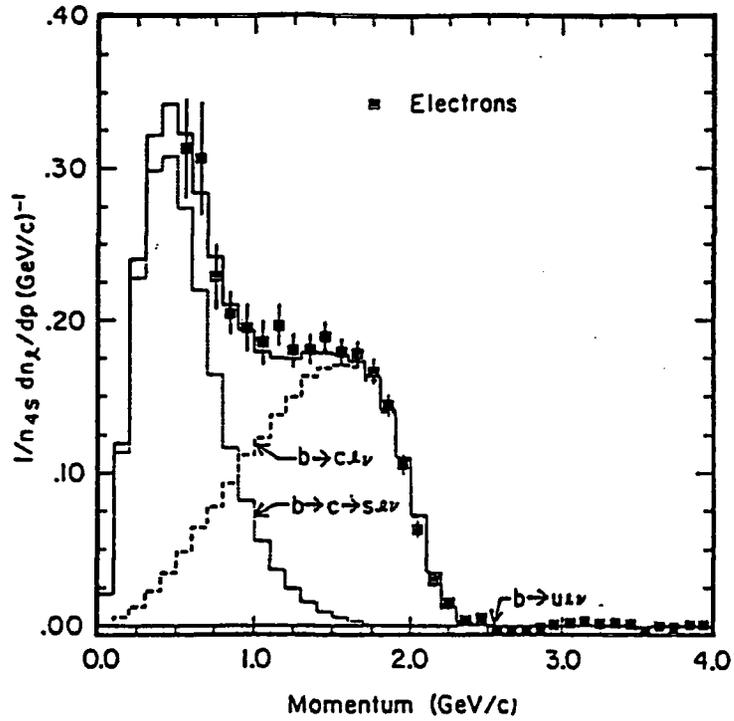
Figure 3.1 Inclusive electron and muon energy spectra from CLEO [1], after continuum subtraction. The dashed and dotted lines show the CLEO fits for the primary and secondary lepton spectra respectively, while the solid line shows the combined total.

channels that have the greatest effect on the endpoint region where the fitting is performed, making the prediction unreliable. For the $b \to u$ decay channel we do not expect the corresponding exclusive channels to be so dominant, so it is hoped that this inclusive approach would be more reasonable.

3.4.2 Exclusive Semileptonic Decays

Many authors choose to use an exclusive approach, whereby the specific final states are built into the model (see chapters 4 to 6). This immediately solves the main problem of the above inclusive analysis, which was is its inability to predict the D and D^* exclusive channels. From an experimental point of view the data is more difficult to extract, since it is necessary to reconstruct the decay completely in order to detect the outgoing meson, so less data is available for the analysis.

Theoretically there is only one significant problem, which is that we need to know the matrix elements of the quark charged-current of (1.10) between initial and final meson states. Although not directly calculable it is possible to estimate these hadronic matrix elements, and, more importantly, to test the hypotheses, as described in chapter 5 and 6.

Theoretical predictions of $B \to Dl\nu$ and $B \to D^*l\nu$ are nearly all in good agreement, both with each other and with the experimental data. Predictions for $B \to \pi l\nu$ and $B \to \rho l\nu$ are considerably less consistent, for the reasons outlined in section 3.3.

3.5 Experimental Data

The most accurate experimental measurements of B meson decays are made by the CLEO collaboration, using the Cornell Electron Storage Ring (CESR) at Cornell University, New York, and by the ARGUS collaboration, using the DORIS II storage ring at DESY, in Hamburg. Both experiments operate on the $\Upsilon(4S)$ resonance, which is just above the threshold for producing $B\overline{B}$ pairs. Since $m_{\Upsilon(4S)} \approx 10.58\,GeV$ and $m_B \approx 5.28\,GeV$, the B mesons are produced almost, but not exactly at rest ($|\mathbf{p}_B| \approx 0.33\,GeV$). Data taken just below the $B\overline{B}$ threshold is used to remove the continuum contribution from the data.

The data given below is restated in chapters 6 and 7, where it is compared to

the theoretical models. Before presenting the results, it is worthwhile to outline some of the other procedures and assumptions used by the experimentalists in their analyses.

3.5.1 Discussion of CLEO Experimental Data

The most recent CLEO analysis [4] has been done on a data sample with integrated luminosity of $212\,pb^{-1}$ on the $\Upsilon(4S)$ and $102\,pb^{-1}$ at an energy just below the $B\overline{B}$ threshold (the continuum data sample). This data sample contains about 480,000 B meson decays. The momentum resolution in the detector is given by $(\delta p/p)^2 = (0.23\%p)^2 + (0.7\%)^2$, which means the detector is accurate to better than 1% for $p \lesssim 2.5\,GeV$.

There are several problems with the data that will be outlined here, and which should be kept in mind in the following discussions. Firstly, it has conventionally been assumed that the $\Upsilon(4S)$ decays to $B\overline{B}$ pairs with very nearly 100% branching ratio. A recent analysis by the CLEO collaboration [5], however, indicates a significant rate for the decay $\Upsilon(4S) \rightarrow \psi X$. The measured branching ratio is $\text{Br}(\Upsilon(4S) \rightarrow \psi X) = (0.22 \pm 0.06 \pm 0.04)\%$ for ψ's with momenta greater than $2.0\,GeV$ (above the endpoint for the decay $B \rightarrow \psi X$). Since the branching ratio to lower energy ψ's is unknown it is not yet possible to determine $\text{Br}(\Upsilon(4S) \rightarrow B\overline{B})$. Furthermore, the ratio of charged to neutral $B\overline{B}$ pairs produced is also unknown, although the near-equality of masses, $|m_{B^0} - m_{B^\pm}| = 0.8 \pm 0.5\,MeV$ [6], indicates that this ratio should be close to unity (see, for instance, the coupled channel analysis of ref. [7]). The results are quoted below in terms of f_{+-} and f_{00}, the branching fractions of $\Upsilon(4S)$ to charged and neutral $B\overline{B}$ pairs respectively, relative to the values

$$f_{+-} = f_{00} = 0.5. \tag{3.4}$$

In order to analyse the inclusive lepton spectrum of fig.3.1 the whole spectrum is fitted by combining the primary decay spectrum predicted by the ACCMM [2] or ISGW [3] models (discussed in more detail in chapters 7 and 5 respectively), with the secondary decay spectrum predicted by folding the measured D meson momentum spectrum with the theoretical prediction for the lepton spectrum from D meson decay, after correcting for other possible sources of leptons. This can be done for both electron and muon spectra, both of which are well measured.

For the analysis of the exclusive decay channels a lower lepton energy cutoff at $E_l = 1.4\,GeV$ is used to suppress leptons which are not primary B decay products. Also D^+ momenta are required to be greater than $1.5\,GeV$, to reduce background contributions. The CLEO analysis uses the ISGW model to extrapolate into these cutoff regions when calculating branching ratios. Clearly a full analysis of any model requires that the model being tested should be used in the extrapolation, but the different models have very similar spectra shapes, so the above extrapolation can be used reliably for all the models.

Finally, we must remember that the spectra of fig.3.1 are for leptons in the laboratory frame. Since the exact direction of the B mesons in this frame is unknown, a full analysis should include an isotropic boost from the B rest-frame to the laboratory frame. Although the effect of this boost is small, it is noticeable at high lepton momenta. For the exclusive analysis it is safe to neglect this effect at present, due to the lack of precision in the data, but the more accurately measured inclusive lepton spectrum requires its inclusion.

3.5.2 CLEO Results

(i) The inclusive semileptonic lepton energy spectra [1] for electrons and muons are shown in fig.3.1.

(ii) The total semileptonic branching ratio, averaged over electrons and muons, and using the models described above, is [1]

$$
\begin{aligned}
\mathrm{Br}(\overline{B} \to Xl\nu) &= (10.4 \pm 0.1 \pm 0.2)\% \qquad \text{ACCMM} \\
\mathrm{Br}(B \to Xl\nu) &= (10.0 \pm 0.1 \pm 0.2)\% \qquad \text{ISGW}
\end{aligned}
\tag{3.5}
$$

(iii) The exclusive branching ratios, using the ISGW model, are [4]

$$
\begin{aligned}
\mathrm{Br}(B^- \to D^0 l^- \overline{\nu}) &= (1.6 \pm 0.6 \pm 0.3)\left(\frac{0.5}{f_{+-}}\right)\% \\
\mathrm{Br}(\overline{B^0} \to D^+ l^- \overline{\nu}) &= (1.8 \pm 0.6 \pm 0.3)\left(\frac{0.5}{f_{00}}\right)\% \\
\mathrm{Br}(B^- \to D^{*0} l^- \overline{\nu}) &= (4.1 \pm 0.8^{+0.8}_{-0.9})\left(\frac{0.5}{f_{+-}}\right)\% \\
\mathrm{Br}(\overline{B^0} \to D^{*+} l^- \overline{\nu}) &= (4.6 \pm 0.5 \pm 0.7)\left(\frac{0.5}{f_{00}}\right)\%
\end{aligned}
\tag{3.6}
$$

(iv) The vector to pseudoscalar (V/PS) ratio is

$$R \equiv \frac{\mathrm{Br}(B^- \to D^{*0}l^-\bar{\nu})}{\mathrm{Br}(B^- \to D^0l^-\bar{\nu})} = \frac{\mathrm{Br}(\overline{B^0} \to D^{*+}l^-\bar{\nu})}{\mathrm{Br}(\overline{B^0} \to D^+l^-\bar{\nu})}, \qquad (3.7)$$

where the latter equality follows from isospin symmetry, which predicts that

$$\begin{aligned} \Gamma(B^- \to D^0l^-\bar{\nu}) &= \Gamma(\overline{B^0} \to D^+l^-\bar{\nu}) \\ \Gamma(B^- \to D^{*0}l^-\bar{\nu}) &= \Gamma(\overline{B^0} \to D^{*+}l^-\bar{\nu}). \end{aligned} \qquad (3.8)$$

Note that R is independent of the $\Upsilon(4S)$ branching fractions f_{+-} and f_{00}. Averaging over the different meson charges, gives [4]

$$R = 2.6^{+1.1+1.0}_{-0.6-0.8} \qquad (3.9)$$

(v) CLEO has not published any exclusive E_l or q^2 spectra.

(vi) The angular distribution of the $D^* \to D\pi$ decay products is proportional to $1 + \alpha \cos^2\theta^*$, where θ^* is the angle betwwen the pion and the decaying B meson in the D^* rest-frame (see chapter 4 for further details). The most recent CLEO measurement is [8]

$$\alpha = 0.65 \pm 0.66 \pm 0.25 \qquad (3.10)$$

(vii) The ratio of charged to neutral B lifetimes is calculated from the exclusive rates given above using

$$\frac{\tau_{B^\pm}}{\tau_{B^0}} = \frac{\mathrm{Br}(B^- \to D^0l\bar{\nu})}{\mathrm{Br}(\overline{B^0} \to D^+l\bar{\nu})} = \frac{\mathrm{Br}(B^- \to D^{*0}l\bar{\nu})}{\mathrm{Br}(\overline{B^0} \to D^{*+}l\bar{\nu})}, \qquad (3.11)$$

again assuming isospin symmetry (3.8). Combining the branching ratios of (3.6) gives [4]

$$\frac{\tau_{B^\pm}}{\tau_{B^0}} = (0.89 \pm 0.19 \pm 0.13) \left(\frac{f_{00}}{f_{+-}}\right). \qquad (3.12)$$

3.5.3 Discussion of ARGUS Experimental Data

In general the ARGUS and CLEO experiments and problems are similar, so only the differences are outlined here.

54

ARGUS has now analysed data from about 150,000 $B\overline{B}$ pairs [9], correspond-ing to an integrated luminosity of $172\,pb^{-1}$ at the $\Upsilon(4S)$ resonance, with another $63\,pb^{-1}$ from below the $B\overline{B}$ threshold. The momentum resolution of the detector is $\delta p/p \approx 0.012\sqrt{1+p^2}$, where p is measured in GeV, which is just over 3% at $p = 2.5\,GeV$.

As above the results are quoted here relative to the charged and neutral branch-ing ratios $f_{+-} = f_{00} = 0.5$, although early ARGUS results used $f_{+-} = 0.55$ and $f_{00} = 0.45$. A lepton energy cutoff of $E_l \geq 1.0\,GeV$, and a momentum cut of $p_{D+} \geq 1.5\,GeV$ are included, as above. The ARGUS collaboration use the WSB model to extrapolate their results into the cutoff region, but again this model has very similar spectrum shapes to the other models.

3.5.4 ARGUS Results

(i) The inclusive lepton energy spectra for electrons and muons [10] are shown in fig.3.2.

(ii) The total semileptonic branching ratio, averaged over electrons and muons, and using the models described above, is [10]

$$\begin{aligned}
\mathrm{Br}(B \to Xl\nu) &= (10.2 \pm 0.5 \pm 0.2)\% \qquad \text{ACCMM} \\
\mathrm{Br}(B \to Xl\nu) &= (9.8 \pm 0.5)\% \qquad\qquad\ \ \text{ISGW}
\end{aligned} \tag{3.13}$$

(iii) The exclusive branching ratios [9], corrected by a more recently measured value of $\mathrm{Br}(D^{*-} \to D^0\pi^-)$ [11] are

$$\begin{aligned}
\mathrm{Br}(\overline{B^0} \to D^+l^-\overline{\nu}) &= (1.7 \pm 0.6 \pm 0.4)\left(\frac{0.5}{f_{00}}\right)\% \\
\mathrm{Br}(\overline{B^0} \to D^{*+}l^-\overline{\nu}) &= (5.4 \pm 0.9 \pm 1.3)\left(\frac{0.5}{f_{00}}\right)\%.
\end{aligned} \tag{3.14}$$

No results are yet published for $B^\pm$ decays.

(iv) The vector to pseudoscalar ratio [9] of (3.7) is

$$R = 3.3^{+3.7}_{-1.1}. \tag{3.15}$$

(v) Tha ARGUS E_l and q^2 spectra [12] for the decay $\overline{B} \to D^*l\overline{\nu}$ are shown later in figs.6.10(d) and 6.11(d) respectively.
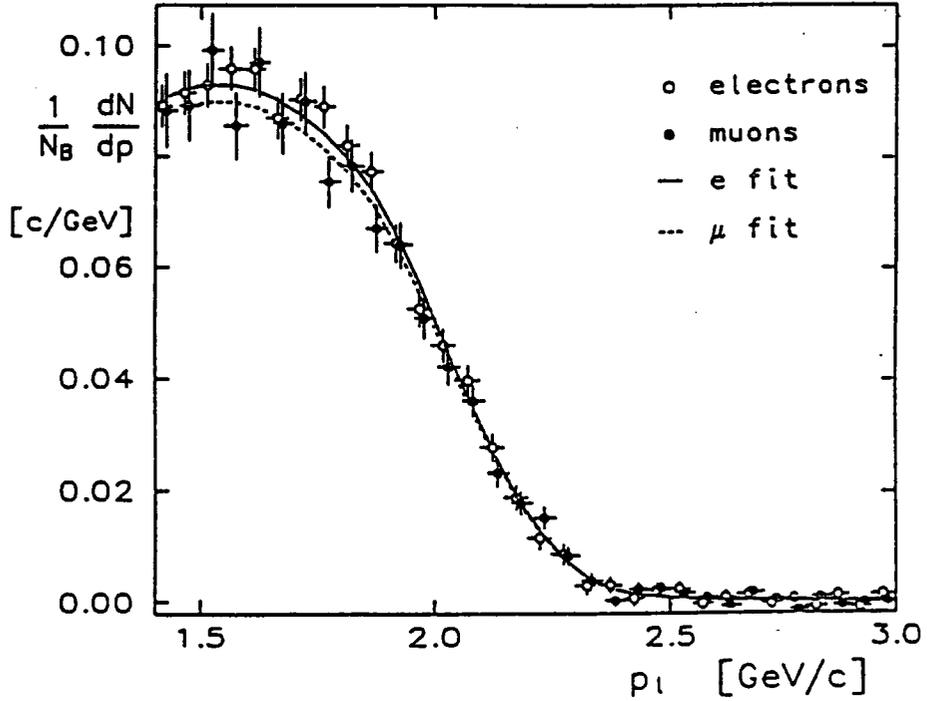
Figure 3.2 Inclusive electron and muon energy spectra from ARGUS, after continuum subtraction, for the region $E_l > 1.4 \, GeV$, where the secondary spectrum is expected to be small.

(vi) The D^* decay angular distribution parameter α is measured to be [12]

$$\alpha = 0.7 \pm 0.9. \tag{3.16}$$

(vii) The ratio of charged to neutral lifetimes, calculated by the same method as the CLEO collaboration above, is [11]

$$\frac{\tau_{B^\pm}}{\tau_{B^0}} = (1.00 \pm 0.23 \pm 0.14) \left(\frac{f_{00}}{f_{+-}} \right) \tag{3.17}$$

3.5.5 Charmless Semileptonic B Decays

The above experimental results are all concerned with $b \rightarrow c l \bar{\nu}$ decays. The detection of charmless decays is also of great theoretical importance. In order for the standard model to be able to describe CP violation it is vital that the KM

matrix element $|V_{ub}|$ be non-zero, as discussed in section 1.5, and discovery of such decays would prove this. While CLEO has not yet reported any completely reconstructed exclusive decays, the ARGUS collaboration has recently done so [13]. They have found two such events, one $\overline{B^0} \to \pi^+\mu^-\overline{\nu}$ and the other $B^- \to \omega^0\mu^-\overline{\nu}$.

Although the detection of these two events proves that $|V_{ub}| \neq 0$, it does not yet allow a precise determination of the magnitude of the KM matrix element. Eventually, when many more such decays are analysed, this will be possible. At the present time the best method to calculate $|V_{ub}|$ is by considering the inclusive lepton spectra of fig.3.1. The maximum lepton energy emitted by the charmed decay of a B meson is $2.31\,GeV$ in the B rest-frame (see chapter 4). After boosting to the laboratory frame, as discussed briefly in section 3.5.1, and in more detail in section 7.4, this becomes $2.47\,GeV$. For a charmless decay these become 2.64 and $2.82\,GeV$ respectively. After subtracting the continuum contribution and all known backgrounds from the observed lepton spectrum, any signal in the region $E_l > 2.47\,GeV$ is thus expected to be from charmless decays.

The analysis of $b \to u$ decays is carried out both by fitting to the measured lepton energy spectrum [10] and by comparing to the partial decay rate in particular energy ranges [14,15]. The second method gives smaller errors than the first, but cannot test the models, while the first method can. The measurements relevant to the second method are discussed below, while the results of the fit to the spectrum will be given in chapter 7.

Unfortunately CLEO has again performed a model-dependent analysis on their data [14], making the phenomenologist's job more difficult. They measure the number of events in two lepton anergy ranges,

$$\Delta_1 \equiv (2.2 - 2.4)\,GeV$$
$$\Delta_2 \equiv (2.4 - 2.6)\,GeV.$$

(3.18)

Events in the second region are expected to be almost entirely from $b \to u$ decays, as the tail produced by the above boost is very small. In order to calculate the $b \to u$ yield in the first region the $b \to c$ contribution is removed by fitting ACCMM and ISGW models to the spectrum in the region $1.5\,GeV \leq E_l \leq 2.2\,GeV$ and extrapolating up to $2.4\,GeV$. Combining their measurements with the total

semileptonic branching ratio (3.5) they obtain the partial branching fractions

$$Br_{sl}(b \rightarrow u, \Delta_1) = (1.5 \pm 0.7 \pm 0.7)\%$$
$$Br_{sl}(b \rightarrow u, \Delta_2) = (1.8 \pm 0.4 \pm 0.3)\%.$$

(3.19)

ARGUS considers the two lepton energy regions [15]

$$\Delta_a \equiv (2.0 - 2.3)\,GeV$$
$$\Delta_b \equiv (2.3 - 2.6)\,GeV,$$

(3.20)

where the first region is expected to be dominated by $b \rightarrow c$ decays. The result is quoted in the form

$$\frac{Br_{sl}(\Delta_b)}{Br_{sl}(\Delta_a)} = (4.7 \pm 1.2)\%.$$

(3.21)

By using models for $b \rightarrow c$ and $b \rightarrow u$ together in the above two regions it is possible to extract a prediction for the ratio $|V_{ub}|/|V_{cb}|$.

The analysis of these measurements is given in chapters 6 and 7.

References

1. Y. Kubota, private communication concerning CLEO preprint, in preparation.

2. G. Altarelli, N. Cabibbo, G. Corbo, L. Maiani and G. Martinelli, *Nucl. Phys.* **B208**, 365 (1982).

3. N. Isgur, D. Scora, B. Grinstein and M.B. Wise, *Phys. Rev.* **D39**, 799 (1989).

4. R. Fulton et al., CLNS 90/989 (August 1990).

5. R. Fulton et al., *Phys. Rev. Lett.* **64**, 2226 (1990).

6. D.L. Kreinick, in *Proceedings of the 14th Lepton-Photon Symposium, Stanford, California, August 7-12, 1989.*

7. A.D. Martin and C.-K. Ng, *Z. Phys.* **C40**, 133 (1988).

8. D. Bortoletto et al., *Phys. Rev. Lett.* **63**, 1667 (1989).

9. H. Albrecht et al., *Phys. Lett.* **B229**, 175 (1989).

10. H. Albrecht et al., DESY 90-088 (July 1990).

11. M. Danilov, DESY 89-147 (November 1989).

12. H. Albrecht et al., *Phys. Lett.* **B219**, 121 (1989).

13. H. Schröder, in *DESY Journal 2-90* p. 3 (1990).

14. R. Fulton et al., *Phys. Rev. Lett.* **64**, 16 (1990).

15. H. Albrecht et al., *Phys. Lett.* **B234**, 409 (1990).

4 Form-Factor Description of Semileptonic $\overline{B}$ Decays

A beauty masked, like the sun in eclipse,
Gathers together more gazers than if it shined out.

<div align="right">William Wycherley, 1640?-1716</div>

4.1 Introduction

This chapter is devoted to the derivation of the formalism for exclusive semileptonic $\overline{B} \to Ml\overline{\nu}$ decays, where $M = D, D^*$. The changes required to extend the formalism to other decays will be discussed briefly in section 4.10.

4.2 Kinematics

The schematic diagram, fig.4.1, shows the decay $\overline{B} \to MW^* \to Ml\overline{\nu}$. The four-momentum of the virtual W boson is

$$q = p_B - p_M = p_l + p_\nu. \tag{4.1}$$

All distributions can be calculated as functions of two variables, which will be taken to be either q^2 and $x \equiv p_l.p_B/m_B^2$, or q^2 and $\cos\theta_l$, the lepton angle in the W^* rest-frame.

The virtual W can be either spin-1, with helicities $\lambda_W = \pm1, 0$, or spin-0, with helicity $\lambda_W = s$ (here a scalar W^* is given a helicity s to distinguish it from the other zero-helicity state). The M-meson is taken to be either a spin-0 D-meson, with $\lambda_M = s$, or a spin-1 D^*-meson, with $\lambda_M = \pm1, 0$. By conservation of angular momentum $\lambda_W = \lambda_M$, since the initial $\overline{B}$-meson is spin-0 (note that 's=0' is of course included here). Finally, the massless antineutrino has $\lambda_\nu = +\frac{1}{2}$, and the charged lepton has $\lambda_l = \pm\frac{1}{2}$ (or $\lambda_l = -\frac{1}{2}$ only, if it is massless). For decays to electrons and muons we can safely neglect the effect of the lepton mass, but for decays to τ leptons the mass must be included.

Although most of the results will be expressed in a frame-independent manner it is convenient to choose a frame for calculational purposes. The two frames that will be used to evaluate the matrix elements are the W^* and $\overline{B}$ rest-frames. In both cases the M-meson is taken to move along the positive z-axis, with the

<div align="center">60</div>
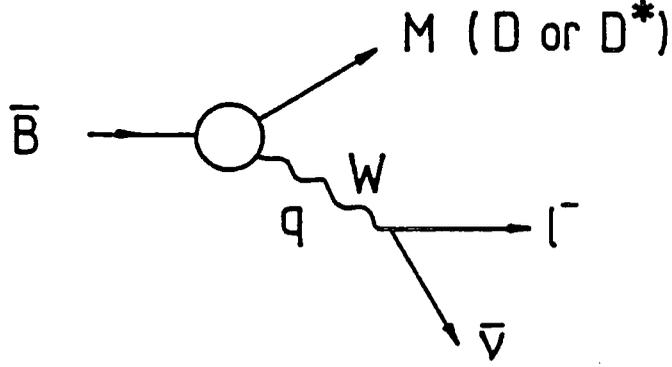
Figure 4.1 The exclusive semileptonic decay $\overline{B} \to M l \overline{\nu}$.

charged lepton in the x-z plane with positive momentum in the x-direction, as shown in fig.4.2. The two frames are related by a simple boost along the z-axis. Note that the helicity of the W^* can be chosen to be unaffected by this boost, as the direction of the W^* is not reversed.

4.2.1 The W^* Rest-Frame

The 4-momenta required in the W^* rest-frame of fig.4.2(a) are

$$
\begin{aligned}
p_B^\mu &= (E_B, 0, 0, p_B), \\
q^\mu &= (\sqrt{q^2}, 0, 0, 0), \\
p_l^\mu &= \frac{q^2 - m_l^2}{2\sqrt{q^2}}\left(\frac{q^2 + m_l^2}{q^2 - m_l^2}, \sin\theta_l, 0, \cos\theta_l\right), \\
p_\nu^\mu &= \frac{q^2 - m_l^2}{2\sqrt{q^2}}(1, -\sin\theta_l, 0, -\cos\theta_l),
\end{aligned}
\tag{4.2}
$$

where $0 \leq \theta_l \leq \pi$, and, using (4.1),

$$
\begin{aligned}
2\sqrt{q^2}E_B &= m_B^2 - m_M^2 + q^2, \\
2\sqrt{q^2}p_B &= \sqrt{Q_+ Q_-},
\end{aligned}
\tag{4.3}
$$

with

$$
Q_\pm = (m_B \pm m_M)^2 - q^2.
\tag{4.4}
$$

Note that

$$
Q_+ Q_- = \lambda(m_B^2, m_M^2, q^2),
\tag{4.5}
$$

61

(a) W^* rest frame   **(b) $\bar{B}$ rest frame**
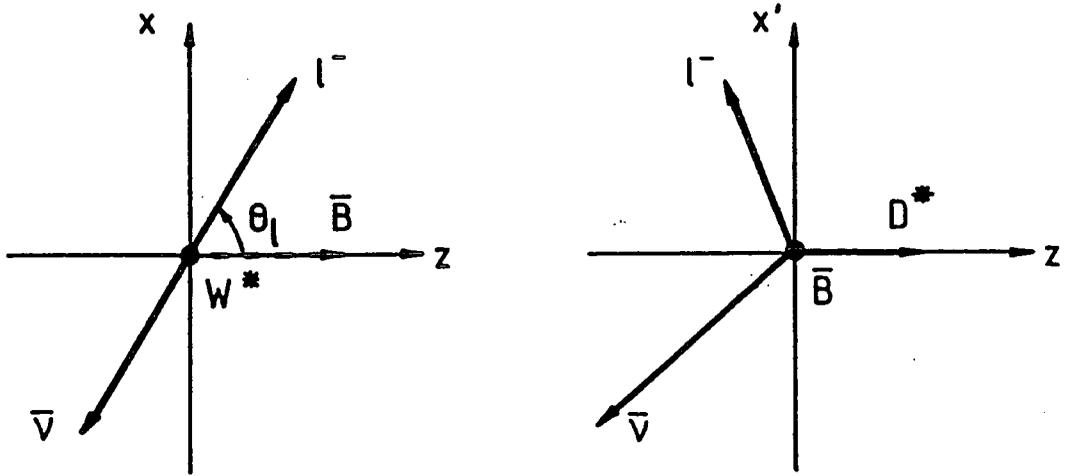
Figure 4.2   The W^* and $\bar{B}$ rest-frames used for the calculation of the matrix elements and the phase-space factor.

the well-known triangle function $\lambda(a, b, c) = a^2 + b^2 + c^2 - 2(ab + bc + ca)$.

In this frame we can write, using (4.2), the invariant variable,

$$x \equiv \frac{p_l \cdot p_B}{m_B^2} = \frac{(m_B^2 - m_M^2 + q^2)(q^2 + m_l^2) - \sqrt{Q_+ Q_-}(q^2 - m_l^2)\cos\theta_l}{4m_B^2 q^2}. \qquad (4.6)$$

4.2.2 The $\bar{B}$ Rest-Frame

The 4-momenta required in the $\bar{B}$ rest-frame of fig.4.2(b) are

$$
\begin{aligned}
p_B^\mu &= (m_B, 0, 0, 0), \\
p_M^\mu &= (E_M, 0, 0, p_M), \\
q^\mu &= (q^0, 0, 0, -p_M), \\
p_l^\mu &= (E_l, p_l \sin\psi_l, 0, p_l \cos\psi_l), \\
p_\nu^\mu &= (p_\nu, -p_\nu \sin\psi_\nu, 0, p_\nu \cos\psi_\nu),
\end{aligned}
\qquad (4.7)
$$

where, again using (4.1),

$$
\begin{aligned}
2m_B E_M &= m_B^2 + m_M^2 - q^2, \\
2m_B p_M &= \sqrt{Q_+ Q_-}, \\
2m_B q^0 &= m_B^2 - m_M^2 + q^2.
\end{aligned}
\qquad (4.8)
$$

In this frame the variable x is proportional to the lepton energy,

$$x \equiv \frac{p_B \cdot p_l}{m_B^2} = \frac{E_l}{m_B}. \tag{4.9}$$

Finally, the leptonic variables are given by

$$p_\nu = q^0 - E_l,$$
$$\cos \psi_l = \frac{q^2 + m_l^2 - 2q^0 E_l}{2 p_M p_l}, \tag{4.10}$$
$$\cos \psi_\nu = \frac{q^2 - m_l^2 - 2q^0 p_\nu}{2 p_M p_\nu},$$

which can be expressed in terms of invariants by using (4.8) and (4.9).

4.3 Allowed Kinematic Region

The available phase-space is given simply in the W^* rest-frame by

$$m_l^2 \leq q^2 \leq (m_B - m_M)^2,$$
$$-1 \leq \cos \theta_l \leq 1. \tag{4.11}$$

These constraints can be rewritten in terms of the invariants q^2 and x using (4.6), and the boundary of the physical region is

$$(1 + b^2 - 2x) \left(\frac{q^2}{m_B^2} \right)^2 - 2(a^2 b^2 - a^2 x + b^2 x + x - 2x^2) \frac{q^2}{m_B^2} \tag{4.12}$$
$$+ b^2(-2a^2 + 2a^2 x + a^4 + 1 - 2x + b^2) = 0,$$

where the constants a and b are

$$a \equiv \frac{m_M}{m_B} \qquad b \equiv \frac{m_l}{m_B}. \tag{4.13}$$

The formula simplifies considerably in the case of massless leptons, reducing to

$$(1 - 2x)q^2 + 2x(a^2 - 1 + 2x) = 0 \qquad \text{or} \qquad q^2 = 0. \tag{4.14}$$

The regions are shown in fig.4.3 for $M = D$ and $l = e, \mu, \tau$ (the results for $M = D^*$
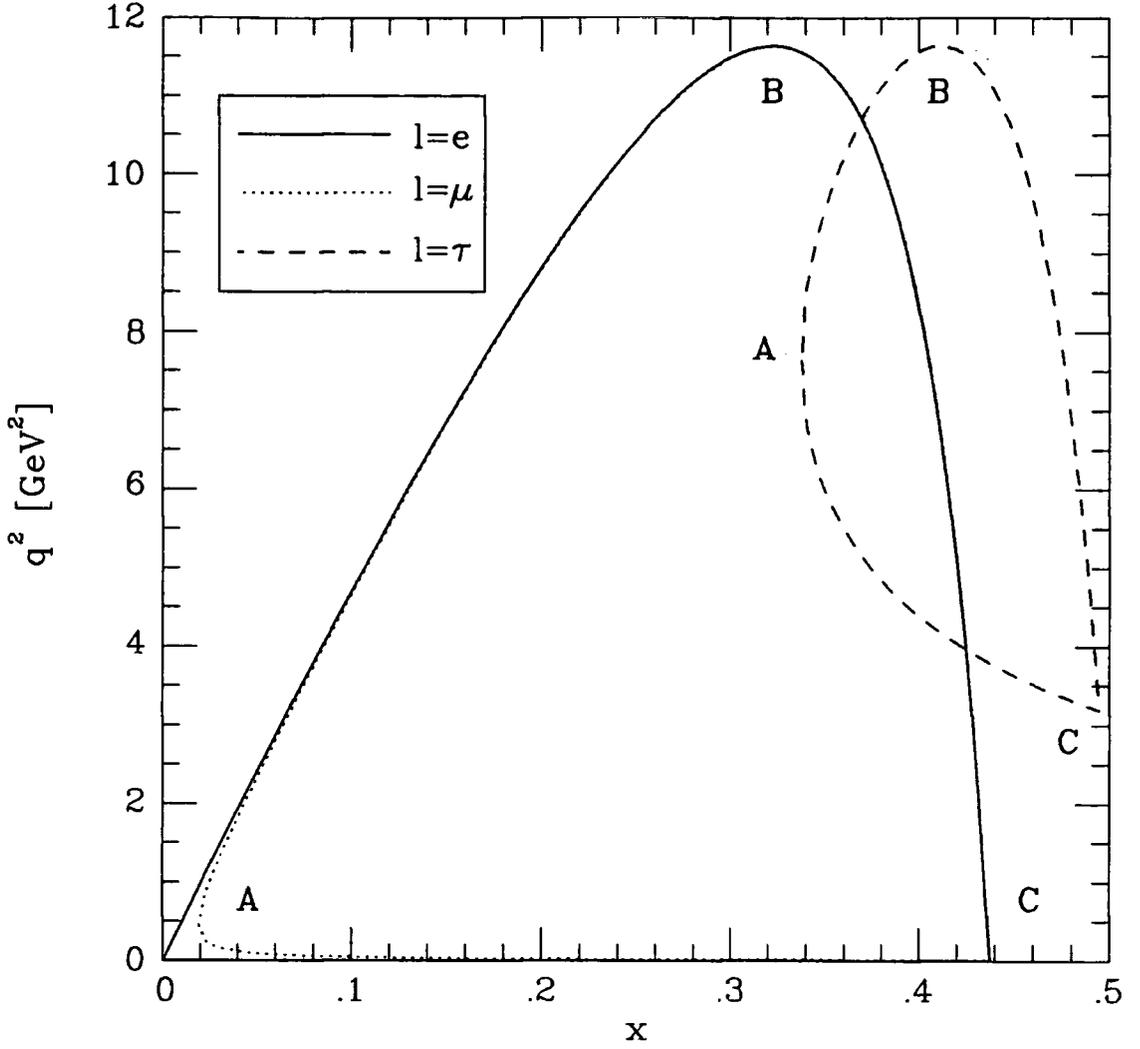
Figure 4.3   The boundaries of the physical region (Dalitz plot) in the (x, q^2) plane for the decay $\overline{B} \to Dl\overline{\nu}$ for the three lepton types. The coordinates of the points A, B and C are given in the text.

are very similar). The coordinates (x, q^2) of the three 'corners', A, B & C, are

$$A : \left(b, \frac{b(1-b-a^2)}{1-b} m_B^2 \right)$$

$$B : \left(\frac{(1-a)^2 + b^2}{2(1-a)}, (1-a)^2 m_B^2 \right) \qquad (4.15)$$

$$C : \left(\frac{1}{2}(1 - a^2 + b^2), b^2 m_B^2 \right).$$

4.4 Matrix Elements for the Decay $\overline{B} \to Ml\overline{\nu}$

The effective Lagrangian for the decay $\overline{B} \to Ml\overline{\nu}$ is given by the four-fermion interaction term

$$\mathcal{L}_{eff} = -\frac{G_F}{\sqrt{2}} V_{cb} J_{\nu l}^{\dagger\mu} J_{cb\mu} + \text{h.c.}, \tag{4.16}$$

as discussed in section 3.2. The two charged currents are defined by (see (1.10))

$$J_{\nu l}^\mu \equiv \overline{\psi}_\nu \gamma^\mu (1 - \gamma_5) \psi_l \qquad \text{and} \qquad J_{cb}^\mu \equiv \overline{\psi}_c \gamma^\mu (1 - \gamma_5) \psi_b. \tag{4.17}$$

The matrix element for the decay to a meson of helicity λ_M and a charged lepton of helicity λ_l is thus

$$\mathcal{M}_{\lambda_M}^{\lambda_l}(x, q^2) = -\frac{G_F}{\sqrt{2}} V_{cb} \langle l^-(p_l, \lambda_l) \overline{\nu}(p_\nu) | J_{\nu l}^{\dagger\mu} | 0 \rangle \langle M(p_M, \lambda_M) | J_{cb\mu} | \overline{B}(p_B) \rangle. \tag{4.18}$$

The matrix element can be written in terms of helicity amplitudes by rewriting the metric tensor in terms of the polarisation vectors of the W^*, $\epsilon_W \equiv \epsilon(q, \lambda_W)$,

$$-g^{\mu\nu} = \sum_{\lambda_W} \eta_{\lambda_W} \epsilon_W^\mu \epsilon_W^{*\nu}, \tag{4.19}$$

where the summation is over the helicity of the virtual W, $\lambda_W = \pm 1, 0, s$ with the metric $\eta_\pm = \eta_0 = -\eta_s = 1$.

The matrix element can now be written as

$$\mathcal{M}_{\lambda_M}^{\lambda_l}(x, q^2) = \frac{G_F}{\sqrt{2}} V_{cb} \sum_{\lambda_W} \eta_{\lambda_W} L_{\lambda_W}^{\lambda_l} H_{\lambda_W}^{\lambda_M}, \tag{4.20}$$

where the hadronic amplitude

$$H_{\lambda_W}^{\lambda_M}(q^2) \equiv \epsilon_{W\mu}^* \langle M(p_M, \lambda_M) | J_{cb}^\mu | \overline{B}(p_B) \rangle \tag{4.21}$$

and the leptonic amplitude

$$L_{\lambda_W}^{\lambda_l}(x, q^2) \equiv \epsilon_{W\mu} \langle l^-(p_l, \lambda_l) \overline{\nu}(p_\nu) | J_{\nu l}^{\dagger\mu} | 0 \rangle, \tag{4.22}$$

describe the decays $\overline{B} \to MW^*$ and $W^* \to l\overline{\nu}$ respectively. Because H and L are Lorentz scalars they can be evaluated in different frames, provided that the W^* helicity is defined to be the same in both frames.

4.5 Differential Decay Distributions

The rate for the decay $\overline{B} \to M(\lambda_M)l(\lambda_l)\overline{\nu}$ is

$$d\Gamma_{\lambda_M}^{\lambda_l} = \frac{1}{2m_B} \left| \mathcal{M}_{\lambda_M}^{\lambda_l} \right|^2 d\Phi_3. \tag{4.23}$$

The Lorentz-invariant three-body phase-space factor $d\Phi_3$ is most conveniently evaluated in the $\overline{B}$ rest-frame of section 4.2.2. In general it is given by

$$d\Phi_3 = d\tilde{p}_M \, d\tilde{p}_l \, d\tilde{p}_\nu \, (2\pi)^4 \delta^4(p_B - p_M - p_l - p_\nu), \tag{4.24}$$

where the invariant measure is defined to be

$$d\tilde{p} \equiv \frac{1}{(2\pi)^3} \frac{d^3 p}{2E} \tag{4.25}$$

$$= \frac{1}{(2\pi)^3} \frac{p^2}{2E} dp \, d\cos\theta \, d\phi \tag{4.26}$$

$$= \frac{1}{(2\pi)^3} d^4 p \, \delta(p^2 - m^2)\theta(p^0). \tag{4.27}$$

To evaluate (4.24), (4.26) is used for the M and l integrals, and (4.27) for the $\overline{\nu}$ integral. Noting that $\theta(p_\nu^0) = 1$, and that the argument of the remaining δ-function is

$$p_\nu^2 = (q - p_l)^2 = q^2 + m_l^2 - 2x m_B^2 + 2(E_M E_l - p_M p_l \cos\psi_l), \tag{4.28}$$

the phase space factor can be written

$$d\Phi_3 = \frac{1}{4} \frac{1}{(2\pi)^3} \frac{p_l}{E_l} \frac{p_M}{E_M} dp_l dp_M. \tag{4.29}$$

Now, using (4.8) and (4.9), this can be re-expressed in terms of the invariants q^2 and x as

$$d\Phi_3 = \frac{1}{64\pi^3} dq^2 \, dx, \tag{4.30}$$

or, using (4.6), as

$$d\Phi_3 = \frac{(q^2 - m_l^2)\sqrt{Q_+ Q_-}}{256\pi^3 m_B^2 q^2} dq^2 \, d\cos\theta_l \tag{4.31}$$

in terms of the lepton angle in the virtual W rest-frame. The latter expression is convenient in Monte-Carlo generation of events.

4.6 Polarisation Vectors

For a spin-1 particle with 4-momentum $p^\mu = (E, p_x, p_y, p_z)$ the polarisation vectors can be chosen to be [1]

$$
\begin{aligned}
\epsilon(p,1)^\mu &= \frac{1}{|\mathbf{p}|p_T}(0, p_x p_z, p_y p_z, -p_T^2), \\
\epsilon(p,2)^\mu &= \frac{1}{p_T}(0, -p_y, p_x, 0), \\
\epsilon(p,0)^\mu &= \frac{E}{|\mathbf{p}|\sqrt{p^2}}(\frac{\mathbf{p}^2}{E}, p_x, p_y, p_z), \\
\epsilon(p,s)^\mu &= \frac{1}{\sqrt{p^2}}p^\mu = \frac{1}{\sqrt{p^2}}(E, p_x, p_y, p_z),
\end{aligned}
\tag{4.32}
$$

where

$$
p_T \equiv \sqrt{p_x^2 + p_y^2}.
\tag{4.33}
$$

The transverse polarisation vectors are

$$
\epsilon(p,\pm)^\mu = \frac{1}{\sqrt{2}}(\mp\epsilon(p,1)^\mu - i\epsilon(p,2)^\mu).
\tag{4.34}
$$

Note that these satisfy (4.19), as any definition of polarisation vectors must. For particles moving along the z-axis, we need to consider the limit $p_x, p_y \to 0$, which is not unique. In order to recover the usual forms for a particle moving in the positive z-direction,

$$
\epsilon(p,\pm)^\mu = \mp\frac{1}{\sqrt{2}}(0, 1, \pm i, 0), \qquad \text{`}
\tag{4.35}
$$

one takes the limit $p_y = 0$ and $p_x \to 0^-$, and hence for a particle moving in the opposite direction one must use $p_y = 0$ and $p_x \to 0^+$.

4.6.1 Polarisation Vectors in the W^* Rest-Frame

Since only the leptonic matrix elements will be evaluated in this frame the only polarisation vectors needed are those of the W^*, which, using the definitions

of (4.32)-(4.34), are simply

$$\epsilon(q,\pm)^\mu = \mp\frac{1}{\sqrt{2}}(0,1,\mp i,0),$$

$$\epsilon(q,0)^\mu = (0,0,0,-1), \tag{4.36}$$

$$\epsilon(q,s)^\mu = \frac{1}{\sqrt{q^2}}q^\mu = (1,0,0,0).$$

4.6.2 Polarisation Vectors in the $\overline{B}$ Rest-Frame

Using the four-momenta defined in (4.7) and (4.32)-(4.34), the polarisation vectors for the W^*, moving along the negative z-axis, are

$$\epsilon(q,\pm)^\mu = \mp\frac{1}{\sqrt{2}}(0,1,\mp i,0),$$

$$\epsilon(q,0)^\mu = \frac{1}{\sqrt{q^2}}(p_M,0,0,-q^0), \tag{4.37}$$

$$\epsilon(q,s)^\mu = \frac{1}{\sqrt{q^2}}q^\mu = \frac{1}{\sqrt{q^2}}(q^0,0,0,-p_M),$$

and for the D^* meson, moving along the positive z-axis, are

$$\epsilon(p_M,\pm)^\mu = \mp\frac{1}{\sqrt{2}}(0,1,\pm i,0),$$

$$\epsilon(p_M,0)^\mu = \frac{1}{m_M}(p_M,0,0,E_M). \tag{4.38}$$

The polarisation vector for the D meson (helicity $\lambda_M = s$) is proportional to its 4-momentum (see (4.32)), and so is not explicitly required.

4.7 Two-Component Spinor Notation

It is most convenient to evaluate the Leptonic and Hadronic matrix elements of (4.20) using the chiral representation of the Dirac γ-matrices [2]:

$$\gamma^\mu = \begin{pmatrix} 0 & \sigma_+^\mu \\ \sigma_-^\mu & 0 \end{pmatrix}, \qquad \gamma^5 = \begin{pmatrix} -1 & 0 \\ 0 & 1 \end{pmatrix}, \tag{4.39}$$

where

$$\sigma_\pm^\mu \equiv (1,\pm\sigma_i), \tag{4.40}$$

and σ_i are the usual Pauli matrices. For the Dirac spinors we use a convention based on that of ref. [2], but adapted so that the spinors satisfy the usual parity

transformation properties [3],

$$\gamma^0 u(p, \lambda) \equiv u(\tilde{p}, -\lambda)$$
$$\gamma^0 v(p, \lambda) \equiv -v(\tilde{p}, -\lambda),$$

(4.41)

where

$$p^\mu \equiv (E, p \sin\theta \cos\phi, p \sin\theta \sin\phi, p \cos\theta) \equiv \tilde{p}_\mu$$

(4.42)

(with $0 \le \theta \le \pi$ and $0 \le \phi < 2\pi$), and λ is the sign of the particle's helicity. The four-component spinors are written

$$u(p, \lambda) \equiv \begin{pmatrix} u(p, \lambda)_- \\ u(p, \lambda)_+ \end{pmatrix}, \qquad v(p, \lambda) \equiv \begin{pmatrix} v(p, \lambda)_- \\ v(p, \lambda)_+ \end{pmatrix},$$

(4.43)

where the two-component spinors are

$$u(p, \lambda)_\pm \equiv \omega(p)_{\pm\lambda} \chi(p)_\lambda, \qquad v(p, \lambda)_\pm \equiv \pm\omega(p)_{\mp\lambda} \phi(p)_\lambda,$$

(4.44)

in terms of the chirality conserving/flipping factors

$$\omega(p)_\pm \equiv \sqrt{E \pm p},$$

(4.45)

and the helicity eigenspinors

$$\chi(p)_+ = \begin{pmatrix} \cos\frac{1}{2}\theta e^{-i\phi} \\ \sin\frac{1}{2}\theta \end{pmatrix} \qquad \phi(p)_+ = \begin{pmatrix} \sin\frac{1}{2}\theta \\ -\cos\frac{1}{2}\theta e^{i\phi} \end{pmatrix}$$
$$\chi(p)_- = \begin{pmatrix} -\sin\frac{1}{2}\theta e^{-i\phi} \\ \cos\frac{1}{2}\theta \end{pmatrix} \qquad \phi(p)_- = \begin{pmatrix} \cos\frac{1}{2}\theta \\ \sin\frac{1}{2}\theta e^{i\phi} \end{pmatrix},$$

(4.46)

for particles (χ) and antiparticles (ϕ).

The reason for defining spinors that satisfy the properties (4.41) is that the fermion annihilation and creation operators then obey simple parity transformation laws [3], such as

$$P a_\lambda(p) P^\dagger = \eta_P a_{-\lambda}(\tilde{p}),$$

(4.47)

with η_P the particle's parity. Under the original spinor conventions of ref. [2], there would be an additional phase factor, depending upon the azimuthal angle ϕ

of (4.42). When defining mesons of definite parity in the quark model, as will be required for $\overline{B}$, D and D^* states, the simple properties of (4.41) are much easier to work with. This mainly results from the fact that, with these conventions,

$$\chi(p)_\lambda = \chi(\tilde{p})_{-\lambda} \qquad \phi(p)_\lambda = \phi(\tilde{p})_{-\lambda}, \tag{4.48}$$

and so, in the $|\mathbf{p}| \to 0$ limit, fermions with opposite directions of motion and opposite helicities have equal spinors, which is not the case for the spinors of ref. [2] which were originally used in ref. [4].

4.8 Leptonic Amplitudes

The leptonic amplitudes for $W \to l\overline{\nu}$ decays, (4.22),

$$L_{\lambda_W}^{\lambda_l}(x, q^2) = \epsilon_{W\mu}(q, \lambda_W)\langle l(p_l, \lambda_l)\overline{\nu}(p_\nu)|J_{\nu l}^{\mu\dagger}|0\rangle, \tag{4.49}$$

can be calculated in any frame, provided that λ_W is defined to be the same as it is in the hadronic amplitudes discussed below. Using the two-component spinor notation (4.39)-(4.44) the matrix element can be written

$$
\begin{aligned}
\langle l(p_l, \lambda_l)\overline{\nu}(p_\nu)|J_{\nu l}^{\mu\dagger}|0\rangle &= \overline{u}(p_l, \lambda_l)\gamma^\mu(1 - \gamma^5)v(p_\nu, +) \\
&= 2u(p_l, \lambda_l)_-^\dagger \sigma_-^\mu v(p_\nu, +)_- \\
&= -2\omega(p_l)_{-\lambda_l}\omega(p_\nu)_+\chi(p_l)_{\lambda_l}^\dagger \sigma_-^\mu \phi(p_\nu)_+.
\end{aligned}
\tag{4.50}
$$

4.8.1 Leptonic Amplitudes in the W^* Rest-Frame

The leptonic amplitudes take a particularly simple form in the W^* rest-frame, because the lepton and neutrino angles are

$$\theta_l = \pi - \theta_\nu \qquad \phi_l = 0 \qquad \phi_\nu = \pi. \tag{4.51}$$

As a result the two-component eigenspinors of (4.46) become [4]

$$\chi(p_l)_+ = \phi(p_\nu)_+ = \begin{pmatrix} \cos \frac{1}{2}\theta_l \\ \sin \frac{1}{2}\theta_l \end{pmatrix} \qquad \chi(p_l)_- = \begin{pmatrix} -\sin \frac{1}{2}\theta_l \\ \cos \frac{1}{2}\theta_l \end{pmatrix}, \tag{4.52}$$

and hence

$$\chi(p_l)^\dagger_- \sigma^\mu_- \phi(p_\nu)_+ = (0, -\cos\theta_l, -i, \sin\theta_l),$$
$$\chi(p_l)^\dagger_+ \sigma^\mu_- \phi(p_\nu)_+ = (1, -\sin\theta_l, 0, -\cos\theta_l). \tag{4.53}$$

Using the polarisation vectors of the W^* in its rest-frame given in (4.36), the leptonic matrix elements of (4.50) and the definitions of (4.7), the leptonic amplitudes (4.49) become (only the sign of λ_l is shown in the superscripts)

$$L^-_\pm(x, q^2) = 2\sqrt{q^2}\, v d_\pm$$
$$L^-_0(x, q^2) = -2\sqrt{q^2}\, v d_0 \tag{4.54}$$
$$L^-_s(x, q^2) = 0$$

and

$$L^+_\pm(x, q^2) = \pm\sqrt{2}\, m_l v d_0$$
$$L^+_0(x, q^2) = \sqrt{2}\, m_l v (d_+ - d_-) \tag{4.55}$$
$$L^+_s(x, q^2) = -2m_l v,$$

with

$$v = \sqrt{1 - \frac{m_l^2}{q^2}}$$
$$d_\pm = \frac{1 \pm \cos\theta_l}{\sqrt{2}} \tag{4.56}$$
$$d_0 = \sin\theta_l.$$

Note that the L^+ amplitudes with $\lambda_l = \frac{1}{2}$ are suppressed by a factor of m_l, due to the V-A form of the charged current. The amplitude L^-_s vanishes due to angular momentum conservation (since the lepton and antineutrino helicities are parallel in the W rest-frame, so the W must be spin-1). The lepton decay angle θ_l in the virtual W rest-frame is expressed in terms of the invariants q^2 and $x \equiv p_l.p_B/m_B^2$, using (4.6), as

$$\cos\theta_l = \frac{(q^2 + m_l^2)(m_B^2 - m_M^2 + q^2) - 4m_B^2 q^2 x}{(q^2 - m_l^2)\sqrt{Q_+ Q_-}}. \tag{4.57}$$

4.8.2 Leptonic Amplitudes in the $\overline{B}$ Rest-Frame

In the $\overline{B}$ rest-frame, with the lepton azimuthal angles ϕ_l, ϕ_ν as in (4.51), the

required two-component eigenspinors are

$$
\chi(p_l)_+ = \begin{pmatrix} \cos\frac{1}{2}\psi_l \\ \sin\frac{1}{2}\psi_l \end{pmatrix},
$$

$$
\chi(p_l)_- = \begin{pmatrix} -\sin\frac{1}{2}\psi_l \\ \cos\frac{1}{2}\psi_l \end{pmatrix}, \tag{4.58}
$$

$$
\phi(p_\nu)_+ = \begin{pmatrix} \sin\frac{1}{2}\psi_\nu \\ \cos\frac{1}{2}\psi_\nu \end{pmatrix},
$$

and so

$$
\chi(p_l)_-^\dagger \sigma_-^\mu \phi(p_\nu)_+ = (\cos\psi_+, \sin\psi_-, -i\sin\psi_+, \cos\psi_-),
$$

$$
\chi(p_l)_+^\dagger \sigma_-^\mu \phi(p_\nu)_+ = (\sin\psi_+, -\cos\psi_-, i\cos\psi_+, \sin\psi_-), \tag{4.59}
$$

where

$$
\psi_\pm \equiv \frac{1}{2}(\psi_l \pm \psi_\nu). \tag{4.60}
$$

The leptonic amplitudes now become [5]

$$
L_\pm^-(x, q^2) = 2\omega_+ \sqrt{p_\nu}(\sin\psi_+ \mp \sin\psi_-),
$$

$$
L_{0,s}^-(x, q^2) = -\frac{2\omega_+}{\sqrt{q^2}}\sqrt{2p_\nu}(p_M \cos\psi_{+,-} + q^0 \cos\psi_{-,+}), \tag{4.61}
$$

and

$$
L_\pm^+(x, q^2) = -2\omega_- \sqrt{p_\nu}(\cos\psi_+ \mp \cos\psi_-),
$$

$$
L_{0,s}^+(x, q^2) = -\frac{2\omega_-}{\sqrt{q^2}}\sqrt{2p_\nu}(p_M \sin\psi_{+,-} + q^0 \sin\psi_{-,+}), \tag{4.62}
$$

where (see (4.45))

$$
\omega_\pm \equiv \omega(p_l)_\pm. \tag{4.63}
$$

The variables given here can be written in terms of q^2 and x using (4.7) and (4.10). Note that in the $m_l = 0$ limit these amplitudes are the same as those calculated in the W^* rest-frame, since the lepton helicity is then unaffected by the frame chosen, and so all the amplitudes L^+ vanish in this limit, as can also be seen from the fact that $\omega_- = 0$.

4.9 Hadronic Amplitudes

The hadronic amplitude for the $\overline{B} \to MW^*$ decay, (4.21), is

$$H^{\lambda_M}_{\lambda_w}(q^2) \equiv \epsilon^*_{W\mu}\langle M(p_M, \lambda_M)|J^\mu_{cb}|\overline{B}(p_B)\rangle. \tag{4.64}$$

We may write the weak current for the $\overline{B} \to M$ transition in the form $J^\mu_{cb} = V^\mu_{cb} - A^\mu_{cb}$, in terms of vector and axial-vector currents. The most general forms of the matrix elements of interest here are [4,6-8]

$$\begin{aligned}
\langle D(p_M)|V^\mu_{cb}|\overline{B}(p_B)\rangle &\equiv f_+(q^2)(p_B + p_M)^\mu + f_-(q^2)(p_B - p_M)^\mu \\
\langle D(p_M)|A^\mu_{cb}|\overline{B}(p_B)\rangle &\equiv 0
\end{aligned} \tag{4.65}$$

for $\overline{B} \to D$, and

$$\begin{aligned}
\langle D^*(p_M, \lambda_M)|V^\mu_{cb}|\overline{B}(p_B)\rangle &\equiv if_1(q^2)\epsilon^{\mu\nu\rho\sigma}\epsilon^*_{M\nu}(p_B + p_M)_\rho(p_B - p_M)_\sigma \\
\langle D^*(p_M, \lambda_M)|A^\mu_{cb}|\overline{B}(p_B)\rangle &\equiv f_2(q^2)\epsilon^{*\mu}_M \\
&\quad + (f_3(q^2)(p_B + p_M)^\mu + f_4(q^2)(p_B - p_M)^\mu)(\epsilon^*_M \cdot p_B),
\end{aligned} \tag{4.66}$$

for $\overline{B} \to D^*$. Here $\epsilon_M \equiv \epsilon(p_M, \lambda_M)$ is the polarisation vector of the D^* meson, as defined in (4.38) for the $\overline{B}$ rest-frame, and the form-factors $f_i(q^2)$ are real (neglecting very small CP-violation effects). Thus the hadronic matrix elements of the charged current,

$$\begin{aligned}
\langle D|J^\mu_{cb}|\overline{B}\rangle &= \langle D|V^\mu_{cb}|\overline{B}\rangle \\
\langle D^*|J^\mu_{cb}|\overline{B}\rangle &= \langle D^*|V^\mu_{cb}|\overline{B}\rangle - \langle D^*|A^\mu_{cb}|\overline{B}\rangle,
\end{aligned} \tag{4.67}$$

are given in terms of six form-factors $f_\pm(q^2)$ and $f_i(q^2)$ with $i = 1, 2, 3, 4$. In the $m_l = 0$ limit the form-factors $f_-(q^2)$ and $f_4(q^2)$ do not contribute, because

$$(p_B - p_M)_\mu\langle l(p_l, \lambda_l)\overline{\nu}(p_\nu)|J^{\mu\dagger}_{\nu l}|0\rangle = 0, \tag{4.68}$$

as shown by the fact that $L^-_s = 0$ in the W^* and $\overline{B}$ rest-frames.

On substituting (4.65) and (4.66) into (4.21) and using (4.7), (4.8) and (4.37), we find that the only non-zero $\overline{B} \to D$ amplitudes are [4]

$$
\begin{aligned}
H_0^s(q^2) &= f_+(q^2)\frac{\sqrt{Q_+Q_-}}{\sqrt{q^2}} \\
H_s^s(q^2) &= f_+(q^2)\frac{(m_B^2 - m_M^2)}{\sqrt{q^2}} + f_-(q^2)\sqrt{q^2},
\end{aligned}
\tag{4.69}
$$

whereas for $\overline{B} \to D^*$ we have four amplitudes [4]

$$
\begin{aligned}
H_\pm^\pm(q^2) &= f_2(q^2) \mp f_1(q^2)\sqrt{Q_+Q_-} \\
H_0^0(q^2) &= -\frac{1}{2m_M\sqrt{q^2}}\left\{(m_B^2 - m_M^2 - q^2)f_2(q^2) + Q_+Q_-f_3(q^2)\right\} \\
H_s^0(q^2) &= -\frac{\sqrt{Q_+Q_-}}{2m_M\sqrt{q^2}}\left\{f_2(q^2) + (m_B^2 - m_M^2)f_3(q^2) + q^2 f_4(q^2)\right\}.
\end{aligned}
\tag{4.70}
$$

In the $m_l = 0$ limit H_s^s and H_s^0 may be ignored, since $L_s^\pm = 0$, showing again that f_+ and f_4 do not contribute, leaving one hadronic amplitude describing $\overline{B} \to Dl\overline{\nu}$ decay and three for $\overline{B} \to D^*l\overline{\nu}$.

4.10 Matrix Elements of Related Decays

There are other related decays to which the above formalism may be applied, such as $B \to \overline{M}l^+\nu$, $D \to Ml^+\nu$ and $\overline{D} \to \overline{M}l\overline{\nu}$, which require slightly different matrix elements (note that the definitions of B and D mesons are slightly confusing – a $\overline{B}$ meson is defined to contain a b quark, while a D meson contains a c quark). In the leptonic sector one must consider the two decays

$$
W^- \to l^-\overline{\nu} \qquad \& \qquad W^+ \to l^+\nu.
\tag{4.71}
$$

In the latter case the matrix element is given by

$$
\begin{aligned}
\langle l^+(p_l, \lambda_l)\nu(p_\nu, -)|J_{\nu l}^\mu|0\rangle &= -2\omega(p_l)_{\lambda_l}\omega(p_\nu)_+ \chi(p_\nu)_-^\dagger \sigma_-^\mu \phi(p_l)_{\lambda_l} \\
&= -\langle l^-(\tilde{p}_l, -\lambda_l)\overline{\nu}(\tilde{p}_\nu, +)|J_{\nu l\mu}|0\rangle.
\end{aligned}
\tag{4.72}
$$

The last equality can be deduced either from the definitions of the two-component eigenspinors or from the CP transformation properties of the matrix element. By

comparing (4.72) with (4.50) it can be seen that, in the massless lepton limit, the lepton spectra for the two processes of (4.71) may be obtained from each other by interchanging lepton and neutrino, as expected.

The hadronic matrix elements are similarly related, with the result that the distributions for $\overline{B} \to Ml\overline{\nu}$ and $B \to \overline{M}l^+\nu$ are exactly the same, provided helicities are all reversed.

However, matrix elements for D decays are different, because they combine hadronic amplitudes similar to those for $\overline{B}$ decays with leptonic amplitudes for W^+ decays.

4.11 Experimental Determination of the Form-Factors and $|V_{cb}|$

The six hadronic form-factors of (4.65) and (4.66) are difficult to calculate accurately, on account of the non-perturbative nature of low-energy QCD. Chapter 5 describes some attempts to predict the q^2-dependence and normalisation of these functions. However, much can be learnt about them directly from experimental observations.

For this section we will be concerned with the q^2-dependence of the $\overline{B} \to Ml\overline{\nu}$ decays, and so will integrate the decay rates of (4.23) over the leptonic variable x (actually the integration can be accomplished more simply by first changing variables to $\cos\theta_l$, the lepton angle in the W^* rest-frame). Accordingly we define the theoretically calculable function

$$L_{\lambda_1\lambda_2}(q^2) \equiv \int dx\, L_{\lambda_1}^-(x,q^2)\, L_{\lambda_2}^-(x,q^2). \qquad (4.73)$$

The integration in (4.73) is over the allowed kinematic region (shown in fig.4.2), but subject to any required experimental acceptance cuts.

4.11.1 q^2-Dependence of $\overline{B} \to Dl\overline{\nu}$ Decays

In the massless lepton limit the differential decay rate for the process $\overline{B} \to Dl\overline{\nu}$ is

$$\frac{d\Gamma}{dq^2} = \frac{1}{256\pi^3} \frac{G_F^2}{m_B} |V_{cb}|^2 L_{00}(q^2) H_0^s(q^2)^2, \qquad (4.74)$$

after integration over the observable lepton energies, where $L_{00}(q^2)$ is given by

(4.73) and $H_0^s(q^2)$ by (4.69). Hence measuring $d\Gamma/dq^2$ determines $|V_{cb}|H_0^s(q^2)$, or equivalently $|V_{cb}|f_+(q^2)$, up to a sign. If $f_+(q^2)$ is known at any value of q^2 then we can determine $|V_{cb}|$, as well as the full functional dependence of f_+. As will be discussed in section 5.1 this normalisation can be predicted fairly reliably for $\overline{B} \to D, D^*$ decays. Conversely, if $|V_{cb}|$ is known, then the normalisation of $f_+(q^2)$ can be measured.

Once accomplished the same can then be done for $f_-(q^2)$, by measuring $d\Gamma/dq^2$ for the decay $\overline{B} \to D\tau\overline{\nu}$.

4.11.2 Angular Correlations for Decay $\overline{B} \to D^* l\overline{\nu} \to (D\pi)l\overline{\nu}$

As above we will initially concentrate on the $l = e, \mu$ decay modes and hence neglect the lepton mass. As emphasised in refs. [4,9], the angular correlation of the decay products in the decay $\overline{B} \to D^* l\overline{\nu} \to (D\pi)l\overline{\nu}$ measures the individual helicity amplitudes. Other analyses of the angular correlation [10] do not use an amplitude analysis, which we find particularly illuminating.

The two-stage decay is described by an amplitude of the form

$$\mathcal{M}_\lambda^- \propto \frac{G_F}{\sqrt{2}} V_{cb} \sum_\lambda L_\lambda^- H_\lambda^\lambda Y_\lambda^1, \tag{4.75}$$

where $\lambda \equiv \lambda_M = \lambda_W = 0, \pm 1$ is the helicity of the D^*, and also that of the virtual W^-. The scalar component $\lambda_W = s$ does not contribute in the limit of massless leptons. The amplitudes H_λ, L_λ and Y_λ^1 describe the decays $\overline{B} \to D_\lambda^* W_\lambda^{*-}$, $W_\lambda^{*-} \to l^-\overline{\nu}$ and $D_\lambda^* \to D\pi$ respectively. The Feynman rules for the decay of a spin-1 particle to two spin-0 particles give an amplitude of the form

$$Y_\lambda^1 = \epsilon^\mu(p_M, \lambda)\,(a p_{\pi\mu} + b p_{D\mu}) \tag{4.76}$$

for some a, b. For the decay of the D^* it is simplest to evaluate the amplitude in the D^* rest-frame, as shown in fig.4.4, which can be obtained from the two frames of fig.4.3 by a boost along the z-axis, and where the decay amplitudes are easily seen to be the $J = 1$ spherical harmonics

$$Y_\pm^1(\theta^*, \phi^*) = \mp\sqrt{\frac{3}{8\pi}}\sin\theta^* e^{\pm i\phi^*}, \qquad Y_0^1(\theta^*, \phi^*) = \sqrt{\frac{3}{4\pi}}\cos\theta^*. \tag{4.77}$$

The angles $0 \le \theta^* \le \pi$ and $0 \le \phi^* < 2\pi$ are defined in fig.4.4. The azimuthal

D* rest frame
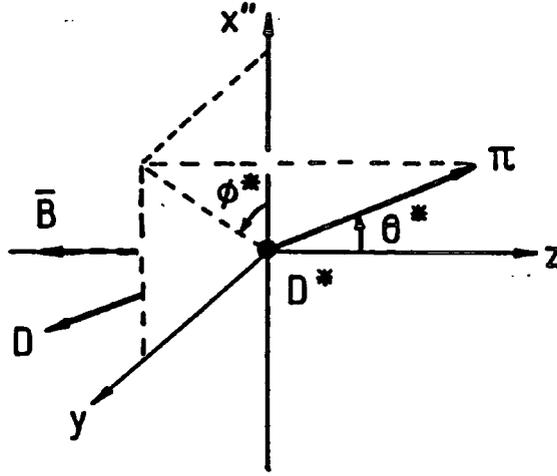
Figure 4.4 The D^* rest-frame, which defines the angular variables used in the $D^* \to D\pi$ decay analysis.

angle ϕ^* is the opening angle between the $W^* \to l\bar{\nu}$ decay plane and the $D^* \to D\pi$ decay plane.

In (4.75) we have omitted the D^* propagator factor and its coupling to $D\pi$. These are effectively taken into account by including the branching-ratio factor $\mathrm{Br}(D^* \to D\pi)$ in the formula for the $\bar{B} \to (D\pi)l\bar{\nu}$ differential decay rate

$$d\Gamma = \frac{G_F^2}{4m_B}|V_{cb}|^2 \,\mathrm{Br}(D^* \to D\pi) \left|\sum_\lambda L_\lambda^- H_\lambda^\lambda Y_\lambda^1\right|^2 d\Phi_3 \, d\cos\theta^* \, d\phi^*. \tag{4.78}$$

The explicit $D\pi$ angular dependence is of the form

$$\frac{8\pi}{3}\left|\sum_\lambda L_\lambda^- H_\lambda^\lambda Y_\lambda^1\right|^2 = \left\{(L_+^- H_+^+)^2 + (L_-^- H_-^-)^2\right\}\sin^2\theta^* + 2(L_0^- H_0^0)^2\cos^2\theta^*$$
$$+ \sqrt{2}(L_0^- H_0^0)(L_-^- H_-^- - L_+^- H_+^+)\sin 2\theta^* \cos\phi^* \tag{4.79}$$
$$- 2(L_-^- H_-^-)(L_+^- H_+^+)\sin^2\theta^* \cos 2\phi^*,$$

where the hadronic amplitudes H_λ^λ are functions only of q^2. Note that the leptonic decay amplitudes L_λ^- are all real in our conventions, and we assume that a basis can be chosen in which the hadronic amplitudes H_λ^λ are also all real (neglecting possible very small CP-violating effects). Since the objective is to measure their q^2

77

dependence we integrate (4.78) over the experimentally detectable lepton energies and obtain

$$\frac{d\Gamma}{dq^2\,d\cos\theta^*\,d\phi^*} = \frac{3}{1024\pi^4}\frac{G_F^2}{m_B}|V_{cb}|^2\,\mathrm{Br}(D^* \to D\pi)$$
$$\times L_{00}(q^2)H_0^0(q^2)^2\left\{1 + \beta_1(q^2)\sin^2\theta^*\right. \qquad (4.80)$$
$$\left. + \beta_2(q^2)\sin 2\theta^*\cos\phi^* + \beta_3(q^2)\sin^2\theta^*\cos 2\phi^*\right\},$$

where the angular coefficients are

$$\beta_1(q^2) = \frac{L_{--}}{2L_{00}}\left(\frac{H_-^-}{H_0^0}\right)^2 + \frac{L_{++}}{2L_{00}}\left(\frac{H_+^+}{H_0^0}\right)^2 - 1$$
$$\beta_2(q^2) = \frac{L_{0-}}{\sqrt{2}L_{00}}\left(\frac{H_-^-}{H_0^0}\right) - \frac{L_{0+}}{\sqrt{2}L_{00}}\left(\frac{H_+^+}{H_0^0}\right) \qquad (4.81)$$
$$\beta_3(q^2) = -\frac{L_{-+}}{L_{00}}\left(\frac{H_-^-}{H_0^0}\right)\left(\frac{H_+^+}{H_0^0}\right),$$

in terms of the hadronic decay amplitudes $H_\lambda^\lambda(q^2)$ and the known leptonic functions $L_{\lambda_1\lambda_2}(q^2)$ of (4.73). We choose to normalise relative to H_{00} rather than the H_{++} or H_{--}, because the the latter two both vanish at $q^2 = 0$. Note that integrating over the full ranges of $\cos\theta^*$ and ϕ^* reproduces the differential decay rate

$$\frac{d\Gamma}{dq^2} = \frac{1}{256\pi^3}\frac{G_F^2}{m_B}|V_{cb}|^2\sum_{\lambda=\pm,0}L_{\lambda\lambda}(q^2)H_\lambda^\lambda(q^2)^2, \qquad (4.82)$$

(except for the branching ratio factor), as expected.

Note that only two of the three $\beta_i(q^2)$ are actually independent. Measurements of the angular distibutions would determine $\beta_{1,2,3}(q^2)$, and hence $H_\pm^\pm(q^2)/H_0^0(q^2)$. If $|V_{cb}|$ is known then $H_0^0(q^2)$ can be determined (up to a sign) from (4.80) and hence so can $H_\pm^\pm(q^2)$. If $|V_{cb}|$ is not known then the overall normalisation is not fixed, but the relative normalisations are. From these three helicity amplitudes the three form-factors $f_{1,2,3}(q^2)$ can be determined, using (4.69), again up to an overall normalisation. Conversely, a theoretical understanding of the normalisation of the form-factors allows a determination of $|V_{cb}|$ to be made.

In the absence of a huge amount of precisely analysed data it is not possible to measure the decay distribution of (4.80). This means that we must integrate

78

over some of the independent variables, and so lose the ability to determine the form-factors individually. Current experimental measurements are of $d\Gamma/dq^2$ and $d\Gamma/d\cos\theta^*$, which can both be used to test the models of hadronic form-factors described in chapter 5.

In analysing the $\cos\theta^*$ distribution it is convenient to introduce the integrated asymmetry parameters

$$\beta_i = \frac{\int dq^2 \, L_{00}(q^2) H_0^0(q^2)^2 \beta_i(q^2)}{\int dq^2 \, L_{00}(q^2) H_0^0(q^2)^2}, \tag{4.83}$$

which give the angular distribution

$$\frac{d\Gamma}{d\cos\theta^* \, d\phi^*} \propto \left\{ 1 + \beta_1 \sin^2\theta^* + \beta_2 \sin 2\theta^* \cos\phi^* + \beta_3 \sin^2\theta^* \cos 2\phi^* \right\}. \tag{4.84}$$

Integrating again, over ϕ^*, yields

$$\frac{d\Gamma}{d\cos\theta^*} \propto (1 + \alpha\cos^2\theta^*), \tag{4.85}$$

where

$$\alpha = -\frac{\beta_1}{\beta_1 + 1}. \tag{4.86}$$

This is the experimentally measured parameter introduced in section 3.5.

The fourth form-factor, $f_4(q^2)$, can be determined from the q^2 dependence of the decay $\overline{B} \to D^* \tau \bar{\nu}$ once $f_{1,2,3}(q^2)$ are known.

4.12 τ Polarisation

The differential decay-rate for $\overline{B} \to M\tau\bar{\nu}$ (with $M = D$ or D^*) is

$$d\Gamma_{\lambda_l} = \frac{1}{256\pi^3} \frac{G_F^2}{m_B} |V_{cb}|^2 \sum_{\lambda_M} \left| \sum_{\lambda_W} \eta_{\lambda_W} L_{\lambda_W}^{\lambda_l} H_{\lambda_W}^{\lambda_M} \right|^2 dq^2 \, dx, \tag{4.87}$$

where $\lambda_l = \pm\frac{1}{2}$ is the helicity of the τ, and $\lambda_W = \pm 1, 0, s$ is the helicity of the virtual W. Here $\lambda_W = s$ denotes the scalar polarisation of the virtual W, and the metric factor $\eta_\pm = \eta_0 = -\eta_s = 1$. For the D^* meson $\lambda_M = \pm 1, 0$, whereas for the (zero helicity) D meson we again use the notation $\lambda_M = s$.

79

The longitudinal polarisation of the τ is [5]

$$P_L(x, q^2) \equiv \frac{d\Gamma_+ - d\Gamma_-}{d\Gamma_+ + d\Gamma_-}, \tag{4.88}$$

with $d\Gamma_{\lambda_l}$ given by (4.87). For massless leptons $\lambda_l = -\frac{1}{2}$ and so $P_L = -1$ always, on account of the standard $V-A$ form of the charged current. For a massive lepton the helicity λ_l, and therefore also the polarisation P_L, are frame-dependent.

To calculate the polarisation in a given frame we must evaluate the leptonic amplitudes in the same frame. Using the leptonic amplitudes calculated in section 4.8 above, we can thus calculate the τ polarisation in either the W or $\overline{B}$ rest-frames.

4.13 Conclusion

The above chapter describes the formalism we use for the analysis of semileptonic $\overline{B}$ decays, as far is it can be taken without detailed models of the hadronic form-factors. Such models are described next, in chapter 5, and their predictions are given in chapter 6.

However, with sufficiently accurate experimental measurements of the q^2 spectra and angular decay distributions, it should be possible to determine the q^2 dependence of all the form-factors, up to an overall normalisation, making form-factor models unnecesary, except to test our understanding of the underlying hadronic transition. Thus, eventually, it is only the accuracy of our predictions of this normalisation that will limit the accuracy of our determination of $|V_{cb}|$.

References

1. K. Hagiwara, R.D. Peccei, D. Zeppenfeld and K. Hikasa, *Nucl. Phys.* **B282**, 253 (1987).

2. K. Hagiwara and D. Zeppenfeld, *Nucl. Phys.* **B274**, 1 (1986).

3. C. Itzykson and J.-B. Zuber, in *Quantum Field Theory* pp.151-156 (McGraw-Hill, New York, 1980).

4. K. Hagiwara, A.D. Martin and M.F. Wade, *Nucl. Phys.* **B327**, 569 (1989).

5. K. Hagiwara, A.D. Martin and M.F. Wade, *Z. Phys* **C46**, 299 (1990).

6. T. Altomari and L. Wolfenstein, *Phys. Rev.* **D37**, 681 (1988).

7. N. Isgur, D. Scora, B. Grinstein and M.B. Wise, *Phys. Rev.* **D39**, 799 (1989).

8. J.G. Körner and G.A. Schuler, *Z. Phys.* **C38**, 511 (1988).

9. K. Hagiwara, A.D. Martin and M.F. Wade, *Phys. Lett.* **B228**, 144 (1989).

10. J.G. Körner and G.A. Schuler, *Phys. Lett.* **B226**, 185 (1989).

    N. Isgur and D. Scora, *Phys. Rev.* **D40**, 1491 (1989).

    F.J. Gilman and R.L. Singleton, Jr., *Phys. Rev.* **D41**, 142 (1990).

5 Models of Hadronic Form-Factors

Heaven is for thee too high
To know what passes there; be lowly wise:
Think only what concerns thee and thy being.

John Milton, 1608-1674

5.1 Introduction

In order to predict the semileptonic decay distributions one must have a model for the hadronic matrix elements, or equivalently for the form-factors. As more data becomes available one should be able to distinguish between the models and thus test the ideas upon which they are based.

In this chapter several models for the form-factors are described and compared. There are some significant differences in theoretical input, but in the end surprisingly little difference in their predictions for $b \to c$ decays. For other decays, involving light quarks, there are significant discrepancies, as might be expected, since light quarks are less easy to quantify.

Most models begin with a quark-model calculation, in which the helicity structure of the $B \to M$ transition is matched to that of the fundamental $b \to c$ quark process (usually this is done at either maximum or minimum momentum transfer, though it is unclear why the momentum-dependence of the helicity overlap is not used). The momentum transfer, or q^2, dependence is then estimated by multiplying the quark-model predictions by some function $F(q^2)$ [1] to simulate the non-perturbative QCD effects.

The most frequent choice for $F(q^2)$ is a single-pole-dominance form [2,3,4]

$$F(q^2) \propto \frac{m_P^2}{m_P^2 - q^2},$$
(5.1)

where the effective pole position m_P^2 is often chosen to correspond to the lowest-lying vector-meson state in the $t \equiv -q^2$ channel, which is $m_{B_c}^2$ in our example (see fig.5.1(a)). This pole form-factor represents a non-perturbative transition of the B meson to an on-shell M and a virtual vector-meson 'P', which then decays to a lepton and neutrino, via a virtual W. In the determination of $|V_{cb}|$ it is

D or D*

$\overline{B}$ ⟍⟍⟍ q

c

$\overline{B}^*_c$

b

W

D or D*

$\overline{B}$ ⟍⟍ q

c

b

W
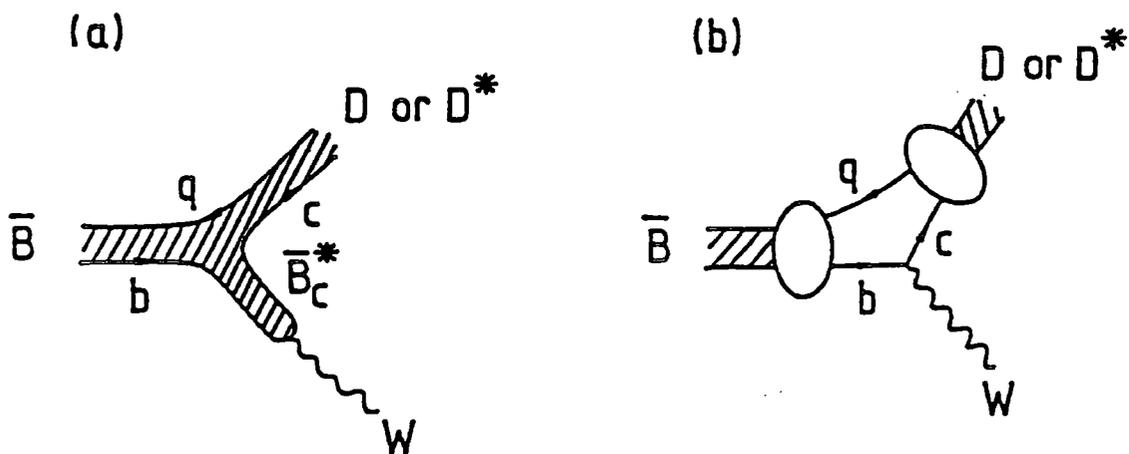
Figure 5.1 Schematic diagrams showing the conceptual difference between (a) nearest pole dominance and (b) spatial wave-function overlap.

vital to know reliably the normalisation of the form-factor in (5.1), as discussed in section 4.11. The normalisation of $F(q^2)$ is unclear in this picture, though the conventional choice is

$$F(q^2_{max}) \approx 1. \tag{5.2}$$

Calculations of the matrix element by Wirbel et al. [4] (see section 5.3.5 below), using infinite-momentum-frame techniques, indicate this to be the case. However, the $B^*_c \to W$ transition coupling (vector meson decay constant) can be estimated in the non-relativistic potential model, and the constraint (5.2) would lead to a very large value of the effective $B^*_c - B - (D, D^*)$ coupling, g, of order $g^2/4\pi \sim 40$ [5]. Furthermore, the level spacing of the B^*_c states is tiny on the scale m_B, so there is no reason why a single resonance should dominate the form-factor, and it is probably better to regard m_P as a free parameter to be determined by experiment.

A second model of the hadronic part of the decay is that the underlying $b \to cW^*$ transition is perturbative, and that $F(q^2)$ corresponds to the spatial overlap of the initial and final meson wave functions [1] (see fig.5.1(b)). In this case one would expect (5.2) to hold, since the mesons are expected to have the same spatial dimensions, up to corrections from the difference in reduced masses $\mu_b = m_b m_q/(m_b + m_q)$ and $\mu_c = m_c m_q/(m_c + m_q)$, a difference which is of the order of

$$\frac{\mu_b - \mu_c}{\mu_b + \mu_c} \approx \frac{m_q}{2m_c}\left(1 - \frac{m_c}{m_b}\right) \tag{5.3}$$

relative to unity. If we take $m_q = 0.3\,GeV$, $m_c = 1.6\,GeV$ and $m_b = 5.0\,GeV$ this is about a 6% effect. Isgur et al. [6] have used variational methods, based on solutions of the non-relativistic harmonic oscillator equation to get

$$F(q^2) = \exp\{-\beta(q^2_{max} - q^2)/2m^2_B\}, \tag{5.4}$$

near $q^2 = q^2_{max}$, with $\beta = 1.65$, although for lack of any better alternative they choose to use this form at all q^2. The value of β extracted from the analysis is actually 0.82, but the authors include a 'relativistic correction' after a comparison with the pion form-factor [6].

Fortunately, as pointed out by Altomari and Wolfenstein [7], the two form-factors of (5.1) and (5.4) do not differ significantly in the case of $b \to c$ transitions. In fact, by expanding the form-factors about $q^2 = q^2_{max}$ one finds

$$F(q^2) = 1 - \frac{q^2_{max} - q^2}{m^2_P - q^2_{max}} + \cdots \tag{5.5}$$

for the pole form-factor, and

$$F(q^2) = 1 - \frac{\beta}{2m^2_B}(q^2_{max} - q^2) + \cdots \tag{5.6}$$

for the exponential form-factor. On comparing (5.5) and (5.6) we see that the two parametrisations approximately coincide when

$$m^2_P = q^2_{max} + \frac{2}{\beta}m^2_B. \tag{5.7}$$

The slope $\beta = 1.65$ hence corresponds, at $q^2 = q^2_{max}$, to a pole at $m_P = 6.74\,GeV$ for $\overline{B} \to D$ and $m_P = 6.67\,GeV$ for $\overline{B} \to D^*$. In fact this correspondence between the two form-factors is true, to a good approximation, over the entire physical range of q^2, and at $q^2 = 0$ the two form-factors differ by at most only 4% in the above case. If the pole mass is chosen to be $m_P = 6.34\,GeV$, as is the case with several of the models discussed below, then the agreement between the exponential and pole form-factors is even closer over the whole q^2 range (see fig.5.2).
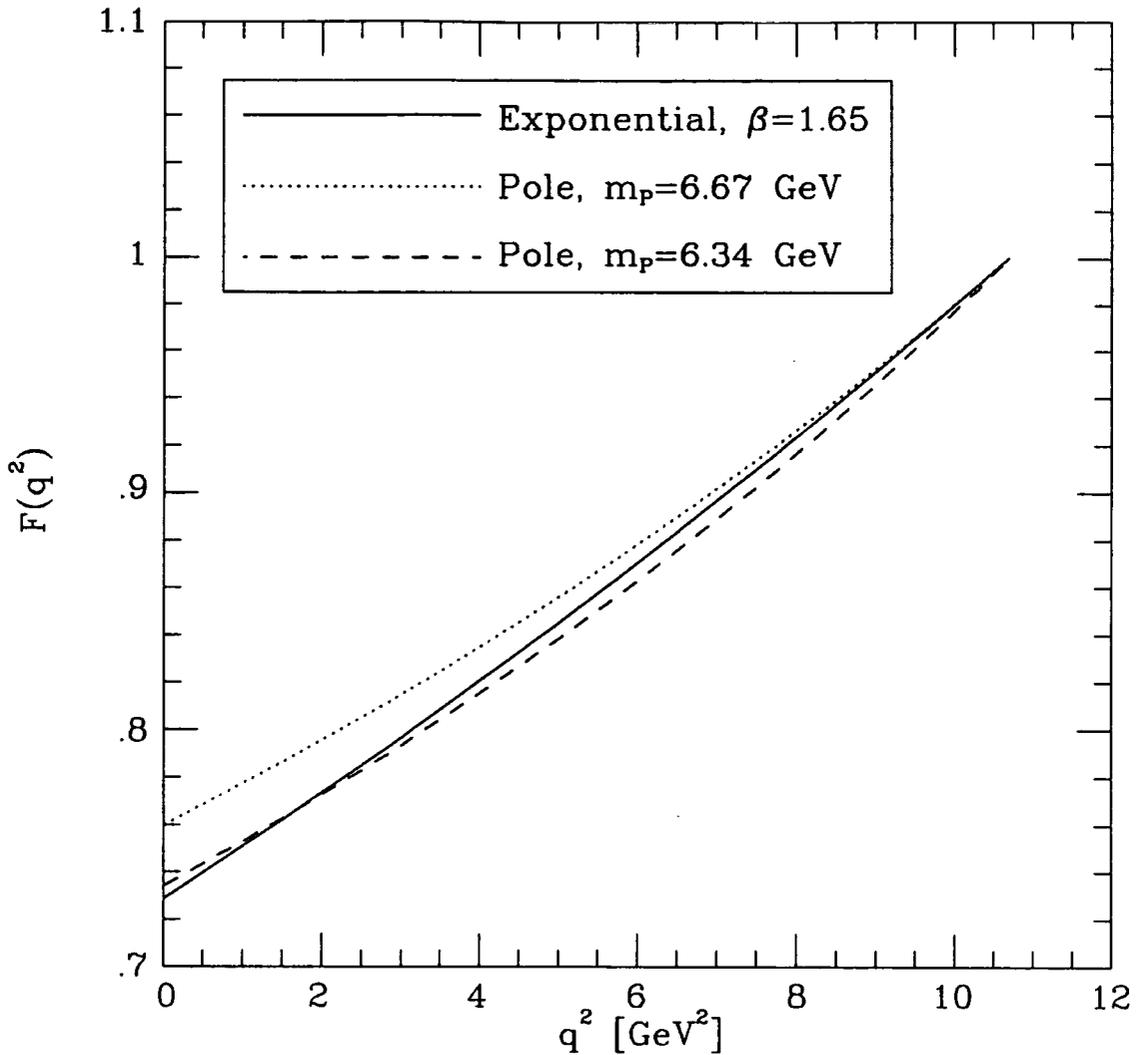
Figure 5.2   Comparison of the q^2 dependence of the pole and exponential wave-function overlaps $F(q^2)$ of (5.1) and (5.4), for some of the parameter values discussed in the text.

5.2 Validity of the Spectator Quark Approach

The hadronic form-factor models described in section 5.3 below are all based on the spectator quark approach, whereby the light quark in the meson has no effect on the decay, other than through its spin. Before detailing the models it is therefore necessary to discuss the validity of such an approach, which will be illustrated using D and B meson decays.

Firstly, we must consider the ratio of charged to neutral meson lifetimes. In the case of D mesons we have [8]
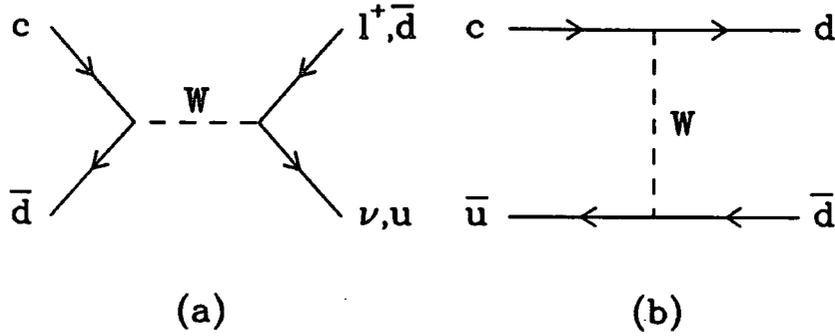
Figure 5.3 Annihilation and exchange diagrams contributing to (a) D^+ and (b) D^0 meson decays.

$$\frac{\tau_{D^+}}{\tau_{D^0}} = 2.52^{+0.13}_{-0.12}. \tag{5.8}$$

The conventional qualitative explanation for the lifetimes being so unequal is that non-spectator annihilation and particle exchange diagrams, such as those shown in fig.5.3, are important. Such diagrams may contribute both constructively or destructively with other mechanisms to produce the above lifetime ratio, showing that not all D decays are well described by the spectator model. However, neither of the diagrams of fig.5.3 can contribute to semileptonic D decay, so one might still expect spectator models to be valid in that case.

Recent measurements of the $K^* \to K\pi$ angular distribution, from K^* mesons produced in the semileptonic decay $D \to K^* l^+ \nu$, are in disagreement with the predictions of spectator models [9]. We believe, however, that this is a problem more with the fact that the $c \to s$ decay does not involve heavy quarks in both initial and final states (as discussed in section 3.3), than with the spectator approach itself.

In the case of B meson decays the current lifetime ratios, given in section 3.5, are [10,11]

$$\frac{\tau_{B^\pm}}{\tau_{B^0}} = (0.89 \pm 0.19 \pm 0.13) \left(\frac{f_{00}}{f_{+-}}\right) \qquad \text{CLEO}$$

$$= (1.00 \pm 0.23 \pm 0.14) \left(\frac{f_{00}}{f_{+-}}\right) \qquad \text{ARGUS,} \tag{5.9}$$

both compatible with a naive spectator approximation, which predicts roughly equal lifetimes. The annihilation and exchange diagrams of fig.5.3 are now less

important, because the relevant KM matrix elements are much smaller in the b-quark case than the c-quark case above.

Secondly, as discussed in chapter 6, predictions of the $D^* \to D\pi$ angular distribution, from D^*s produced in semileptonic B decay, are in good agreement with theoretical predictions (although the experimental errors are very large), consistent with the belief that $b \to c$ decays, involving heavy quarks in both initial and final states, are well described by perturbatively-based calculations.

5.3 Models of hadronic form-factors.

5.3.1 Spectator Quark model

The meson states that occur in the hadronic amplitudes

$$H_{\lambda_w}^{\lambda_M} \equiv \epsilon_{W\mu}^* \langle M(p_M, \lambda_M) | J_{cb}^\mu | \overline{B}(p_B) \rangle \tag{5.10}$$

are parity eigenstates, with quark spins, quantised in the z-direction, given by the usual non-relativistic combinations

$$\frac{1}{\sqrt{2}}(\uparrow\downarrow - \downarrow\uparrow) \qquad \text{for spin 0} \tag{5.11}$$

and

$$\begin{matrix} (\uparrow\uparrow) \\ \frac{1}{\sqrt{2}}(\uparrow\downarrow + \downarrow\uparrow) \qquad \text{for spin 1,} \\ (\downarrow\downarrow) \end{matrix} \tag{5.12}$$

where the first spin is chosen to be that of the b quark and the second that of the $\overline{q}$ antiquark.

The spectator antiquark is taken to be unaffected by the decay of the heavy quark, and the matrix element (5.10) is then evaluated by boosting to a frame where the b quark is at rest and the c quark is moving in the positive z-direction, so that

$$\begin{aligned} p_b &= (m_b, 0, 0, 0), \\ p_c &= (E_c, 0, 0, p_c). \end{aligned} \tag{5.13}$$

We can now choose the quark states to be helicity eigenstates, with spin $\uparrow$ ($\downarrow$) corresponding to helicity $+$ ($-$), by choosing the b quark to be the zero three-momentum

limit of a quark moving in the positive z-direction (although, as explained in section 4.7, we could equally well reverse its 3-momentum and helicity and get exactly the same results). The reason for choosing the spinors as in (4.41) is so that no extra phase factors appear in the definitions of the meson spin wave-functions (5.11) and (5.12).

The two-component eigenspinors in the frame above are

$$\chi(p_b)_+ = \chi(p_c)_+ = \begin{pmatrix} 1 \\ 0 \end{pmatrix}, \qquad \chi(p_b)_- = \chi(p_c)_- = \begin{pmatrix} 0 \\ 1 \end{pmatrix}, \qquad (5.14)$$

so that the four possible quark matrix elements ($\lambda_b, \lambda_c = \pm$) are

$$\begin{aligned} \langle c(p_c, \lambda_c) | J_{cb}^\mu | b(p_b, \lambda_b) \rangle &= \bar{u}(p_c, \lambda_c) \gamma^\mu (1 - \gamma^5) u(p_b, \lambda_b) \\ &= 2 u(p_c, \lambda_c)_-^\dagger \sigma_-^\mu u(p_b, \lambda_b)_- \qquad (5.15) \\ &= 2 \omega(p_b)_{-\lambda_b} \omega(p_c)_{-\lambda_c} \chi(p_c)_{\lambda_c}^\dagger \sigma_-^\mu \chi(p_b)_{\lambda_b}. \end{aligned}$$

In the spectator quark model the light quark is assumed to have no effect upon the heavy quark decay, and its spin is assumed unchanged. Using the notation " " to indicate that here D and D^* are *free* quark-antiquark systems with the correct spin wave-functions, but unconstrained invariant masses, we can form the $\overline{B} \to$ "D" matrix elements

$$\begin{aligned} \langle \text{``}D(p_M)\text{''} | J_{cb}^\mu | \overline{B}(p_B) \rangle &= \frac{1}{2} \left(\langle c(p_c, +) | J_{cb}^\mu | b(p_b, +) \rangle + \langle c(p_c, -) | J_{cb}^\mu | b(p_b, -) \rangle \right) \\ &= \frac{\sqrt{2m_b}}{\sqrt{E_c + m_c}} (E_c + m_c, 0, 0, p_c) \\ &= \frac{\sqrt{2}}{\sqrt{p_b \cdot p_c + m_b m_c}} (m_b p_c^\mu + m_c p_b^\mu), \end{aligned}$$

$$(5.16)$$

where we have assumed non-relativistic S-wave spin-singlet wave-functions of of (5.11) for both the $\overline{B}(b\bar{q})$ and "$D(c\bar{q})$" states. We form the $\overline{B} \to$ "D^*" matrix elements in a similar way and find

$$\begin{aligned} \langle \text{``}D^*(p_M, \pm)\text{''} | J_{cb}^\mu | \overline{B}(p_B) \rangle &= \pm \sqrt{2m_b} \, \omega(p_c)_{\mp} (0, 1, \mp i, 0) \\ \langle \text{``}D^*(p_M, 0)\text{''} | J_{cb}^\mu | \overline{B}(p_B) \rangle &= -\frac{\sqrt{2m_b}}{\sqrt{E_c + m_c}} (p_c, 0, 0, E_c + m_c), \end{aligned} \qquad (5.17)$$

88

which can be combined and rewritten covariantly as

$$\langle ``D^*(p_M, \lambda_M)" | J^\mu_{cb} | \overline{B}(p_B) \rangle$$
$$= \frac{\sqrt{2}}{\sqrt{p_b \cdot p_c + m_b m_c}} (p_b \cdot \epsilon^* p^\mu_c - (p_b \cdot p_c + m_b m_c) \epsilon^{*\mu} - i \epsilon^{\mu\nu\rho\sigma} \epsilon^*_\nu p_{b\rho} p_{c\sigma}), \quad (5.18)$$

where the $\epsilon \equiv \epsilon(p_c, \lambda_M)$ are explicitly given by

$$\epsilon(p_c, \pm)^\mu = \mp \frac{1}{\sqrt{2}}(0, 1, \pm i, 0)$$
$$\epsilon(p_c, 0)^\mu = \frac{1}{m_c}(p_c, 0, 0, E_c), \quad (5.19)$$

and so become the polarisation vectors of the D^* meson when $p_c = p_{D^*}$.

By comparing equations (5.16) and (4.65) we find, in the limit $p_b = p_B$ and $p_c = p_M$, that the spectator quark model gives $\overline{B} \to D$ form-factors

$$f^{SQ}_\pm(q^2) = \pm \frac{(m_B \pm m_M)}{\sqrt{Q_+}}, \quad (5.20)$$

and by comparing (5.18) and (4.66) that the $\overline{B} \to D^*$ form-factors are

$$f^{SQ}_1(q^2) = -f^{SQ}_3(q^2) = f^{SQ}_4(q^2) = \frac{1}{\sqrt{Q_+}}, \qquad f^{SQ}_2(q^2) = \sqrt{Q_+}, \quad (5.21)$$

with $Q_+ \equiv (m_B + m_M)^2 - q^2$. As emphasized by Suzuki [12] these form-factors are intrinsic to the quark-model description of the spin wave-functions, and have nothing to do with the form-factor $F(q^2)$ that arises from the mismatch of the meson wavefunctions in coordinate space.

Many authors have ignored these spectator quark model 'form-factors', which are intrinsic to the description of heavy mesons in terms of non-relativistic quarks, since the non-relativistic quark model with weak binding is only applicable in the vicinity of $q^2 = q^2_{max}$. However, it is natural to include the form-factors at all q^2 under the parton-like assumption that the binding has a negligible effect on the spin properties of the quark-antiquark system.

The expressions of (5.20) and (5.21) have been used to check the formalism described in chapter 4, by comparing the predictions for the total decay rate

against the well-known formula for the lowest order total free-quark decay rate [1]

$$\Gamma_0 \equiv \Gamma(b \to c l \bar{\nu}) = \frac{G_F^2 m_b^5}{192\pi^3} |V_{cb}|^2 \left\{ 1 - 8\epsilon^2 + 8\epsilon^6 - \epsilon^8 - 24\epsilon^4 \ln \epsilon \right\}, \qquad (5.22)$$

with $\epsilon \equiv m_c/m_b$, by choosing $m_b = m_B$ and $m_c = m_D = m_{D^*}$. Agreement is expected in this limit, since summing over the helicity states of the D and D^* mesons is equivalent to spin-averaging in the free-quark decay.

Perturbative QCD corrections to the V_{cb}^μ and A_{cb}^μ currents of (4.65) and (4.66) have been calculated in ref. [13]. These introduce multiplicative factors

$$1 + \frac{\alpha_s}{\pi} F_i(\epsilon), \qquad (5.23)$$

with

$$F_V(\epsilon) = \left(\frac{\epsilon + 1}{\epsilon - 1} \right) \ln \epsilon - 2, \qquad F_A(\epsilon) = F_V(\epsilon) - \frac{2}{3}. \qquad (5.24)$$

For $\epsilon \equiv m_c/m_b \approx 0.3$ we have $F_V \approx 0.24$ and $F_A \approx -0.43$ and so the corrections are less than 3%. Although small, these calculable short-distance contributions should be included in a precise determination of $|V_{cb}|$. However, since they are much smaller than the other uncertainties, we have not actually done so.

5.3.2 KS model

The model of Körner and Schuler [2] is based on matching at $q^2 = 0$. They argue that this is the best region to perform the matching because of threshold effects at q_{max}^2. The results are then continued to $q^2 \neq 0$ by assuming nearest-meson dominance, with a common pole position since the level spacing of the crossed-channel $b\bar{c}$ states is so small. Thus the form-factors are given by

$$f_i^{KS}(q^2) = f_i^{SQ}(0) \times I \times \left(\frac{m_P^2}{m_P^2 - q^2} \right)^{n_i}, \qquad i = (+, -, 1, 2, 3, 4) \qquad (5.25)$$

where

$$I = 0.7$$
$$m_P = 6.34 \, GeV$$
$$n_i = 1 \text{ for } i = (+, -, 2) \qquad (5.26)$$
$$n_i = 2 \text{ for } i = (1, 3, 4).$$

The factor I is included to take account of the wave-function overlap at $q^2 = 0$, and the powers n_i are taken from the power counting rules of QCD. In fact KS

use slightly different conventions for the definitions of the form-factors, but their formulae can be rewritten in the above form using our conventions.

Previously we noted [1] that choosing different powers of q^2 for different form-factors effectively accounts for the power of Q_+ difference between f_1, f_3 and f_2 in (5.21). The KS approach, however, leads to disagreement for the $\overline{B} \rightarrow D$ transition form-factor f_+, which scales as f_1 and f_3 in the free quark model (cf. (5.21)), whereas they assigned the same power $n = 1$ for f_+ and f_2. Such a difference in the relative behaviour of the form-factors leads to different predictions, e.g. of $\mathrm{Br}(\overline{B} \rightarrow Dl\overline{\nu})/\mathrm{Br}(\overline{B} \rightarrow D^*l\overline{\nu})$.

5.3.3 AW model

The Altomari and Wolfenstein model [7] consists of a calculation of the matrix elements at zero recoil ($q^2 = q^2_{max}$) in the non-relativistic quark model, again assuming that the light quark is just a spectator. By neglecting reduced mass effects they are able to calculate the form-factors without needing to choose a specific form for the meson wave-functions. Their results can be summarised as

$$f_i^{AW}(q^2) = f_i^{AW}(q^2_{max}) \times F(q^2), \qquad i = (+, -, 1, 2, 3, 4) \qquad (5.27)$$

where

$$f_\pm^{AW}(q^2_{max}) = \sqrt{\frac{m_D}{m_B}}\left(1 \pm \frac{m_B \mp m_D}{2m_c}\right)$$

$$f_1^{AW}(q^2_{max}) = \frac{1}{2m_c}\sqrt{\frac{m_{D^*}}{m_B}}$$

$$f_2^{AW}(q^2_{max}) = \sqrt{4m_B m_{D^*}} \qquad (5.28)$$

$$f_3^{AW}(q^2_{max}) = -\frac{1}{\sqrt{4m_{D^*}m_B}}\left(1 + \frac{m_{D^*}}{m_B}\left(1 - \frac{m_{D^*}}{m_c}\right)\right)$$

$$f_4^{AW}(q^2_{max}) = \frac{1}{\sqrt{4m_{D^*}m_B}}\left(1 - \frac{m_{D^*}}{m_B}\left(1 - \frac{m_{D^*}}{m_c}\right)\right),$$

where they take $m_c = 1.8\,GeV$. In their calculation AW find the derivation of $f_{3,4}$ to be doubtful, because they expect relativistic effects to be significant. They suggest that these form-factors should be taken to be free parameters of the model, to be fixed by experiment, but for the purposes of the discussion the form-factors are taken as given above. They take a pole-dominance form for $F(q^2)$, with pole mass $m_P = 6.8\,GeV$, corresponding to their estimate of the B_c^* resonance mass.

Note that in the limit $m_c = m_M$ one finds that $f_i^{AW}(q_{max}^2) = f_i^{SQ}(q_{max}^2)$, a correction of order 8% or less.

5.3.4 ISGW model

The model of Isgur, Scora, Grinstein and Wise [6,14,15] is based upon similar assumptions to the AW model, but with two main differences. Firstly, ISGW choose a particular form for the meson wave-functions (they use variational technique with the solutions of the harmonic oscillator), which can be used to estimate the reduced mass effects. Secondly, they use 'weak-binding' masses, $\tilde{m}_B \equiv m_b + m_q$ instead of meson masses, which introduces some uncertainty, since the quark masses are much less well constrained than the meson masses.

The ISGW calculation actually includes matrix elements for decays to all the low-lying ($c\bar{q}$) mesons, rather than just D and D^*, in an attempt to reproduce the inclusive spectrum near the lepton energy endpoint. Their results for decays to D and D^* can be written in the form

$$f_i^{ISGW}(q^2) = f_i^{ISGW}(q_{max}^2) \times F(q^2), \qquad i = (+, -, 1, 2, 3) \qquad (5.29)$$

where

$$F(q^2) = \exp\{-\beta(q_{max}^2 - q^2)/2m_B^2\}. \qquad (5.30)$$

Using the parameters given in [6], we find

$$\begin{aligned}
f_+^{ISGW}(q_{max}^2) &= 1.13 \\
f_-^{ISGW}(q_{max}^2) &= -0.539 \\
f_1^{ISGW}(q_{max}^2) &= 0.163 \, GeV^{-1} \\
f_2^{ISGW}(q_{max}^2) &= 6.83 \, GeV \\
f_3^{ISGW}(q_{max}^2) &= -0.146 \, GeV^{-1},
\end{aligned} \qquad (5.31)$$

(unfortunately, the form-factor f_4 is not given). As discussed in section 5.1 the result of the variational calculation is the exponential form (5.30), with the prediction of $\beta = 1.65$, after including a 'relativistic correction' factor.

We can compare the naive SQ form-factors of (5.20) and (5.21) with the more careful estimates of the overlap integrals of (5.31). At $q^2 = q^2_{max}$ we find

$$\frac{f_i^{ISGW}}{f_i^{SQ}} = 1.00, 1.06, 1.05, 0.95 \tag{5.32}$$

for the four form-factors which contribute to the $e\bar{\nu}$ and $\mu\bar{\nu}$ decay modes (that is $i = +$ for $\overline{B} \to Dl\bar{\nu}$ and $i = 1, 2, 3$ for $\overline{B} \to D^*l\bar{\nu}$ respectively), which gives a 5% change in $d\Gamma/dq^2$.

5.3.5 WSB model

The model of Wirbel, Stech and Bauer [4] is based on nearest meson dominace in the appropriate J^P crossed channel, matched at $q^2 = 0$. Unlike the KS model, WSB choose different pole masses for the different possible J^P values of the exchanged mesons. When decomposing the hadronic matrix elements of (4.65) and (4.66) the polarisation vectors corresponding to the different mesons are taken into account. For instance, in the $\overline{B} \to D$ transition this results in

$$\langle D|J^\mu|\overline{B}\rangle = \left((p_B + p_D)^\mu - \frac{m_B^2 - m_D^2}{q^2}q^\mu\right) F_{1-}(q^2) + \left(\frac{m_B^2 - m_D^2}{q^2}q^\mu\right) F_{0+}(q^2), \tag{5.33}$$

with $F_{1-}(0) = F_{0+}(0)$. The second term, corresponding to the emission of a 0^+ meson, is thus proportional to the meson's momentum q^μ, while the 1^- meson term is orthogonal to q^μ (angular momentum and parity conservation imply that only 0^+ and 1^- mesons are possible in this case). The form-factors $F_i(q^2)$ are chosen to have the form

$$F_i(q^2) = \frac{h_i}{1 - q^2/m_i^2}, \tag{5.34}$$

where the pole masses, determined by numerical estimates, are

$$m_{1-} = 6.34\,GeV \qquad m_{0-} = 6.80\,GeV. \tag{5.35}$$

The values of the form-factors at $q^2 = 0$ are obtained by describing the mesons as

relativistic bound-states in the infinite-momentum frame, which yields

$$h_{1-} = h_{0+} = 0.690. \tag{5.36}$$

In terms of the form-factors $f_{\pm}$ we may write

$$f_+^{WSB}(q^2) = F_{1-}(q^2)$$
$$f_-^{WSB}(q^2) = \frac{m_B^2 - m_D^2}{q^2} \left(F_{0+}(q^2) - F_{1-}(q^2) \right). \tag{5.37}$$

Since the pole positions of the two WSB form-factors are close, there is rough cancellation in f_-^{WSB}, with the result that it is much smaller than predicted in other models. However, matching at $q^2 = 0$ when there is a $1/q^2$ term in the hadronic matrix element of (5.33) may well result is the omission of important terms in the form-factors, making f_- and f_4 artificially small.

A similar matrix element decomposition for the $\overline{B} \to D^*$ matrix element can also be made [4], with terms corresponding to 1^-, 1^+ and 0^- spin-parities in the $b\bar{c}$ channel. The pole masses and h_i's are tabulated in ref. [16]. As with f_-^{WSB}, the form-factor f_4^{WSB} also turns out to be much smaller than in other models.

5.3.6 SP model

The final model we will take from the literature is that of Schöberl and Pietschmann [17]. This model, based on a quark-model calculation, gives, without detailed reasoning, the following form-factors

$$f_{\pm}^{SP}(q^2) = \sqrt{\frac{m_B^2 + m_D^2 - q^2}{2m_B^2}}$$
$$f_1^{SP}(q^2) = 0$$
$$f_2^{SP}(q^2) = \sqrt{2(m_B^2 + m_{D^*}^2 - q^2)} \tag{5.38}$$
$$f_3^{SP}(q^2) = 0,$$

with no correction for the wave-function overlap. The basis of this model is unclear and it is only really included for completeness, and to show that not all models are in perfect agreement with experiment.

5.3.7 FAC, MAX and MIN models

Except for SP the above models all extrapolate the hadronic form-factors from the quark model form-factors fixed at one particular value of q^2. However, the explicit forms for general q^2 given in (5.21) show that the form-factor f_2^{SQ} has a different behaviour to the other five form-factors and so it cannot be correct to assume exactly the same q^2-dependence for all of them.

There seems no reason to completely ignore this spin-overlap q^2-dependence, so we introduced the following factorisation ansatz [1,18,19] :

$$f_i^{FAC}(q^2) = f_i^{SQ}(q^2) \times F(q^2). \tag{5.39}$$

Such a factorisation of form-factors is motivated by the 'parton model' assumption that the binding force does not affect the spin-structure of the valence quark-antiquark pair; within the non-relativistic quark model this may be justified in the vicinity of $q^2 = q_{max}^2$, where the correlation between the spin and spatial wave-functions can be neglected and where the factor $F(q^2)$ can be interpreted as the overlap of the $\overline{B}$ and D (or D^*) spatial wave-functions. Of course, as a non-relativistic treatment may be questionable when dealing with mesons containing a light quark there is no guarantee that the ansatz of (5.39) will work, even in the vicinity of $q^2 = q_{max}^2$.

For the spatial wave-function overlap factor $F(q^2)$ we may use either the exponential form (5.4) or the pole-dominated form (5.1), as there is no clear reason to show one is superior, as explained above. In fact we use the pole-dominance form, with the same pole mass as KS, $m_P = 6.34\,GeV$.

Two other variations of the FAC model are also of interest:

$$\begin{aligned} f_i^{MAX}(q^2) &= f_i^{SQ}(q_{max}^2) \times F(q^2) \\ f_i^{MIN}(q^2) &= f_i^{SQ}(0) \times F(q^2). \end{aligned} \tag{5.40}$$

These incorporate the two philosophies of matching at $q^2 = 0$ and $q^2 = q_{max}^2$ respectively. Comparison of (5.40) and (5.39) shows that FAC agrees with MAX at $q^2 = q_{max}^2$ and with MIN at $q^2 = 0$ (hence the names). The predictions of MAX are thus similar to those of AW and ISGW, while those of MIN are similar to those of KS and WSB. By comparing the predictions within these two groups it is possible to see the effect of slight changes in normalisation of the form-factors.

5.4 Comparison of models

The above discussions include the most commonly used form-factor models (BSW, ISGW and KS), although one could be forgiven for thinking that their use by CLEO and ARGUS stems from the geographical locations of the various institutions. We introduced the FAC model in order to include the full q^2-dependence predicted by the meson spins, and the MAX and MIN models to see the effect of ignoring this dependence. The 9 models (SQ, FAC, MAX, MIN, KS, ISGW, WSB, AW and SP) are derived from various different physical pictures, which we will now compare. Firstly, the SP model is very different from any of the others. Its physical basis is unclear, and it turns out to be incompatible with most of the experimental data for $b \rightarrow c$ decays (see chapter 6).

The WSB and KS models both use pole-dominance for calculating the q^2-dependence. The KS model also uses the spectator quark approach to calculate the spin wave-function overlap at $q^2 = 0$, which seems to be self-contradictory, as the two pictures, shown in fig.5.1, are very different views of the hadronic transition. The WSB model is entirely based upon the vector-meson dominance hypothesis of fig.5.1(a) but does seem to be unreliable in its prediction of the two extra form-factors relevant to decays to τ leptons, because of its matching at $q^2 = 0$, as discussed above.

The remaining six models are all based upon the spectator quark approach, as depicted in fig.5.1(b). The q^2-dependence of the form-factors is derived by assuming that the spin and spatial wave-function overlaps factorise when the outgoing meson is at rest in the $\overline{B}$ rest-frame (i.e. at $q^2 = q^2_{max}$). Since the non-relativistic quark model is only valid in this region, many models (ISGW, AW, MAX) ignore the q^2-dependence of the spectator quark model form-factors of (5.20) and (5.21), and use a common q^2 variation for all of them. However, under the 'parton-model' assumption that the binding force does not affect the spin-structure of the valence quark-antiquark pair, it seems reasonable to use the full q^2-dependence of the f_i^{SQ}. Furthermore, as stated in section 5.3.7, in the vicinity of q^2_{max}, the form-factor f_2^{SQ} behaves differently to the other form-factors, so making the assumption of equal q^2-dependence for all form-factors dubious. Both SQ and FAC models do include this 'full' dependence. The MIN model, which uses matching at $q^2 = 0$ does not really have a firm basis in this approach, which is only justifiable at q^2_{max}. However,

it is included as a simplified version of KS (it does not have dipole form-factors).

The spatial overlap $F(q^2)$ for these spectator models is harder to determine. Only the ISGW approach actually predicts it (the exponential form of (5.4)), but the naive calculation is again only valid at q^2_{max}. However, by including the 'relativistic correction factor' as explained in section 5.1, and using the exponential form-factor at all q^2, good agreement with experiment is obtained. Since there is little variation between the pole and exponential overlap functions, as shown in fig.5.2, we choose to use the pole form in FAC, MAX and MIN, even though we actually believe the hadronic transition does not involve an intermediate $b\bar{c}$ state. Comparison of SQ and FAC allows us to see the overall effect of the spatial overlap function $F(q^2)$.

In section 4.11 it was shown how precise measurements of the q^2 spectra and angular correlations of decay products could be used to determine the form-factors. If we assume a particular model, we can use the measurements to determine $F(q^2)$ instead, up to an overall normalisation. Since most of the models use a common overlap there is no need to do the full angular analysis, as then $d\Gamma/dq^2 \propto |F(q^2)|^2$, for decays to both D and D^*.

A final point to note is that the models ISGW and SP do not give predictions for the form-factor $f_4(q^2)$ and so cannot be used to predict the decay $\overline{B} \to D^* \tau \overline{\nu}$.

The most basic comparison of the models is given by their predictions of the six form-factors, as shown in fig.5.4 (for $\overline{B} \to D$) and fig.5.5 (for $\overline{B} \to D^*$). The most striking feature of the graphs is that the SP model is very different from all the others, due to f_1 and f_3 being zero, and the lack of any wave-function overlap. The WSB model is only significantly different in its predictions for f_- and f_4, which are both much smaller than those of the other models. Clearly this can only affect the predictions for decays involving τ leptons. The wave-function overlap $F(q^2)$ has a large effect, as can be seen by comparing the SQ and FAC models, which are otherwise identical. For f_+, f_- and f_2 the gradients of the ISGW and KS predictions are very similar, as expected from the similarity of the exponential and pole form-factors. However, this is clearly not true for f_1 and f_3, where the KS model uses dipole form-factors. A comparison of the slopes of the FAC and ISGW predictions shows the effect of including the spin-overlap q^2-dependence.

Comparison of the hadronic matrix elements shown in fig.5.6, which are just
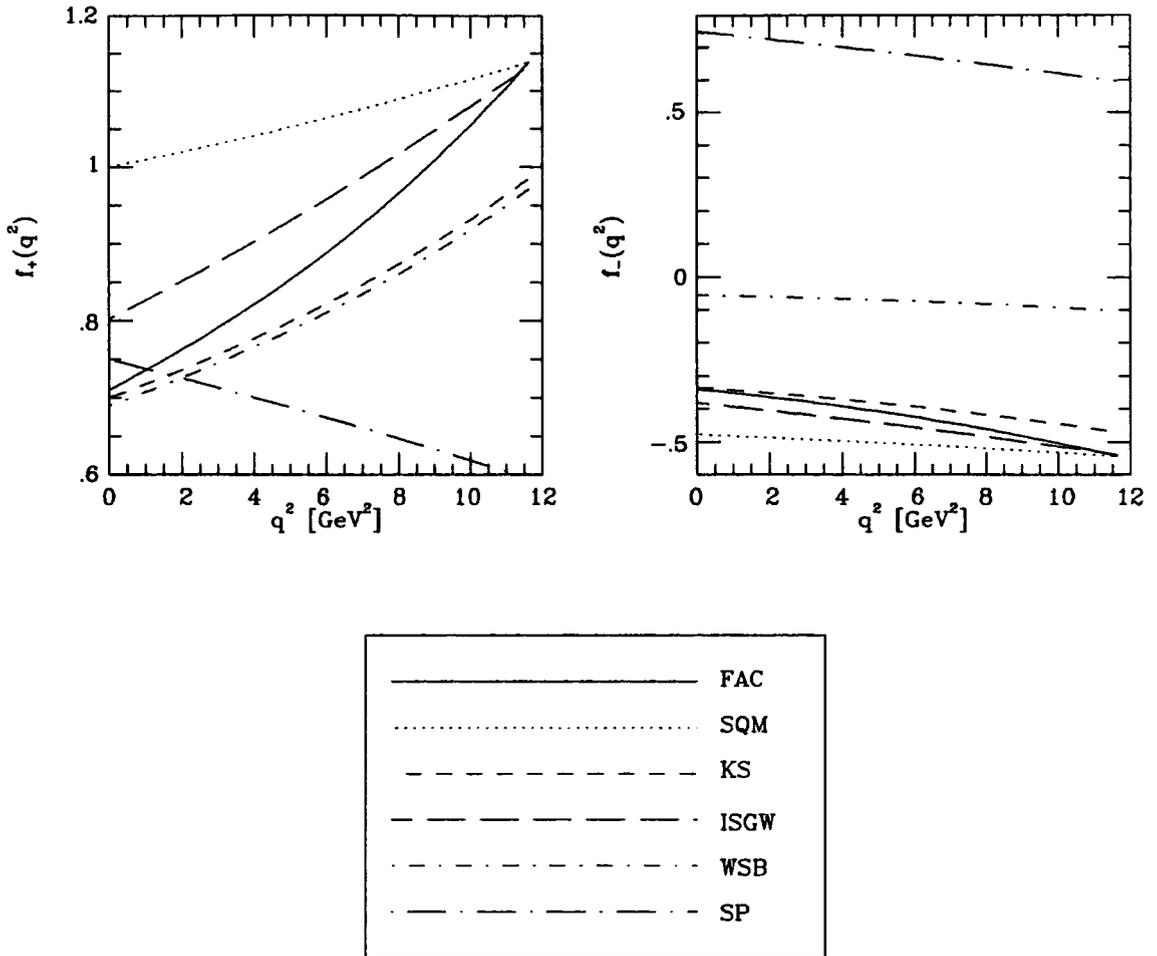
Figure 5.4 The hadronic form-factors $f_\pm(q^2)$, of (4.65), which are relevant for the decay $\overline{B} \to D l \overline{\nu}$, for six of the models discussed in the text.

linear combinations of the six form-factors, as given by (4.69) and (4.70), show little variation for the case $\overline{B} \to D$, in spite of the very low prediction for $f_-(q^2)$ given by WSB. The $\overline{B} \to D^*$ matrix elements show much greater spread, particularly in the case of SP. Note that some of the scales have a suppressed zero.

Predictions for x and q^2 spectra, as given by five representative models, are given in figs.5.7 and 5.8 respectively. These figures include the rates to the three helicity states of the D^* meson (even though not directly observable). Simple kinematical arguments can be used to check some of the features of the graphs, with reference to the Dalitz plot of fig.4.3, by considering the $\overline{B}$ meson rest-frame of fig.4.2. Firstly, at high x (high lepton energy) we have $q^2 \approx 0$, which means, from (4.8), that the outgoing meson is also highly energetic, and therefore moving
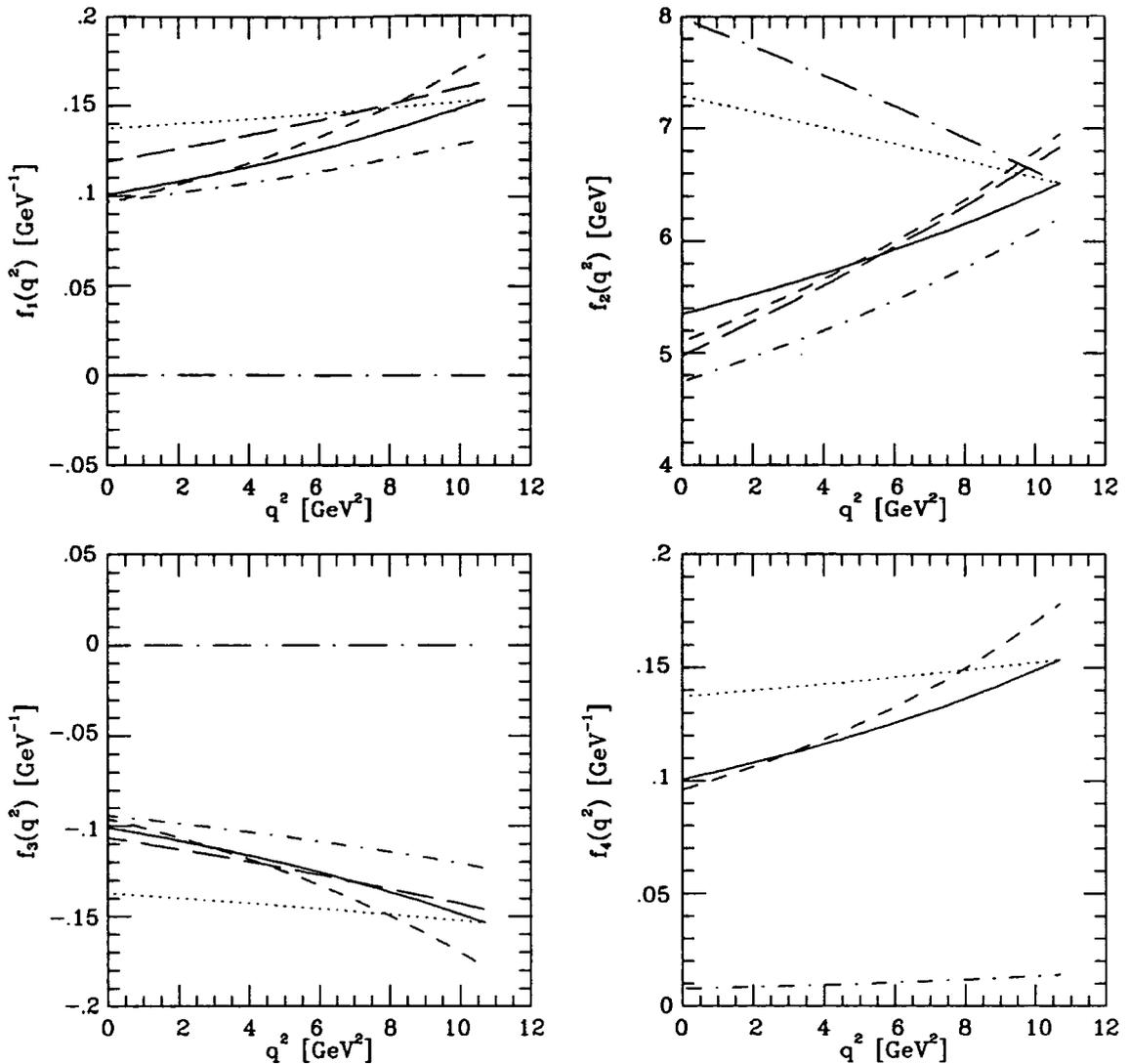
Figure 5.5   The hadronic form-factors $f_i(q^2)$ for $i = 1, 2, 3, 4$, of (4.66), which are required for the prediction of the decay $\overline{B} \to D^* l \overline{\nu}$. The key is given in fig.5.4.

in the opposite direction to the lepton, while the antineutrino has very low energy. Since the decaying $\overline{B}$ meson was spin-0, and the lepton has negative helicity, conservation of angular momentum tells us that the produced meson cannot be right-handed, as demonstrated by the spectra of fig.5.7. Similarly, at low x we again have $q^2 \approx 0$, so the antineutrino and meson are back-to-back and the meson cannot be left-handed, as again shown by fig.5.7. Finally, at $q^2 = 0$, where again the outgoing meson has maximum energy, we expect both lepton and antineutrino to be moving along the negative z-axis, so that the meson must have helicity zero in the z-direction, as shown by fig.5.8. This also demonstrates the point raised in

99
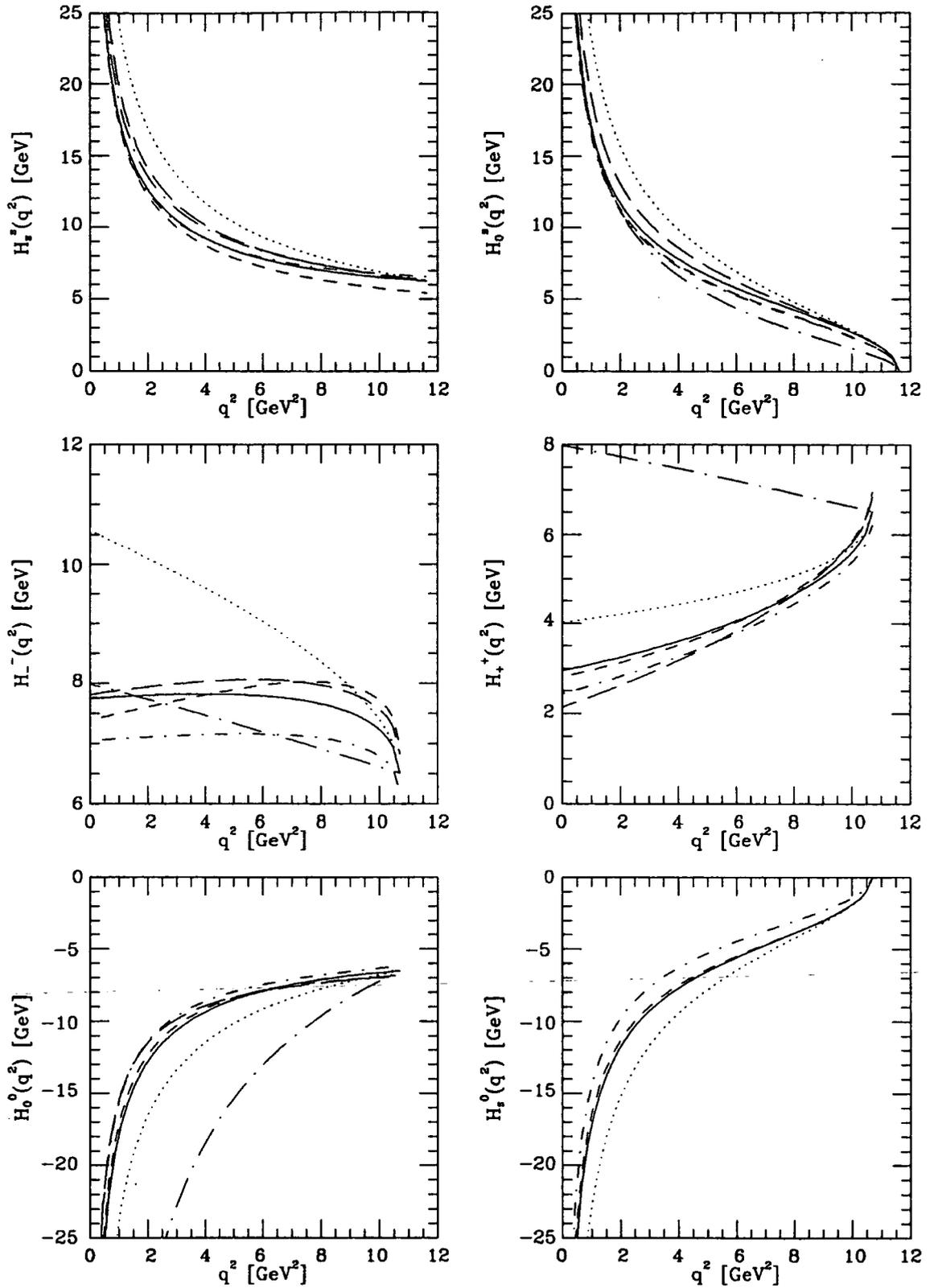
Figure 5.6 The six hadronic matrix elements of (4.69) and (4.70), as predicted by the six models used in fig.5.4.

100
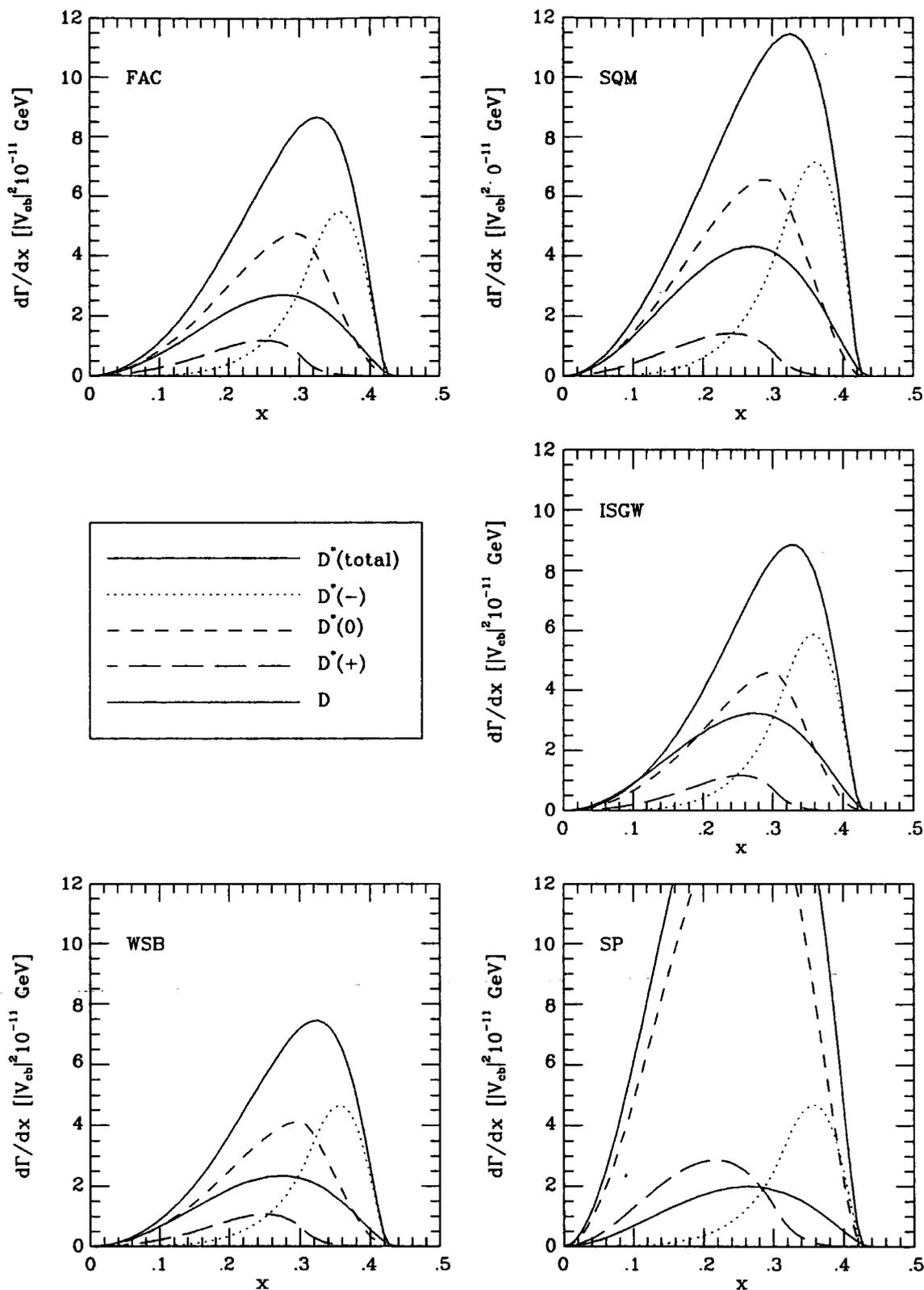
Figure 5.7   Lepton energy spectra of five representative models, for the decays $\overline{B} \to Dl\overline{\nu}$ and $\overline{B} \to D^*l\overline{\nu}$. The partial rates to the various possible helicities of the D^* are also shown.
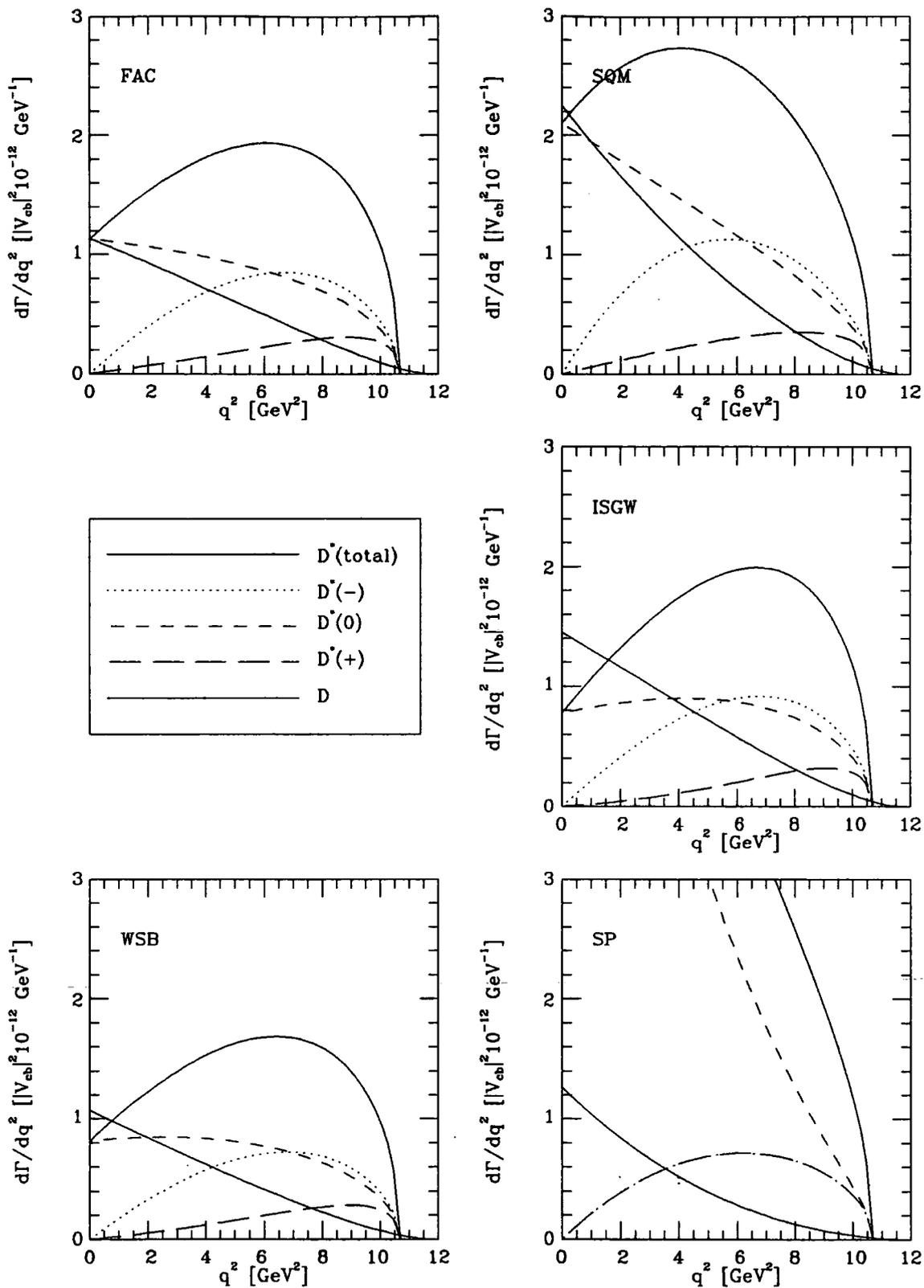
Figure 5.8 q^2 spectra of five representative models, for the decays $\overline{B} \rightarrow Dl\overline{\nu}$ and $\overline{B} \rightarrow D^*l\overline{\nu}$. The partial rates to the various possible helicities of the D^* are also shown.

section 4.11, that while $H_{\pm}^{\pm}(q^2) \to 0$ as $q^2 \to 0$, $H_0^0(q^2)$ does not.

The prediction of SP for the decay to the helicity zero D^* is huge. This is because in all other models there is a rough cancellation in H_0^0 of (4.70) since f_2 and f_3 are of opposite sign. Since $f_3 = 0$ in SP this cancellation does not occur, leading to the large contribution from such decays. The effect is also noticeable in the decay to positive helicity D^*, although the effect is smaller since the cancellation in H_+^+ is less complete. Apart from this model all spectra are similar in shape and relative size, and differ significantly only in overall normalisation.

Finally fig.5.9 shows the predictions for the angular distribution parameters $\beta_i(q^2)$. Ideally the above figures would include the experimental cut on the lepton momentum, but since the CLEO and ARGUS collaboration both insist on extrapolating to the whole momentum range this does not seem worthwhile. Note again that the model predictions are very similar (with the exception of SP), which unfortunately means that distinguishing between models will be very difficult. The predictions for FAC and SQ are identical, since the wave-function overlap factor $F(q^2)$ cancels in the ratios of (4.81).

5.5 Conclusion

This chapter describes several models of the hadronic form-factors currently in use. In general they are all in close agreement with each other numerically, in spite of their different physical bases. This will unfortunately make it difficult to test the physical ideas behind the models without very precise experimental measurements, which are not yet available.

The determination of the form-factor normalisation at q_{max}^2 is vital to the accurate determination of the KM matrix element $|V_{cb}|$. The comparison between models seems to indicate that this is known to within a few percent, but the problem deserves more careful study.
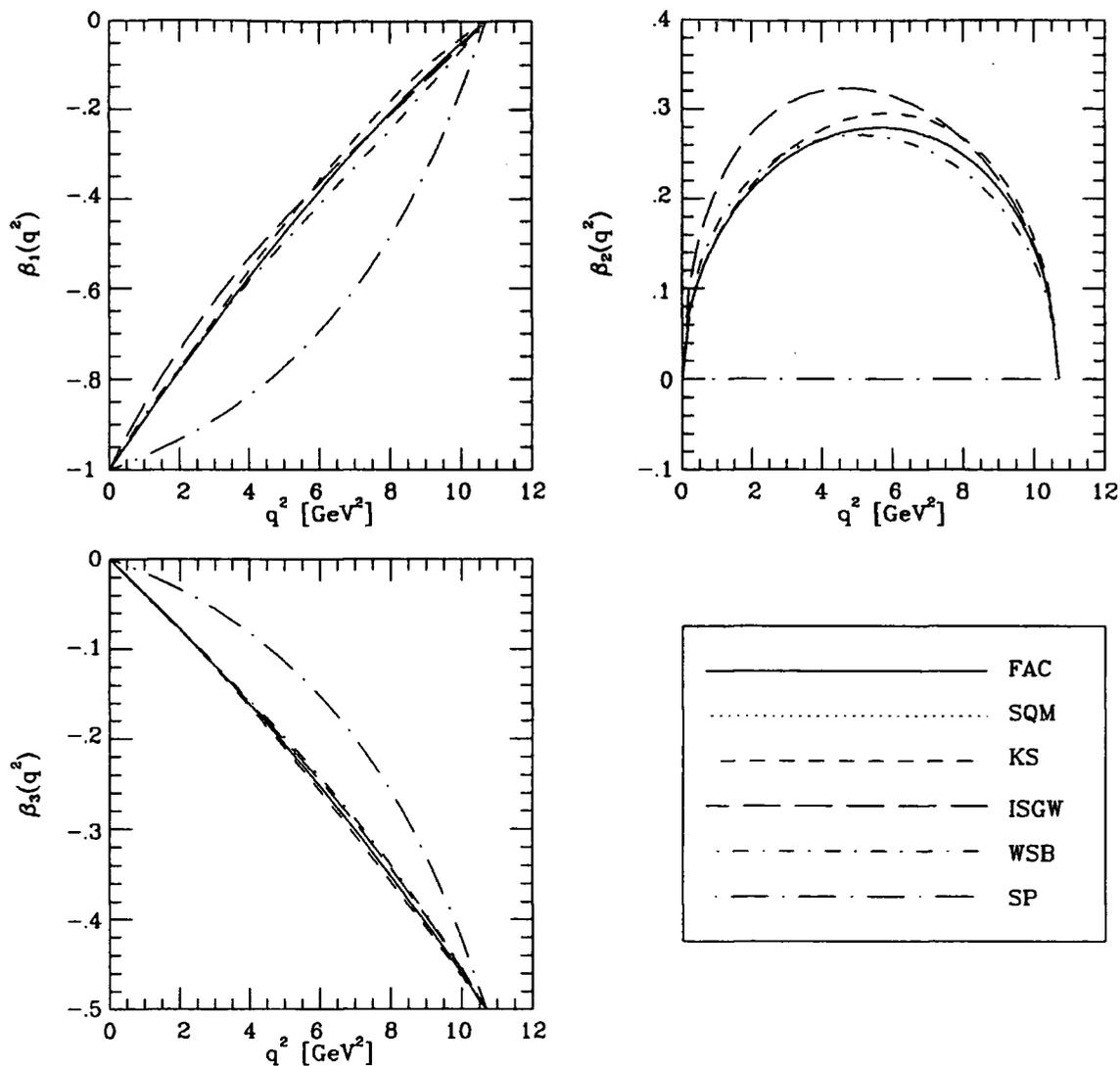
Figure 5.9 Angular asymmetry parameters $\beta_i(q^2)$ of (4.81), for the six models shown in the key.

References

1. K. Hagiwara, A.D. Martin and M.F. Wade, *Nucl. Phys.* **B327**, 569 (1989).

2. J.G. Körner and G.A. Schuler, *Z. Phys.* **C38**, 511 (1988).

   J.G. Körner and G.A. Schuler, *Phys. Lett.* **B226**, 185 (1989).

   J.G. Körner and G.A. Schuler, *Phys. Lett.* **B231**, 306 (1989).

3. J.G. Körner and G.A. Schuler, *Z. Phys.* **C46**, 93 (1990).

4. M. Wirbel, B. Stech and M. Bauer, *Z. Phys* **C29**, 637 (1985).

   M. Bauer and M. Wirbel, *Z. Phys.* **C42**, 671 (1989).

5. K. Hagiwara, private communication.

6. N. Isgur, D. Scora, B. Grinstein and M.B. Wise, *Phys. Rev.* **D39**, 799 (1989).

7. T. Altomari and L. Wolfenstein, *Phys. Rev.* **D37**, 681 (1988).

8. Particle Data Group: Review of Particle Properties, *Phys. Lett.* **B239**, 1 (1990).

9. J.C. Anjos et al., FERMILAB-PUB-90-124-E (June 1990).

10. R. Fulton et al., CLNS 90/989 (August 1990).

11. M. Danilov, DESY 89-147 (November 1989).

12. M. Suzuki, *Nucl. Phys.* **B258**, 553 (1985).

13. M.B. Voloshin and M.A. Schifman, *Sov. J. Nucl. Phys.* **45**, 292 (1987).

14. B. Grinstein, M.B. Wise and N. Isgur, *Phys. Rev. Lett.* **56**, 298 (1986).

15. N. Isgur and D. Scora, *Phys. Rev.* **D40**, 1491 (1989).

16. M. Wirbel, B. Stech and M.Bauer, *Z. Phys.* **C34**, 103 (1987).

17. F. Schöberl and H. Pietschmann, *Europhys. Lett.* **2**, 583 (1986).

18. K. Hagiwara, A.D. Martin and M.F. Wade, *Phys. Lett.* **B228**, 144 (1989).

19. K. Hagiwara, A.D. Martin and M.F. Wade, *Z. Phys.* **C46**, 299 (1990).

6 Comparison of Exclusive Models with Experiment and Determination of $|V_{cb}|$ and $|V_{ub}|$

Our best is bad, nor bears Thy test;
Still, it should be our very best.

Robert Browning, 1812-1889

6.1 Introduction

Ideally we would like to perform the model-independent analysis described in section 4.11, in order to extract the q^2-dependence of the $\overline{B} \rightarrow D$ and $\overline{B} \rightarrow D^*$ form-factors. Unfortunately, the semileptonic B decay data is not yet anywhere near precise enough for this, or even to try to extract the q^2-dependence of the spatial overlap of the initial and final meson wave-functions, as described in section 5.4. All we can do at present is try to determine which of the models are compatible with experiment, and then extract the model predictions for the KM matrix elements $|V_{cb}|$ and $|V_{ub}|$. Of course, many of the models have variable parameters in them, so disagreement with experiment will not immediately rule them out. As will be seen below, the models are all in good agreement with experiment, except for SP, so no adjustment of parameters is yet necessary. Further data is required before the models can be seriously tested.

In the analysis below it will be assumed, for convenience, that the $\Upsilon(4S)$ branching fractions to B^+B^- and $B^0\overline{B^0}$ pairs, introduced in section 3.5.1, are

$$f_{+-} = f_{00} = 0.5. \tag{6.1}$$

However, any changes to this assumption can easily be incorporated, since the branching ratios are inversely proportional to the relevant branching fraction f.

6.2 Testing the Models

Before trying to predict the KM matrix elements, we will first compare the models with the data given in chapter 3. For this purpose we can use the ratio R of semileptonic $\overline{B}$ decays to vector (D^*) and pseudoscalar (D) states, the E_l and q^2 spectra, and the angular asymmetry parameter α for $\overline{B} \rightarrow D^* \rightarrow D\pi$ decay (as defined in (4.85)).

6.2.1 The Vector to Pseudoscalar Ratio R

The vector to pseudoscalar (V/PS) ratio R of (3.7), which is independent of the $\Upsilon(4S)$ branching fractions, is measured to be [1,2]

$$R \equiv \frac{\Gamma(\overline{B} \to D^*l\overline{\nu})}{\Gamma(\overline{B} \to Dl\overline{\nu})} = 2.6^{+1.1+1.0}_{-0.6-0.8} \quad \text{(CLEO)}$$
$$= 3.3^{+3.7}_{-1.1} \quad \text{(ARGUS)} \quad (6.2)$$

Table 6.1 shows the model predictions for the total rates to D and D^* mesons, along with the V/PS ratio.

Model	$\overline{B} \to Dl\overline{\nu}$	$\overline{B} \to D^*l\overline{\nu}$	R
FAC	6.1	17.2	2.8
SQ	10.1	24.2	2.4
MAX	7.4	14.3	1.9
MIN	5.7	19.6	3.4
KS	5.5	17.3	3.1
ISGW	7.4	16.7	2.3
WSB	5.4	14.6	2.7
AW	8.3	15.6	1.9
SP	4.8	46.0	9.6

Table 6.1. Exclusive decay rates (to $l = e, \mu$) and the vector to pseudoscalar ratio R of (6.2), as predicted by the models defined in section 5.3. All the decay rates are given in units of $10^{-12}|V_{cb}|^2\,GeV$.

Comparison of the predictions of R with the experimental values of (6.2) shows that all models except SP are in good agreement with the data. However, the predictions are far enough apart to give encouragement to the hope that they might be distinguishable in time. It must be noted here that changing any of the variable parameters of the models, such as m_P of (5.1) or β of (5.4), will affect the V/PS ratio R. The total rates all show reasonable agreement between models, except for the spectator quark model (SQ), which is slightly high due to lack of suppression by the spatial overlap, and the unmotivated SP model, which predicts an enormous rate for decays to D^* mesons.

Unfortunately the only available spectra for exclusive B decays are the AR-GUS E_l and q^2 spectra for the decay $\overline{B} \to D^* l\overline{\nu}$, which are shown in figs.6.1(d) and 6.2(d) respectively. Since we are trying to determine $|V_{cb}|$ we do not know the normalisation of the predictions, and can thus only test their shapes. With enough data we will be able to determine the spatial wave-function overlap $F(q^2)$ as discussed in section 5.4, if the data is made available without using the model-dependent extrapolations currently employed. Figs.6.1 and 6.2 are organised as follows: (a) and (b) show the spectra for $\overline{B} \to D l\overline{\nu}$, while (c) and (d) show those for $\overline{B} \to D^* l\overline{\nu}$. The curves of (b) and (d) are normalised by the total rate, to allow comparison of the predicted shapes with the experimental data.

For the lepton energy spectra the predictions all have very similar shapes (except for SP), and it is only the normalisations that differentiate between them at present. For the q^2 spectra the predictions are again very similar in shape, the only significant differences being the SQ and SP models. The great similarity between most of the q^2 spectra demonstrates how difficult it will be to distinguish between models, except by extremely precise measurements. Comparison with the ARGUS data shown in figs.6.1(d) and 6.2(d) shows that only SP is incompatible.

6.2.3 The D^* Decay Angular Distribution Parameter α

The $D^* \to D\pi$ decay angular distribution parameter α, discussed in section 4.11, is measured to be [3,4]

$$
\begin{aligned}
\alpha &= 0.65 \pm 0.66 \pm 0.25. &\quad \text{CLEO} &\quad (E_l > 1.0\,GeV) \\
\alpha &= 0.7 \pm 0.9 &\quad \text{ARGUS} &\quad (E_l > 1.4\,GeV).
\end{aligned}
\tag{6.3}
$$

The decay angular spectra are given in refs. [3,4], but there is little point in reproducing them here. Because the lepton energy cuts are not the same it is not possible to combine the two measurements.

The predictions for the decay angular distribution parameter α are shown in table 6.2, for the values of the lepton energy cut used in the experiments, and also for no cut, for comparison.
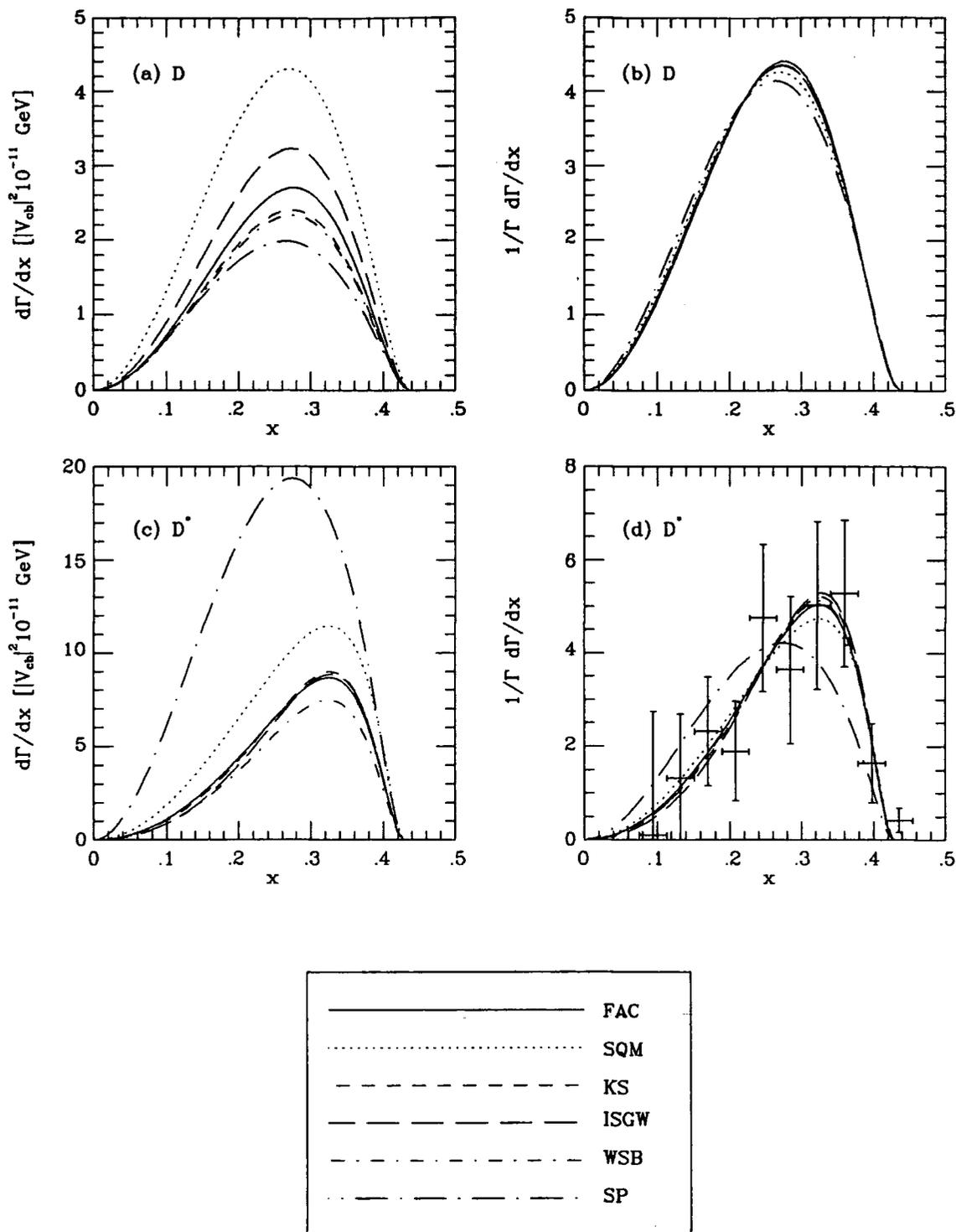
Figure 6.1 Lepton spectra for $b \to c$ decays, for the six models shown in the key. (a) and (b) are for $\overline{B} \to Dl\overline{\nu}$, while (c) and (d) are for $\overline{B} \to D^* l\overline{\nu}$. The spectra of (b) and (d) have been normalised by their corresponding total rates in order to allow comparison with the experimentally measured spectrum from ARGUS [3].
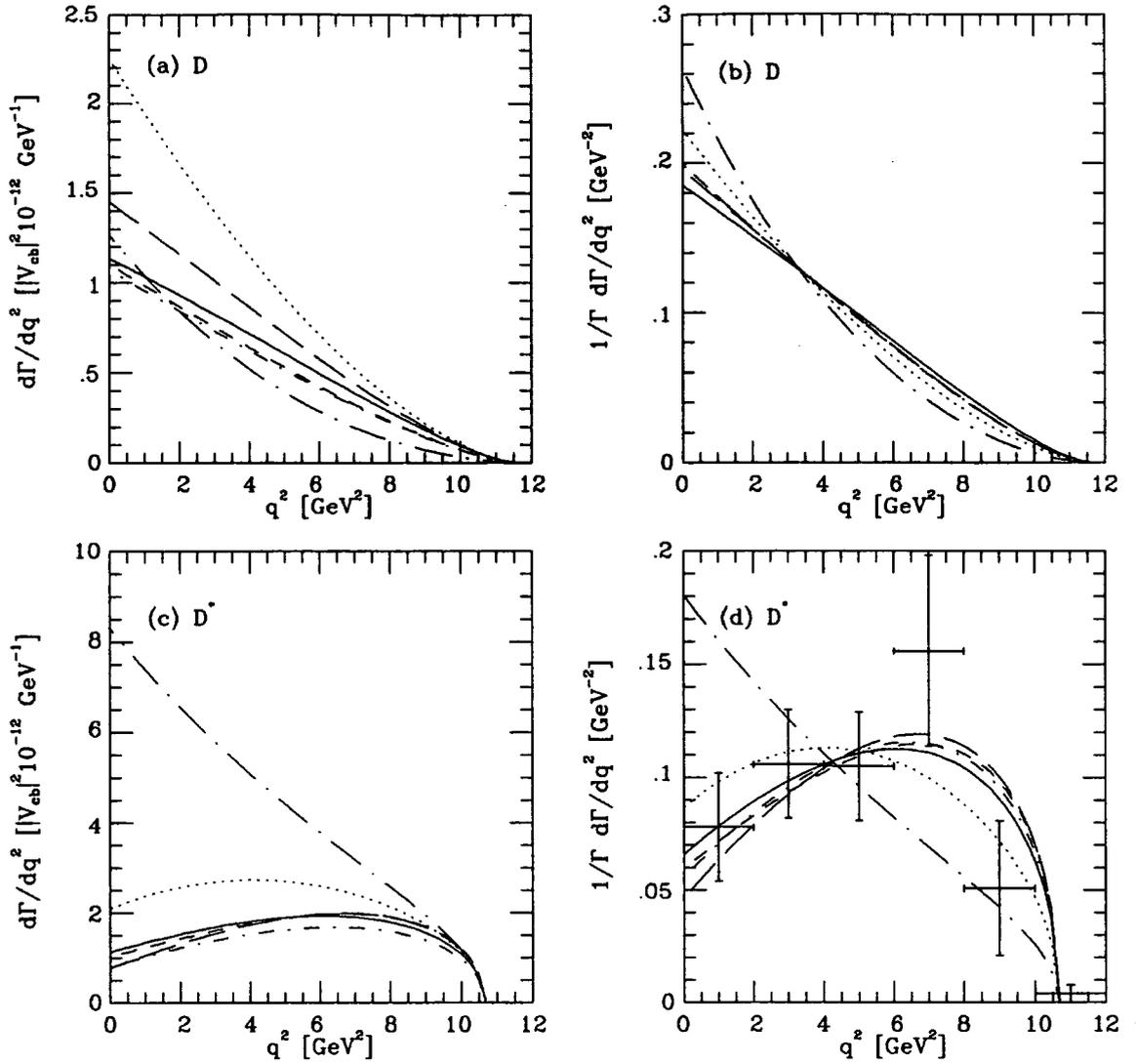
Figure 6.2 q^2 spectra for $b \to c$ decays. (a) and (b) are for $\overline{B} \to Dl\overline{\nu}$, while (c) and (d) are for $\overline{B} \to D^*l\overline{\nu}$. The spectra of (b) and (d) have been normalised by their corresponding total rates in order to allow comparison with the experimentally measured spectrum from ARGUS [3]. The key to the models used can be found in fig.6.1.

Model	$E_l > 0.0\,GeV$	$E_l > 1.0\,GeV$	$E_l > 1.4\,GeV$
FAC	1.19	0.90	0.44
SQ	1.41	1.06	0.53
MAX	0.75	0.56	0.19
MIN	1.27	1.01	0.55
KS	1.06	0.80	0.36
ISGW	0.93	0.70	0.29
WSB	1.16	0.90	0.45
AW	0.82	0.58	0.19
SP	5.38	5.04	4.07
Expt.	–	0.7±0.9 [3]	0.65±0.71 [4]

Table 6.2. D^* angular decay parameter α of (4.85), as predicted by the models discussed in section 5.3, for various values of lepton energy cutoff, appropriate to the experimental results.

The measured values of α have such large errors that they are still compatible with zero, and with all the models (again except for SP). Again, changing the spatial overlap function $F(q^2)$ will change the prediction for α, as can be seen, for instance, from the differences between the predictions of the FAC and SQ, which differ only by $F(q^2)$.

6.2.4 Conclusions

Having compared the models with the existing data, we can, unfortunately, only rule out the SP model. All the other models are easily compatible with the tests that can be performed at the current level of accuracy, and we must wait for more data before any precision tests can be carried out. Given the ability to change $F(q^2)$ it will probably require a combination of all the above tests and very precise experimental measurements to distinguish between any of the models except SQ and SP, which have no free parameters.

6.3 Determination of $|V_{cb}|$

Given that above tests only exclude the SP model, we can now turn our at-

tention to the determination of $|V_{cb}|$ from the exclusive branching ratios given in chapter 3. The CLEO collaboration gives [1]

$$\mathrm{Br}(B^- \to D^0 l^- \overline{\nu}) = (1.6 \pm 0.6 \pm 0.3)\%$$

$$\mathrm{Br}(\overline{B^0} \to D^+ l^- \overline{\nu}) = (1.8 \pm 0.6 \pm 0.3)\%$$

$$\mathrm{Br}(B^- \to D^{*0} l^- \overline{\nu}) = (4.1 \pm 0.8^{+0.8}_{-0.9})\%$$

$$\mathrm{Br}(\overline{B^0} \to D^{*+} l^- \overline{\nu}) = (4.6 \pm 0.5 \pm 0.7)\%$$

(6.4)

while ARGUS quotes [2]

$$\mathrm{Br}(\overline{B^0} \to D^+ l^- \overline{\nu}) = (1.7 \pm 0.6 \pm 0.4)\%$$

$$\mathrm{Br}(\overline{B^0} \to D^{*+} l^- \overline{\nu}) = (5.4 \pm 0.9 \pm 1.3)\%.$$

(6.5)

On adding the statistical and systematic errors in quadrature and then combining the results of the two groups we obtain (assuming that $\tau_{B^\pm} = \tau_{B^0}$)

$$\mathrm{Br}(\overline{B} \to D l^- \overline{\nu}) = (1.7 \pm 0.4)\%$$

$$\mathrm{Br}(\overline{B} \to D^* l^- \overline{\nu}) = (4.6 \pm 0.6)\%.$$

(6.6)

Assuming the compatability of the models with the above experimental constraints, the mean branching ratios may be combined with the measured B-meson lifetime [5] $\tau_B = (1.18 \pm 0.11) \times 10^{-12}\,s$, and the theoretical predictions of table 6.1, to predict the value of the KM matrix element $|V_{cb}|$, as shown in table 6.3.

Model	$\overline{B} \to D l^- \overline{\nu}$	$\overline{B} \to D^* l^- \overline{\nu}$
FAC	0.039 ± 0.007	0.039 ± 0.005
SQ	0.031 ± 0.005	0.033 ± 0.004
MAX	0.036 ± 0.006	0.042 ± 0.005
MIN	0.041 ± 0.007	0.036 ± 0.004
KS	0.042 ± 0.007	0.039 ± 0.005
ISGW	0.036 ± 0.006	0.039 ± 0.005
WSB	0.042 ± 0.007	0.042 ± 0.005
AW	0.034 ± 0.006	0.041 ± 0.005
(SP	0.044 ± 0.007	$0.024 \pm 0.003)$

Table 6.3. Model values of $|V_{cb}|$, using the experimental mean branching ratios of (6.6).

A simple averaging of the above models, omitting SQ and SP, yields the result

$$|V_{cb}| = 0.039 \pm 0.004 \pm 0.003, \qquad (6.7)$$

where the first error is experimental, and the second represents the variation between the models as an estimate of the theoretical error. Note that this is of course still dependent upon the above assumptions about the $\overline{B^0}$ and B^- lifetimes and the production ratios f_{00} and f_{+-}, and on the form-factor normalisation at q^2_{max}.

At present we are not able to learn much about the physics occuring in the hadronic transition. To do so we will need much more precise data than is currently available. For instance, with a sufficiently accurate determination of the q^2 spectra, we should be able to determine the spatial overlap $F(q^2)$ well enough to know whether the pole-dominated form of (5.1) is compatible with the data for a reasonable value of the pole mass m_P.

6.4 Model Dependence

In the previous section we used the difference between model predictions in order to estimate the model-dependence. As an alternative to this we now consider the effect of varying the parameter m_P that appears in the spatial overlap function $F(q^2)$ discussed in section 5.1, using the FAC model as an example. As the fitting uses the ARGUS x and q^2 spectra of fig.6.1(d) and 6.2(d) we will use only the ARGUS data, rather than the combined results used above.

The determination of $|V_{cb}|$ above has not used this fit to the data for several reasons. Firstly, the data values used have been read from the graphs of ref. [3], which introduces some error, particularly in the case of the $10.0\,GeV \leq q^2 \leq 12.0\,GeV$ bin, where the experimental error is very small. Secondly, the quoted errors for the other data points are still very large, and the value $m_P = 6.34\,GeV$ is easily compatible with the data (in fact we shall see that arbitrarily large values of m_P are possible).

The FAC model predictions for the total exclusive semileptonic rates, as a function of m_P are shown in fig.6.3(a), and the V/PS ratio is shown in figure.6.3(b), with the ARGUS experimental result included. For each value of m_P the x and q^2 spectra are fitted to the ARGUS results, varying the normalisation (i.e. $|V_{cb}|$) to
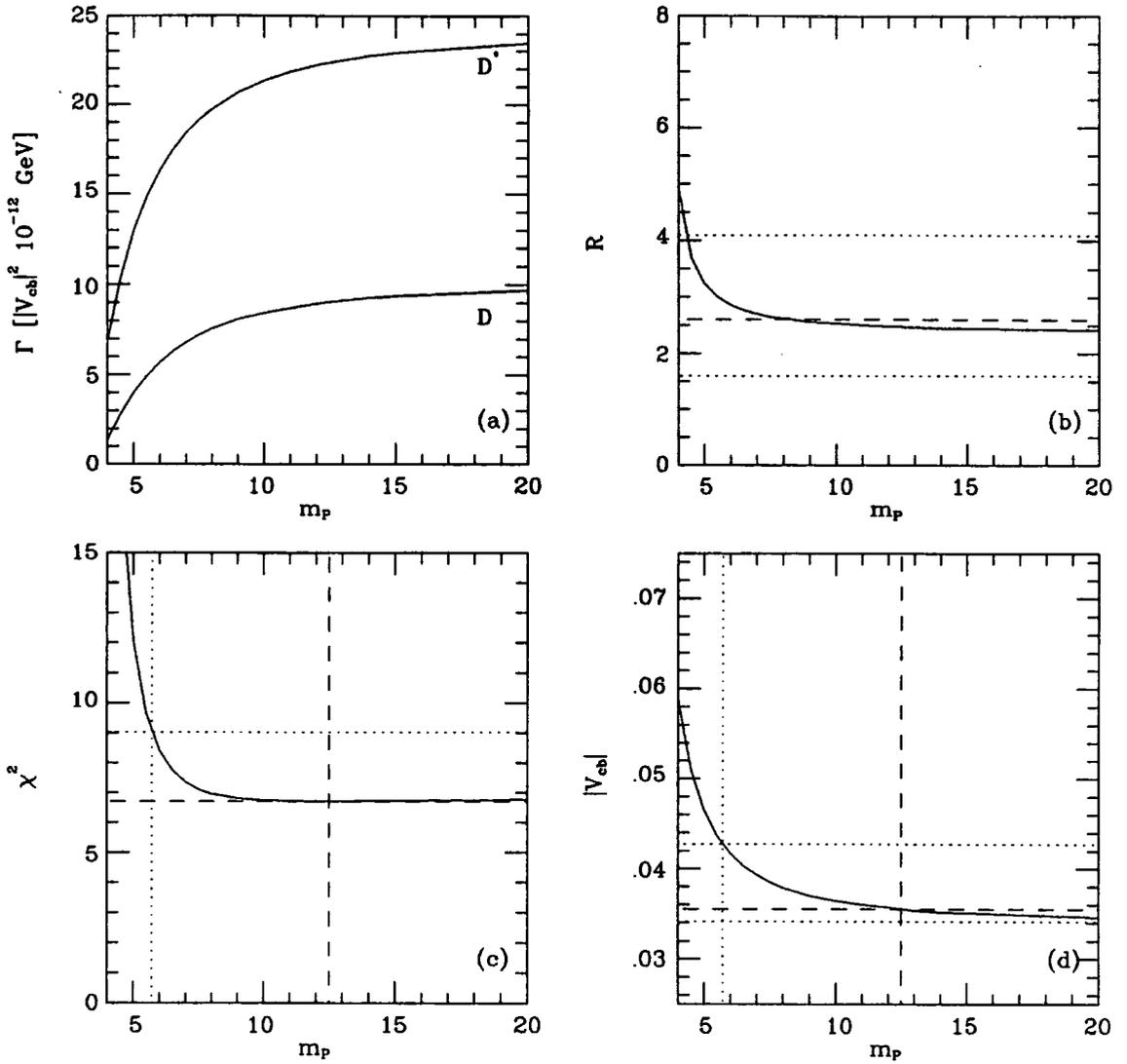
Figure 6.3 The results of the fit of the FAC model of section 5.3.7 to the ARGUS $\overline{B} \rightarrow D^* l \overline{\nu}$ spectra of figs.6.1(d) and 6.2(d). Figs.6.3(a) and (b) show the total rates for the decays $\overline{B} \rightarrow D, D^* l \overline{\nu}$ and the V/PS ratio R of (6.2) as a function of m_P, with the ARGUS experimental result for the latter included. Fig.6.3(c) shows the χ^2 variation, with the best-fit (dashed lines) and 1σ-limit (dotted lines). Finally, fig.6.3(d) shows the corresponding fitted values of $|V_{cb}|$, again with the central value and 1σ errors marked (the lower error corresponds to $m_P = \infty$).

minimise the χ^2. Fig.6.3(c) shows this χ^2 as a function of m_P. The best fit occurs at $m_P \approx 12.5\,GeV$, with $\chi^2 = 6.72$, although any larger value fits the data well (for $m_P = \infty$, which is the same as the spectator quark model, the fit gives $\chi^2 = 6.84$). Considerably lower m_P values are also compatible; taking $\Delta\chi^2 \equiv \chi^2 - \chi^2_{min} = 2.30$ (for two free parameters, m_P and $|V_{cb}|$) as an estimate for the 1σ variation, we find that $m_P \gtrsim 5.7\,GeV$.

The corresponding values for $|V_{cb}|$ are shown in fig.6.3(d). Using the above range of χ^2 values, we find

$$|V_{cb}| = 0.036^{+0.007}_{-0.002}, \qquad (6.8)$$

with the upper limit corresponding to $m_P = 5.7\,GeV$, the central value to $m_P = 12.5\,GeV$, and the lower limit to $m_P = \infty$. The lower limit is slightly artificial, since the form of $F(q^2)$ used is a non-decreasing function of q^2, as is expected from its interpretation as the overlap of spatial wave-functions. The value $m_P = 6.34\,GeV$ used previously also fits the data well, giving $|V_{cb}| = 0.041$.

The size of the upper error from this determination of $|V_{cb}|$ is close to that obtained by comparison of calculated rates and branching ratios above, but the central value is different, mainly because only the ARGUS data is being used, and the value of m_P is different.

The V/PS ratio changes from 2.94 down to 2.39 over the given m_P range, which is well within the ARGUS errors quoted in (6.2). This demonstrates how important it is to have measurements of the x and q^2 spectra, since the only other real test of the models is the V/PS ratio. The use of the equivalent spectra for $\overline{B} \to D$ decays would also help greatly in determining the form of $F(q^2)$. Eventually a combined fit to the x and q^2 spectra of both $\overline{B} \to Dl\overline{\nu}$ and $\overline{B} \to D^*l\overline{\nu}$ decays should give the best determination of $|V_{cb}|$.

6.5 Predictions for Decay to τ Leptons

Semileptonic B meson decays to τ-leptons have yet to be observed. However, as discussed in section 4.11, they do offer the simplest way to study the two extra hadronic form-factors, $f_-(q^2)$ and $f_4(q^2)$, that are not involved significantly in decays to the light leptons $l = e, \mu$. Several groups have discussed predictions [6,7,8].

Table 6.4 gives the total rate predictions for the decays $\overline{B} \to D\tau\overline{\nu}$ and $\overline{B} \to D^*\tau\overline{\nu}$, and for the vector to pseudoscalar ratio R. As for the decays to 'massless' leptons the models are all in fair agreement with each other.

Model	$\overline{B^0} \to D^+\tau\overline{\nu}$	$\overline{B^0} \to D^{*+}\tau\overline{\nu}$	R
FAC	1.7	4.1	2.4
SQ	2.3	5.0	2.2
MAX	1.9	3.8	2.0
MIN	1.5	4.9	3.3
KS	1.4	4.3	3.1
ISGW	1.9	–	–
WSB	1.6	3.6	2.2
AW	2.0	4.0	2.0
SP	1.5	–	–

Table 6.4. Exclusive decay rates to τ leptons and the vector to pseudoscalar ratio R, as predicted by the models described in the text. Decay rates are given in units of $10^{-12}|V_{cb}|^2\,GeV$.

Figs.6.4 and 6.5 show the lepton energy and q^2 spectra for the models FAC, SQ and WSB. In all three cases the predictions for the spectra shapes are very similar, and only the normalisation offers any possibility for testing between models.

In contrast to the decays discussed previously the models can also, in theory, be tested by considering the polarisation of the τ-lepton. This should be detectable in an asymmetric B factory, since then the B mesons are not produced at rest and so the decay vertices can be found by sufficiently accurate vertex detectors. Although not directly measureable, it is interesting to calculate the longitudinal polarisation of (4.88), which is shown in fig.6.6 as function of x and of q^2, in the $\overline{B}$ meson rest-frame (at an asymmetric B factory we would really need to use the laboratory frame, but we use the meson rest-frame here as a demonstration).

For a very slowly moving τ, helicities $\lambda_l = \pm\frac{1}{2}$ are equally likely, and hence $P_L \to 0$ as $x \to x_{min}$. At the other limit $x \to x_{max}$, that is the maximum momentum of the lepton, we expect P_L to be closer to -1; indeed if $|\mathbf{p}_l| \gg m_l$ were kinematically possible then $P_L \approx -1$, which is indeed the case for electrons
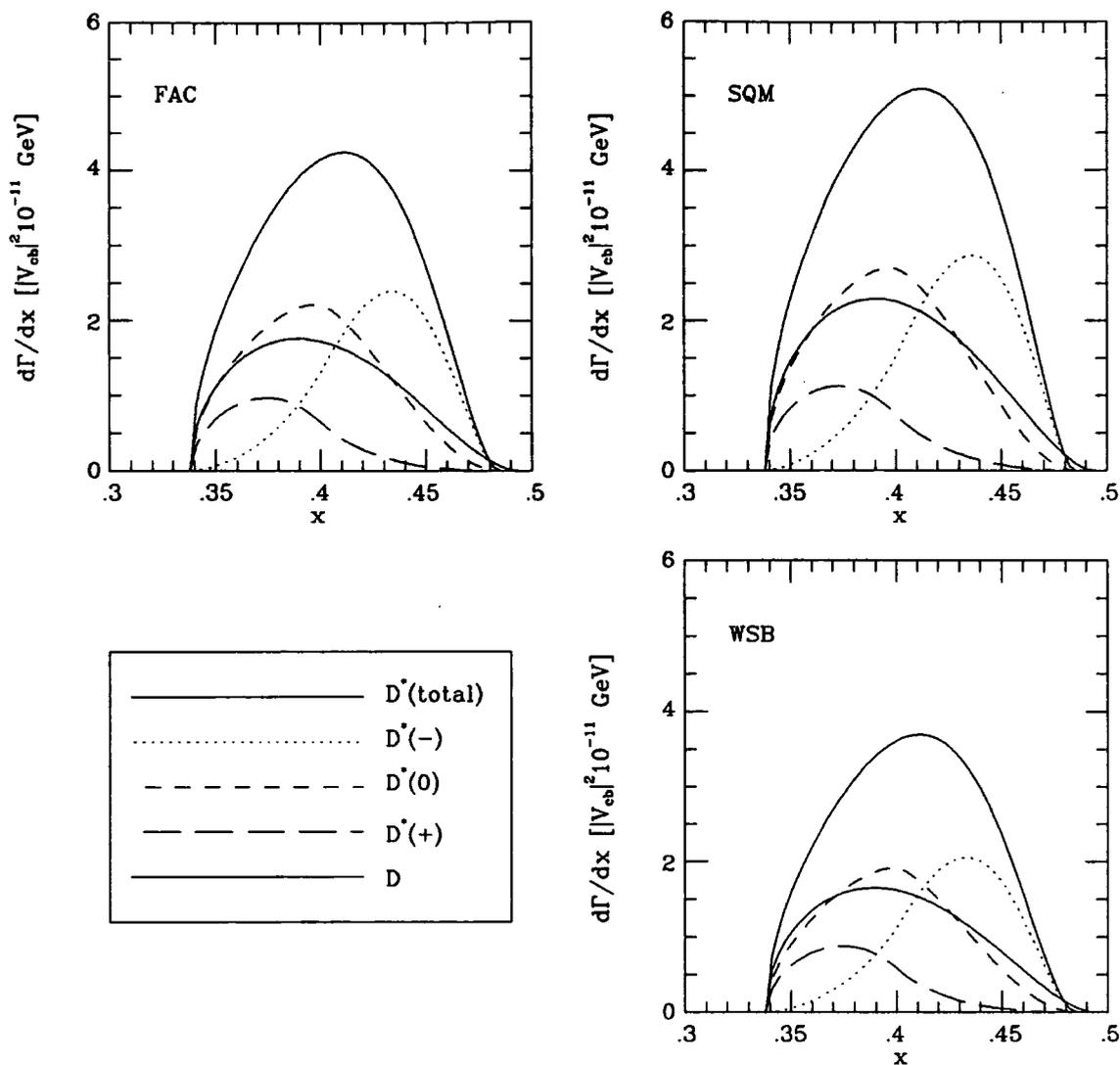
Figure 6.4 Lepton energy spectra of three representative models, for the decays $\overline{B} \rightarrow D\tau\overline{\nu}$ and $\overline{B} \rightarrow D^*\tau\overline{\nu}$. The partial rates to the various possible helicities of the D^* are also shown.

117
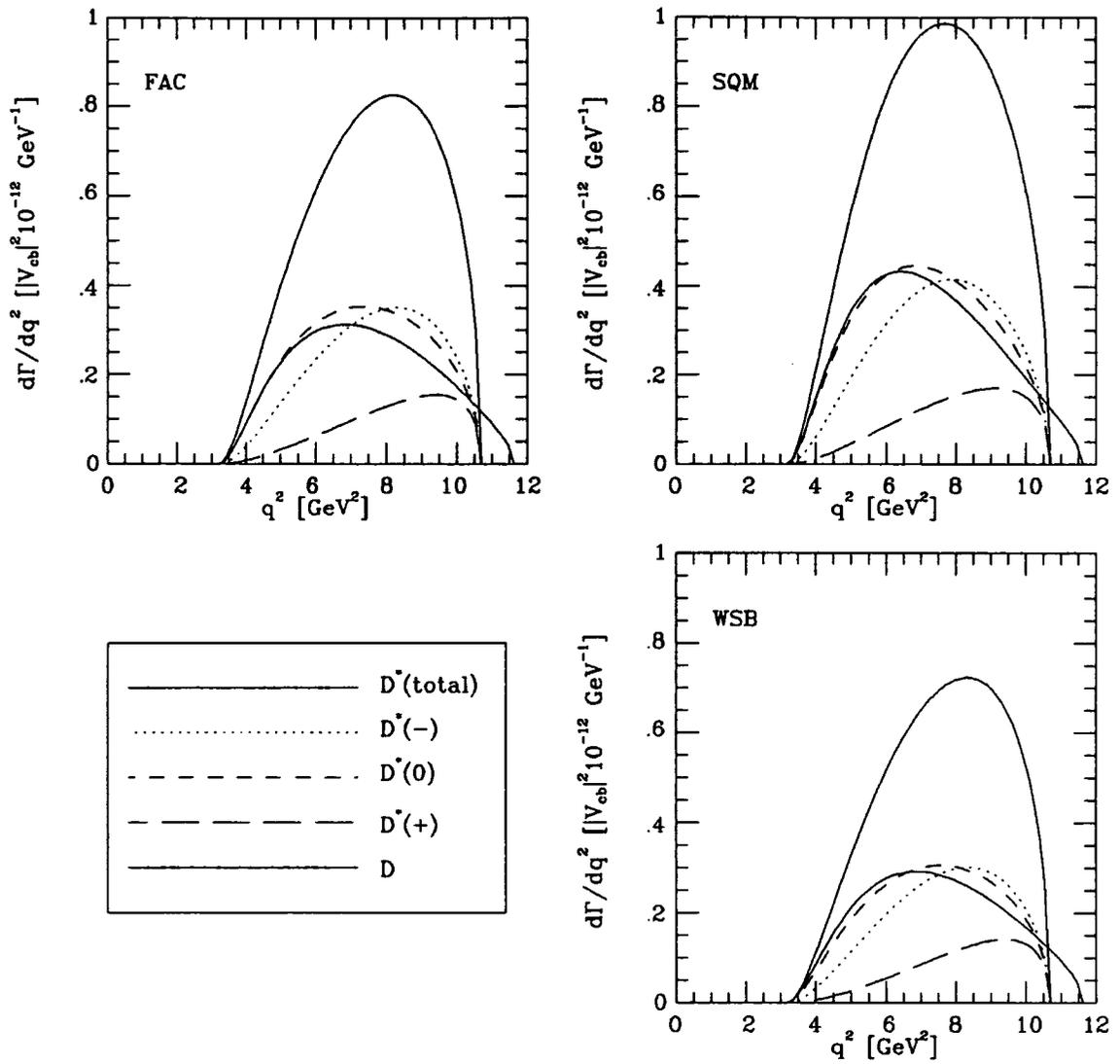
Figure 6.5 q^2 spectra of three representative models, for the decays $\overline{B} \to D\tau\overline{\nu}$ and $\overline{B} \to D^*\tau\overline{\nu}$. The partial rates to the various possible helicities of the D^* are also shown.
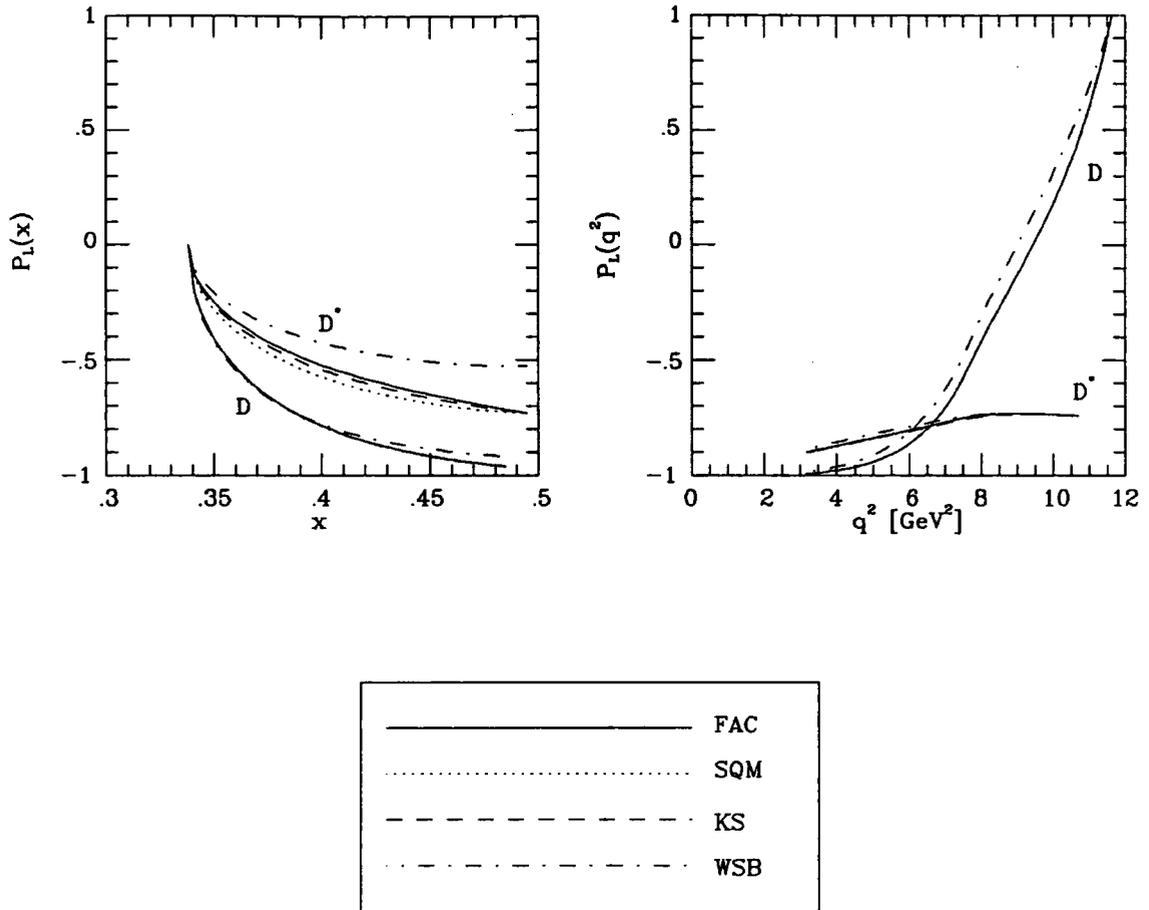
Figure 6.6   Longitudinal Polarisation (4.88) of the emitted τ lepton in the $\overline{B}$ rest-frame.

and muons.

At q^2_{min}, P_L is close to -1 since again $x = x_{min}$. For the decay $\overline{B} \to D\tau\overline{\nu}$, at q^2_{max} the $\overline{B}$ and W rest-frames coincide. As $H^s_0(q^2_{max}) = 0$ (see (4.69)) only a scalar W can be produced, and so, by angular momentum conservation, the τ must have the same helicity as the $\overline{\nu}$, so $P_L(q^2_{max}) = 1$.

6.6 Exclusive $b \to u$ Decays

The models described in the previous chapter are, for the most part, only intended to be used for heavy quark to heavy quark decays, such as the $b \to c$ decays discussed above. However, they are often also used for heavy to light quark decays (such as $b \to u$ and $c \to s$). Since the produced quark is light the theoretical reliability of the form-factor models is clearly suspect, but they can at least be

119

used to give rough estimates of the exclusive decay rates, and hence for the KM matrix elements.

In this section we consider exclusive semileptonic decays of B mesons to the 0^- states π, η and η' and to the 1^- states ρ and ω, which involve a $b \to u$ transition, and so can be used to try to determine $|V_{ub}|$. The definitions of these states in terms of quarks are

$$
\begin{aligned}
\pi^+ &= \bar{d}u \qquad \pi^- = \bar{u}d \\
\pi^0 &= \frac{1}{\sqrt{2}}(\bar{u}u - \bar{d}d) \\
\eta &= \frac{1}{\sqrt{6}}(\bar{u}u + \bar{d}d - 2\bar{s}s) \\
\eta' &= \frac{1}{\sqrt{3}}(\bar{u}u + \bar{d}d + \bar{s}s)
\end{aligned}
\tag{6.9}
$$

and

$$
\begin{aligned}
\rho^+ &= \bar{d}u \qquad \rho^- = \bar{u}d \\
\rho &= \frac{1}{\sqrt{2}}(\bar{u}u - \bar{d}d) \\
\omega &= \frac{1}{\sqrt{2}}(\bar{u}u + \bar{d}d)
\end{aligned}
\tag{6.10}
$$

(we neglect the effects of mixing between the states). Thus we may write the neutral 0^- and 1^- states as

$$
\bar{u}u = \frac{1}{\sqrt{2}}\pi^0 + \frac{1}{\sqrt{6}}\eta + \frac{1}{\sqrt{3}}\eta' \qquad \text{and} \qquad \bar{u}u = \frac{1}{\sqrt{2}}\rho^0 + \frac{1}{\sqrt{2}}\omega
\tag{6.11}
$$

respectively. For the analysis we consider only the WSB, ISGW and FAC models from chapter 5. Since only two exclusive $b \to u$ events have been observed, it is not yet possible to test the models, and so they will not be discussed in great detail. We will try, however, to identify the problems that occur, and how they effect the reliability of the possible determination of $|V_{ub}|$.

Theoretical difficulties with such decays are numerous. Section 5.1 explains the coupled-channel and spatial overlap pictures of the hadronic part of the decay, and it was argued that for the $b \to c$ case the latter seems more reasonable. However, for the decay $b \to u$ the coupled channel processes are probably important (indeed Isgur and Wise, who are supporters of the spatial overlap approach for $b \to c$ decays have stressed the importance of the B^* resonance in $b \to u$ decays [9]). The low

masses of the mesons produced mean that the q^2 range is very much larger than for $B \rightarrow D, D^*$ decays, so that the form-factors display much greater variation between models, and are much more sensitive to model parameters. Finally, in the case of $B \rightarrow \rho$ decays, a precise prediction should include the effect of the large width of the ρ meson (the decay widths of the other mesons are negligible).

The WSB form-factors are defined exactly as in section 5.3.5, with pole masses and spatial overlaps given explicitly in ref. [10].

The ISGW model form-factors are easily calculable from the formulae given in ref. [11], as was done for $B \rightarrow D, D^*$ decays in section 5.3.4. We have not included the effect of the B^* resonance contribution mentioned above, as it is not yet known whether it interferes constructively or destructively with the $b \rightarrow cW^*$ vertex. The exponential parameter of (5.4) is predicted in this case to be $\beta = 6.52$, but unfortunately the results are very sensitive to it, on account of the large q^2 range. For instance, reducing β by 5% increases the $B \rightarrow \pi, \rho$ rates by 18% and 9% respectively, whereas a similar change for $B \rightarrow D, D^*$ decays produces only a 2% increase in the rates. The ISGW model also gives predictions for the decays to low-mass resonances other than the 0^- and 1^- states, but these are not included here.

The FAC model, using the form-factors of section 5.3.7, was not intended for $b \rightarrow u$ decays, since it relies on both initial and final quarks being heavy. The first problem is to decide what masses to use in the SQ model form-factors, which originate from a quark level calculation. ISGW use 'weak-binding' meson masses, determined by summing up the constituent quark masses, but as a comparison we have chosen to use meson masses in the FAC predictions, as before. For $B \rightarrow D, D^*$ decays it was argued in section 5.1 that the spatial overlap could be normalised by $F(q^2_{max}) = 1$ due to the near-equal sizes of initial and final meson, but for $B \rightarrow \pi, \rho$ decays this argument no longer holds. However, without any definite alternative we continue to use this normalisation. Finally, by predicting $F(q^2)$ by a pole-dominated form we introduce severe dependence on the value of the pole mass m_P for $B \rightarrow \pi$ decays. We use the measured value of $m_{B^*} = 5.33\,GeV$ [5], but even a slight change to $m_{B^*} = 5.32\,GeV$ would decrease the rate by about 10%. This effect is not apparent in the WSB model, even though they use the same extrapolation, since the $q^2 = 0$ region dominates their spectrum (see fig.6.7), and that is where their form-factors are normalised.

The lepton energy and q^2 spectra of the three models for the decays $\overline{B} \to \pi, \rho$ are shown in fig.6.7, and demonstrate the very large range of predictions in the $B \to \pi$ case both in normalisation and shape. If the q^2 spectrum of this decay is ever measured it should easily distinguish between the models. The predictions for $B \to \rho$ are much closer in shape, thought still rather different in overall normalisation, on account of its larger mass.

The total decay rates are given in table 6.5 below. Neglecting small effects due to differences between charged and neutral meson masses, the decay rates to neutral π and ρ mesons are half those to the corresponding charged mesons, on account of the factor $1/\sqrt{2}$ in (6.11). Similarly, the rates to η, η' and ω include factors 1/6, 1/3 and 1/2 respectively. The table shows again that the greatest variation between models occurs in the decays to pions, due to the very low pion mass (the predictions for η and η', which differ only in the particle masses and in the spatial overlap factors of WSB, are much closer). There are also significant differences between the predictions for decays to the 1^- mesons.

Model	$\overline{B^0} \to \pi^+ l\overline{\nu}$	$B^- \to \pi^0 l\overline{\nu}$	$B^- \to \eta l\overline{\nu}$	$B^- \to \eta' l\overline{\nu}$
FAC	0.4	0.2	0.4	1.4
ISGW	1.4	0.7	0.4	1.3
WSB	5.0	2.5	0.6	1.1
	$\overline{B^0} \to \rho^+ l\overline{\nu}$	$B^- \to \rho^0 l\overline{\nu}$	$B^- \to \omega l\overline{\nu}$	
FAC	11.4	5.7	5.8	
ISGW	5.5	2.7	2.7	
WSB	17.5	8.7	8.6	

Table 6.5. Exclusive decay rates for decays to 0^- (π, η and η') and 1^- (ρ and ω) mesons, as predicted by the three models discussed in the text. Decay rates are given in units of $10^{-12}|V_{ub}|^2 \, GeV$.

6.7 Extraction of $|V_{ub}|$ from the Inclusive Spectrum

These exclusive models are often used in an attempt to extract the KM matrix element $|V_{ub}|$ from the inclusive spectra near the lepton endpoint [12,13,14] (the experimental results were introduced in section 3.5.5).
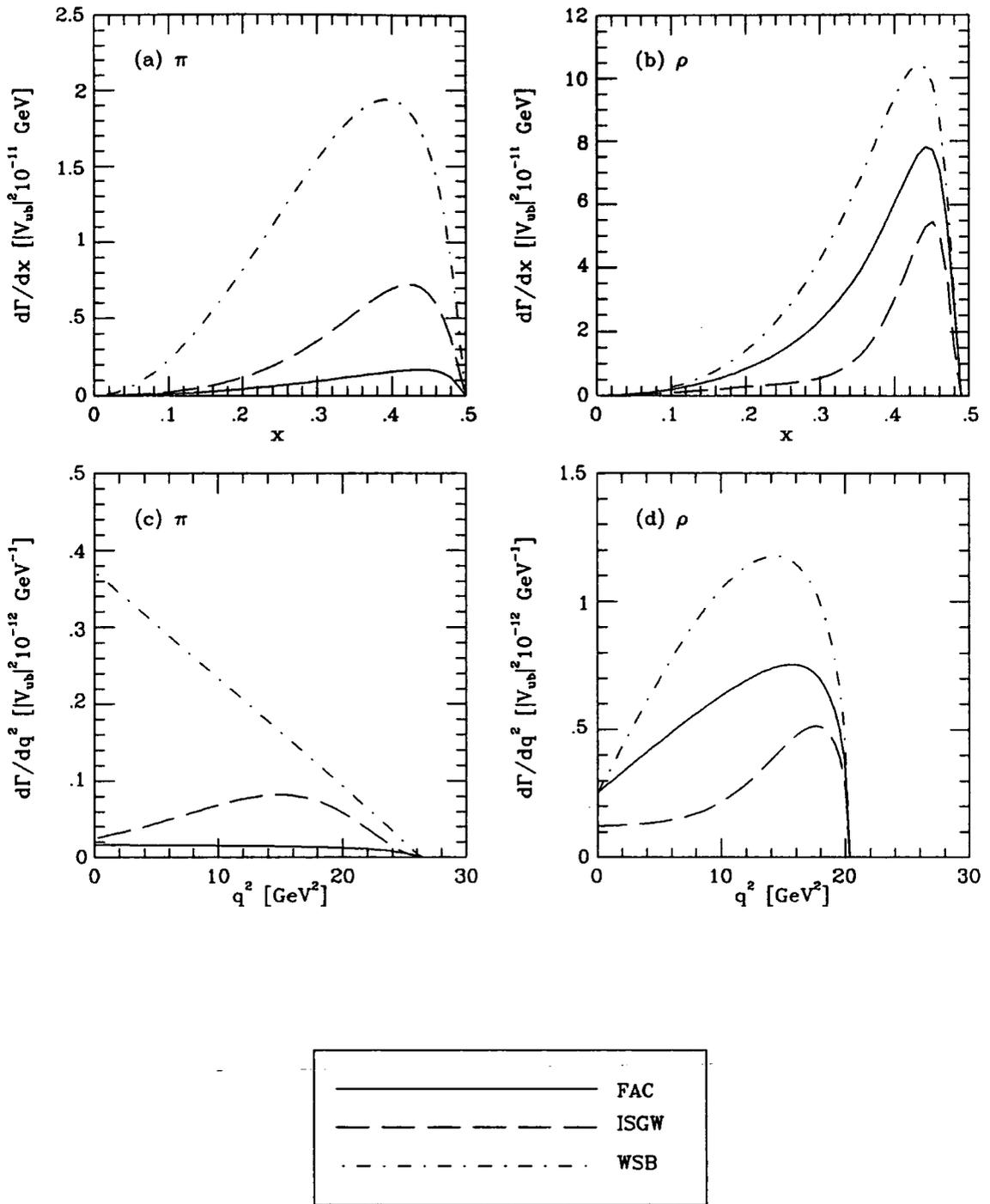
Figure 6.7   Lepton energy and q^2 spectra of exclusive $b \to u$ decays, for the three models shown in the key. (a) and (c) are for $\overline{B} \to \pi l \overline{\nu}$, while (b) and (d) are for $\overline{B} \to \rho l \overline{\nu}$.

The analysis of the experimental data should, of course, be made using a determination of the inclusive lepton spectrum for the $b \rightarrow c, ul\bar{\nu}$ decays, but the exclusive models can be used to give a rough estimate for the matrix element. For $b \rightarrow c$ decays we already know from the measured semileptonic branching fractions of section 3.5 that $(60 - 70)\%$ of the inclusive spectrum comes from the two exclusive channels $B \rightarrow D, D^*$. Furthermore, these two channels dominate the lepton energy endpoint region to an even greater extent, since the most energetic electrons are produced by the lowest mass final states. For $b \rightarrow u$ decays such dominance by a few exclusive channels is no longer certain. There are many low-mass states available, including multihadron states, which can produce sufficiently energetic leptons. Thus using models that predict only the decay rates to 0^- and 1^- states may seriously underestimate the inclusive spectrum. The ISGW model attempts to include all the single resonances that can contribute to the high-energy lepton region, but rather then repeating their whole calculation, we estimate the effect by considering the relevant figure from ref. [11]. This shows that the extra resonances considered increase the rate by a factor of about 2. Using the prediction of the free-quark decay spectrum in the same figure as an upper limit, this factor could increase to about 10.

The model predictions for the lepton spectrum are be boosted from the B rest-frame to the $\Upsilon(4S)$ frame as discussed in section 3.5.1, as this gives a significant effect for high lepton energies. The boosted distribution is given by [15] (see chapter 7 for discussion)

$$\frac{d\Gamma}{dE_l} = \int_{E_-}^{E_+} dE_l' \frac{d\Gamma}{dE_l'} \frac{1}{2E_l'\beta\gamma}, \tag{6.12}$$

where $2m_B\gamma \equiv m_{\Upsilon(4S)}$, $\beta\gamma \equiv \sqrt{\gamma^2 - 1}$, and

$$E_- = \frac{E_l}{\gamma(1+\beta)}$$
$$E_+ = \text{Min}\left\{ \frac{E_l}{\gamma(1-\beta)}, \frac{m_B^2 - m_M^2}{2m_B} \right\}. \tag{6.13}$$

The ARGUS result [13], (3.21), is

$$B \equiv \frac{\mathrm{Br}_{sl}(\Delta_b)}{\mathrm{Br}_{sl}(\Delta_a)} = (4.7 \pm 1.2)\%, \tag{6.14}$$

where the lepton energy ranges, originally defined in (3.20), are

$$\begin{aligned} \Delta_a &\equiv (2.0 - 2.3)\,GeV \\ \Delta_b &\equiv (2.3 - 2.6)\,GeV. \end{aligned} \tag{6.15}$$

In analysing this result the inclusive spectrum for $b \to c l \bar{\nu}$ decays is assumed to be sufficiently well described by the $B \to D, D^*$ contributions for $E_l \geq 2.0\,GeV$. The inclusive $b \to u l \bar{\nu}$ contribution is approximated by assuming that the $\Upsilon(4S)$ braching fractions are $f_{+-} = f_{00} = 0.5$ and summing over the $\pi^{\pm}$ and $\rho^{\pm}$ channels for the neutral B meson decays and the $\pi^0, \eta, \eta', \rho^0$ and ω channels for the charged B decays. A factor 'k' is introduced to allow for the difference between this sum of exclusive channels and the true inclusive spectrum. This factor depends on the energy range under study, decreasing with increasing energy, but for simplicity, and since the other uncertainties are large, k will be taken to be the same for all $E_l > 2.0\,GeV$. From the above discussion of the ISGW results, we will take $1 \lesssim \sqrt{k} \lesssim 3$ as a 'most pessimistic' assumption of the uncertainty. Most analyses [12,13] just use $k = 1$.

Under these assumptions we may write

$$B = \frac{|V_{cb}|^2 \tilde{\Gamma}_{sl}(b \to c, \Delta_b) + |V_{ub}|^2 \tilde{\Gamma}_{sl}(b \to u, \Delta_b)}{|V_{cb}|^2 \tilde{\Gamma}_{sl}(b \to c, \Delta_a) + |V_{ub}|^2 \tilde{\Gamma}_{sl}(b \to u, \Delta_a)}, \tag{6.16}$$

where $\tilde{\Gamma}(b \to q) \equiv \Gamma(b \to q)/|V_{qb}|^2$. On rearrangement this gives

$$k \left| \frac{V_{ub}}{V_{cb}} \right|^2 \approx \frac{B\tilde{\Gamma}_{sl}(b \to c, \Delta_a) - \tilde{\Gamma}_{sl}(b \to c, \Delta_b)}{\tilde{\Gamma}_{sl}(b \to u, \Delta_b) - B\tilde{\Gamma}_{sl}(b \to u, \Delta_a)}, \tag{6.17}$$

where the decay rates are now understood to be sums over the relevant exclusive states.

Table 6.6 shows the relevant partial decay rates, summed over the above exclusive channels, and the corresponding predictions for the ratio $\sqrt{k}|V_{ub}/V_{cb}|$ and for $\sqrt{k}|V_{ub}|$, calculated using the model predictions for $|V_{cb}|$ given in table 6.3. The errors quoted are derived solely from the experimental errors. The ISGW and WSB predictions agree with those given in ref. [13] for $k = 1$.

Model	$\tilde{\Gamma}(b \rightarrow c, \Delta_a)$	$\tilde{\Gamma}(b \rightarrow c, \Delta_b)$		
FAC	1.77	0.02		
ISGW	1.87	0.02		
WSB	1.49	0.01		
	$\tilde{\Gamma}(b \rightarrow u, \Delta_a)$	$\tilde{\Gamma}(b \rightarrow u, \Delta_b)$	$\sqrt{k}|V_{ub}/V_{cb}|$	$\sqrt{k}|V_{ub}|$
FAC	3.9	3.0	0.15 ± 0.03	0.006 ± 0.002
ISGW	2.5	2.2	0.18 ± 0.03	0.007 ± 0.003
WSB	6.3	4.1	0.12 ± 0.02	0.005 ± 0.002

Table 6.6. Partial exclusive decay rates for decays to charmless mesons, summed over the 0^- and 1^- states, as described in the text, and the corresponding predictions for the KM matrix elements. The energy ranges, Δ_i, are defined in (6.15) and the decay rates are given in units of $10^{-12}|V_{ub}|^2 \, GeV$.

An estimate of the theoretical uncertainty can be made from the variations between the models and by allowing the factor $\sqrt{k}$ to range from 1 to 3. Combining these with the experimental errors, we can write

$$0.03 \lesssim \left|\frac{V_{ub}}{V_{cb}}\right| \lesssim 0.21 \qquad (6.18)$$

and

$$0.001 \lesssim |V_{ub}| \lesssim 0.010. \qquad (6.19)$$

6.7.2 Analysis of the CLEO Result

In order to analyse the CLEO data [12], (3.19), we use the same assumptions about the relative sizes of exclusive and inclusive rates as in the previous section.

The CLEO partial branching ratios, (3.19), are

$$B_1 \equiv \mathrm{Br}_{sl}(b \to u, \Delta_1) = (1.5 \pm 0.7 \pm 0.7) \times 10^{-4}$$

$$B_2 \equiv \mathrm{Br}_{sl}(b \to u, \Delta_2) = (1.8 \pm 0.4 \pm 0.3) \times 10^{-4},$$

(6.20)

where the lepton energy intervals, first defined in (3.18), are

$$\Delta_1 \equiv (2.2 - 2.4)\, GeV$$

$$\Delta_2 \equiv (2.4 - 2.6)\, GeV.$$

(6.21)

Using the B meson lifetime $\tau_B = 1.79 \times 10^{12}\, GeV^{-1}$, we can extract $|V_{ub}|$ directly, via

$$k|V_{ub}|^2 = \frac{B_i}{\tilde{\Gamma}(b \to u, \Delta_i)\tau_B}.$$

(6.22)

The predictions for the partial decay rates in the relevant lepton energy regions are given in table 6.7 below. The region Δ_2 presumably gives the most reliable of the two measurements, since it is expected that $b \to cl\bar{\nu}$ decays have negligible effect there, and so the model-dependent subtraction of the $b \to c$ contribution used for Δ_1 is not required, resulting in smaller experimental errors. Table 6.7 also gives the model predictions for $\sqrt{k}|V_{ub}|$ and $\sqrt{k}|V_{ub}/V_{cb}|$ for the two regions, again using the model predictions for $|V_{cb}|$ from table 6.3 for the latter.

Model	$\tilde{\Gamma}(b \to u, \Delta_1)$	$\sqrt{k}|V_{ub}|$	$\sqrt{k}|V_{ub}/V_{cb}|$
FAC	2.8	0.005 ± 0.001	0.13 ± 0.06
ISGW	2.0	0.006 ± 0.002	0.17 ± 0.09
WSB	4.2	0.004 ± 0.001	0.10 ± 0.05
Model	$\tilde{\Gamma}(b \to u, \Delta_2)$	$\sqrt{k}|V_{ub}|$	$\sqrt{k}|V_{ub}/V_{cb}|$
FAC	1.6	0.008 ± 0.001	0.21 ± 0.06
ISGW	1.2	0.009 ± 0.001	0.24 ± 0.07
WSB	2.1	0.007 ± 0.001	0.17 ± 0.05

Table 6.7. Partial exclusive decay rates for decays to charmless mesons, summed over the 0^- and 1^- states, as described in the text, and the corresponding predictions for the KM matrix elements. The energy ranges, Δ_i, are defined in (6.21) and the decay rates are given in units of $10^{-12}|V_{ub}|^2\, GeV$.

Despite measuring partial rates that are expected to be independent of $|V_{cb}|$ the CLEO analysis [12] does not predict $|V_{ub}|$ directly. Instead they include in the analysis the model predictions for the total semileptonic $b \to c$ rate and the measured semileptonic branching ratio and extract a value for $|V_{ub}/V_{cb}|$. This is presumably in the hope that the errors introduced by approximating the inclusive spectrum by summing exlusive channels are the same for $b \to c$ and $b \to u$ calculations and so cancel. Since we introduced the factor k instead a direct comparison with their results is difficult. Furthermore, as stated before, we have not included all possible resonances in the ISGW calculation.

The results of table 6.7 for the two energy regions are in slight disagreement, but only at the 1σ level. Since k is expected to decrease with increasing energy they are, in fact, slightly further apart than they first appear. The limiting values from the above table, allowing the same range of k as before, gives

$$0.001 \lesssim |V_{ub}| \lesssim 0.010 \qquad (6.23)$$

and

$$0.02 \lesssim \left| \frac{V_{ub}}{V_{cb}} \right| \lesssim 0.30 \qquad (6.24),$$

in agreement with the ranges (6.18) and (6.19), deduced from the ARGUS data.

For the analysis of chapter 2 we take

$$\left| \frac{V_{ub}}{V_{cb}} \right| = 0.07^{+0.14}_{-0.04}, \qquad (6.25)$$

where the central value corresponds to $k = 2$ and the range to the more accurate ARGUS result of (6.18).

6.8 Conclusion

As discussed in the previous chapter it is not yet possible to distinguish experimentally between the models of chapter 5, except for the SP model, which is ruled out by the data. It is also not yet possible to attempt the experimental measurement of the q^2 dependence of the form-factors. It is hoped that spectra for the decay $\overline{B} \to Dl\overline{\nu}$ will become available, and that the CLEO collaboration will also publish exclusive spectra in addition to the branching ratios.

Unfortunately, since there is no reliable determination of the branching ratio of the $\Upsilon(4S)$ to non-$B\overline{B}$ final states, there is a large uncertainty about the charged and neutral branching ratios f_{+-} and f_{00}. If these are reduced from the values used above the predicted value of $|V_{cb}|$ rises accordingly. Since the changes could be substantial it is very important that this problem be solved as soon as possible. Also, as discussed briefly in chapter 5, the normalisation of the form-factor models at q^2_{max} needs to be investigated further, to ensure the reliability of the prediction of $|V_{cb}|$.

References

1. R. Fulton et al., CLNS 90/989 (August 1990).

2. M. Danilov, DESY 89-147 (November 1989).

3. H. Albrecht et al., *Phys. Lett.* **B219**, 121 (1989).

4. D. Bortoletto et al., *Phys. Rev. Lett.* **63**, 1667 (1989).

5. Particle Data Group: Review of Particle Properties, *Phys. Lett.* **B239**, 1 (1990).

6. K. Hagiwara, A.D. Martin and M.F. Wade, *Z. Phys.* **C46**, 299 (1990).

7. J.G. Körner and G.A. Schuler, DESY 89-122 (September 1989).

8. P. Heiliger and L.M. Sehgal, *Phys. Lett.* **B229**, 409 (1989).

9. N. Isgur and M.B. Wise, *Phys. Rev.* **D41**, 151 (1990).

10. M. Wirbel, B. Stech and M.Bauer, *Z. Phys.* **C34**, 103 (1987).

11. N. Isgur, D. Scora, B. Grinstein and M.B. Wise, *Phys. Rev.* **D39**, 799 (1989).

12. R. Fulton et al., *Phys. Rev. Lett.* **64**, 2226 (1990).

13. H. Albrecht et al., *Phys. Lett.* **B234**, 409 (1990).

14. G. Kramer and W.F. Palmer, DESY 90-011 (February 1990).

15. G. Altarelli, N. Cabibbo, G. Corbo, L. Maiani and G. Martinelli, *Nucl. Phys.* **B208**, 365 (1982).

7 Inclusive Semileptonic B Meson Decays

Unasham'd, though foil'd he does the best he can.
John Dryden, 1631-1700

7.1 Introduction

As described in chapter 3, the inclusive lepton energy (E_l) spectrum arising from semileptonic B meson decays, $\overline{B} \rightarrow Xl\overline{\nu}$, is composed of leptons from both primary and secondary decays. Without the benefit of a prediction for the shape of the secondary lepton spectrum it is necessary to fit predictions of the primary lepton spectrum to just the high energy end of the measured data. This fit is usually for data with $E_l \geq 1.5\,GeV$. As explained in section 3.4.1, the maximum lepton energy is $2.47\,GeV$ for $b \rightarrow c$ decays and $2.82\,GeV$ for $b \rightarrow u$ decays. Given that the contribution of $b \rightarrow u$ decays to the spectrum is very small, one can either fit the spectrum from $b \rightarrow c$ decays up to about $2.2\,GeV$, or, better, fit the sum of the two contributions up to the $b \rightarrow u$ endpoint.

7.1.1 'Exclusive' Approximations to 'Inclusive' Spectra

Many theoretical studies of the lepton energy spectrum arising from inclusive decays use the exclusive models described in the previous chapters, on the pretext that the spectrum is dominated by the D and D^* channels, particularly near the endpoint. As previously explained, the ISGW model [1] also includes several other low-mass resonances in order to approximate the inclusive spectrum more accurately. All these models ignore non-resonant contributions, whose size is not well known. Furthermore, since the predictions of the models for the relative strength of the exclusive channels may be incorrect, the spectrum will also be wrong (in fact the CLEO analysis [2], using the ISGW model, actually scales the exclusive rates to agree with its exclusive analysis).

The most recent results for the KM matrix elements, obtained from the inclusive lepton spectrum, using the ISGW model predictions for both $b \rightarrow u$ and $b \rightarrow c$ decays, are as follows: The ARGUS collaboration [3], fitting to the lepton

spectrum for $E_l \geq 1.5\,GeV$, obtain the values

$$|V_{cb}| = 0.046 \pm 0.006$$

$$\left|\frac{V_{ub}}{V_{cb}}\right| = 0.14^{+0.05}_{-0.06}. \tag{7.1}$$

Using, instead, the partial decay rates for specific lepton energy regions, as discussed in section 3.5.5, ARGUS obtain [4]

$$\left|\frac{V_{ub}}{V_{cb}}\right| = 0.18 \pm 0.02, \tag{7.2}$$

while CLEO find [5]

$$\left|\frac{V_{ub}}{V_{cb}}\right| = 0.11^{+0.03}_{-0.04} \qquad \text{for } E_l \in \Delta_1$$

$$= 0.19^{+0.02}_{-0.03} \qquad \text{for } E_l \in \Delta_2, \tag{7.3}$$

for the two energy regions $\Delta_1 = (2.2 - 2.4)\,GeV$ and $\Delta_2 = (2.4 - 2.6)\,GeV$.

7.1.2 The ACCMM Model of Inclusive Decays

The most common theoretical model of the inclusive spectrum is based on the work of Altarelli et al. [6], called the ACCMM model. The model is based upon a free quark model calculation of the lepton spectrum of the decay $b \to cl\bar{\nu}$, including first order QCD corrections. The differential decay rate is

$$\frac{d\Gamma}{dx} = \frac{d\Gamma^{(0)}}{dx}\left(1 - \frac{2\alpha_s}{3\pi}G(x,\epsilon)\right), \tag{7.4}$$

where $d\Gamma^{(0)}/dx$ is the lowest order rate and $G(x,\epsilon)$, defined in ref. [7], contains the first order corrections. The variables are $x \equiv 2E_l/m_b$ and $\epsilon \equiv m_c/m_b$. The function $G(x,\epsilon)$ contains a logarithmic singularity at the maximum value of x. In the case of decays to a charmed quark the effect of the singularity is negligible, due to the vanishing of phase-space in this limit. However, for decays to a final u quark this is no longer the case. The standard technique is to take the u quark to be massless, which makes the singularity a double log, and to exponentiate this singularity in the lepton energy distribution, as discussed in ref. [6].

The quark decay is converted to the meson decay by treating the spectator quark as a particle of definite mass, m_{sp}, and the heavy quark as a virtual particle whose invariant mass is given by

$$m_b^2 \equiv m_B^2 + m_{sp}^2 - 2m_B\sqrt{m_{sp}^2 + p^2}, \tag{7.5}$$

where p is the magnitude of the three-momentum of the two quarks in the B meson rest-frame. The distribution of the three-momentum p is usually chosen to be gaussian, with an adjustable width parameter p_F (see section 7.4 below). The resulting lepton distribution must then be boosted from the rest-frame of the b quark to the rest-frame of the $\overline{B}$ meson, and then to the laboratory (i.e. the $\Upsilon(4S)$) frame, in order to recreate the experimental situation. The parameters of the fit are thus the gaussian width p_F, the spectator quark mass m_{sp} and the charmed quark mass m_c.

The results for the KM matrix elements, using the ACCMM model, are as follows. Fitting to the spectrum [3], ARGUS find

$$|V_{cb}| = 0.047 \pm 0.004$$
$$\left|\frac{V_{ub}}{V_{cb}}\right| = 0.09^{+0.03}_{-0.05}, \tag{7.6}$$

while using the partial decay rates given in section 3.5.5 they obtain [4],

$$\left|\frac{V_{ub}}{V_{cb}}\right| = 0.10 \pm 0.01. \tag{7.7}$$

Similarly CLEO [5] find

$$\left|\frac{V_{ub}}{V_{cb}}\right| = 0.07^{+0.02}_{-0.03} \qquad \text{for } E_l \in \Delta_1$$
$$= 0.12 \pm 0.02 \qquad \text{for } E_l \in \Delta_2, \tag{7.8}$$

for the two energy regions. While the results for $|V_{cb}|$ are in good agreement with those from the ISGW analysis of the inclusive spectrum, the results for $|V_{ub}|$ are significantly smaller.

The main drawback of the ACCMM model is that it makes no attempt to reproduce the correct invariant mass spectrum for the hadronic decay products.

This perturbative calculation cannot reproduce the sharp peaks that would be observed at the D and D^* masses, and since these are dominant, especially at high lepton energies, the predictions must be in doubt. The discussions below attempt to model these resonances in order to improve the model.

A further drawback is that the gaussian width p_F turns out to be very important in the fit, and to have a significant effect on the total rate, and hence on the determination of $|V_{cb}|$. Since the smearing of the quark momenta described above is an 'ad-hoc' description of the quark dynamics, the large dependence upon p_F is unfortunate.

In ref. [8] the choice

$$m_D = m_c + m_{sp} \qquad (7.9)$$

is made, reducing the number of free parameters to two, in order that the minimum possible invariant mass takes the correct value, $m_X = m_D$. In fact this choice turns out to ensure the correct endpoint in the E_l and q^2 spectra also. Conversely, those fits which do not use this choice do not have the correct endpoints, although the fits tend to predict values of the quark masses that almost satisfy the constraint (7.9), so no noticeable problems arise.

One final point that must be made here concerns the experimental verification of the model. As was often stressed in the preceding chapters, the measurement of the various exclusive spectra will allow the hadronic models of chapter 5 to be tested. Such tests are not possible for the ACCMM model, since only the inclusive lepton spectrum is measurable.

7.2 Possible improvements to the ACCMM model

Most of the remainder of this chapter is concerned with attempts to improve upon the ACCMM model, essentially in an effort to fit both the lepton spectrum and the invariant mass spectrum simultaneously. Rather than refitting to the data, we instead use the experimentally determined parameters as the starting point in the calculation, and then study the effects of the changes we make.

An attempt to fit the invariant mass spectrum has been made by Barger et al. (BKP) [8]. However, rather than redoing the quark model calculation, as is done below, their calculation is essentially the lowest order result scaled by the
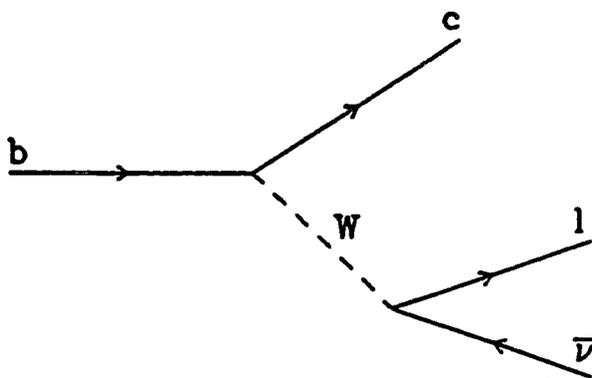
Figure 7.1   Lowest order Feynman diagram.

magnitude of the first order QCD corrections. This turns out to be a good approximation to the more rigorous method used below, which considers the invariant mass of the quark gluon system directly.

Having calculated the invariant mass distribution, BKP divide it into mass regions designed to approximate the D and D^* masses, and then fit to the experimentally measured exclusive branching ratios for these two decays, in addition to the inclusive lepton spectrum. Their results show that this additional fit to the m_X spectrum does change the results slightly, but not significantly.

The following discussion includes all the first order QCD effects and then tests the above model of the D and D^* contributions.

7.3 Free Semileptonic Quark Decay

7.3.1 Matrix Elements

The lowest order matrix element for the decay $b \rightarrow cl\bar{\nu}$ is calculated from the diagram of fig.7.1. The $O(\alpha_s)$ contributions can be divided into virtual and bremsstrahlung corrections. The virtual corrections, shown in fig.7.2, include those diagrams where a gluon is emitted and reabsorbed, while the bremsstrahlung corrections of fig.7.3 describe the process $b \rightarrow cgl\bar{\nu}$, where a real gluon is emitted. We define Y to denote the produced c or $c + g$ system, and X to denote the final hadronic system, after the inclusion of the spectator quark.

The kinematics of the decay can be taken directly from the discussion of ex-
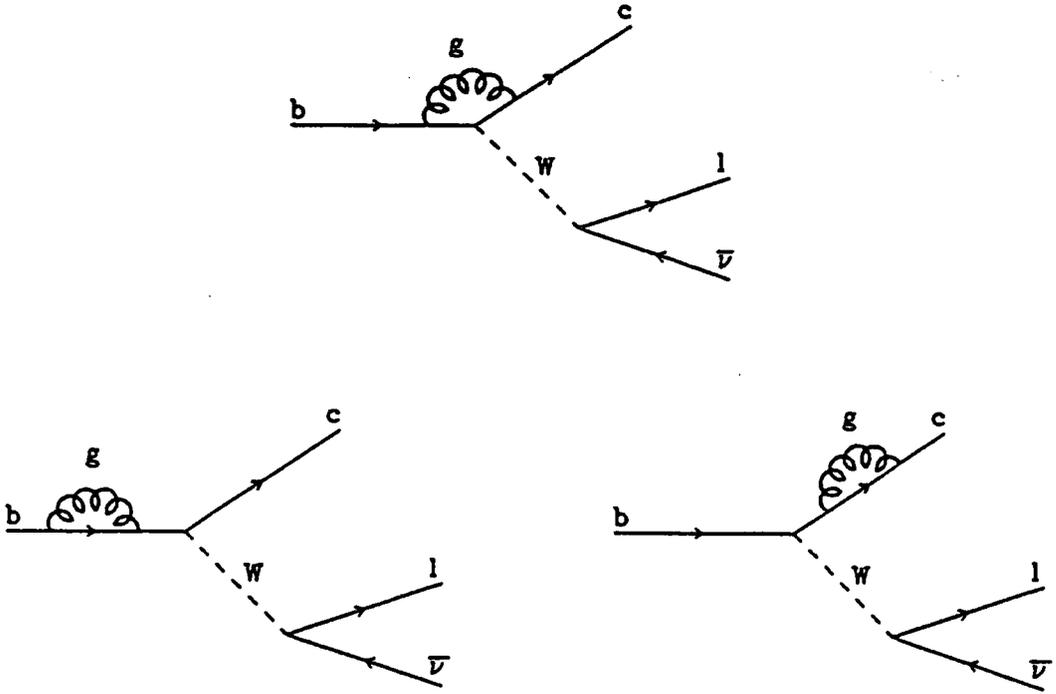
Figure 7.2 First order virtual Feynman diagrams.

clusive processes. For the free quark decay this means we can use the kinematics derived in chapter 4, providing we replace the $\overline{B}$ meson by the b quark and the M meson by the c (or $c + g$) system, Y.

The squared matrix elements, averaged over initial spins and summed over final spins, are given in ref. [9] (in fact that paper describes the decays of charge $+2/3$ quarks to charge $-1/3$ quarks, which means that we must interchange the lepton and neutrino momenta to recover the matrix elements required here). Thus, in the notation of ref. [9], the first order matrix element squared is

$$|M_0|^2 = 64G_F^2(p_c \cdot p_l)(p_b \cdot p_\nu), \tag{7.10}$$

and the bremsstrahlung term is

$$|M_2|^2 = 512G_F^2 \frac{4\pi\alpha_s}{3} \left[\frac{B_1}{D_1^2} + \frac{B_2}{D_1 D_2} + \frac{B_3}{D_2^2} \right], \tag{7.11}$$

where

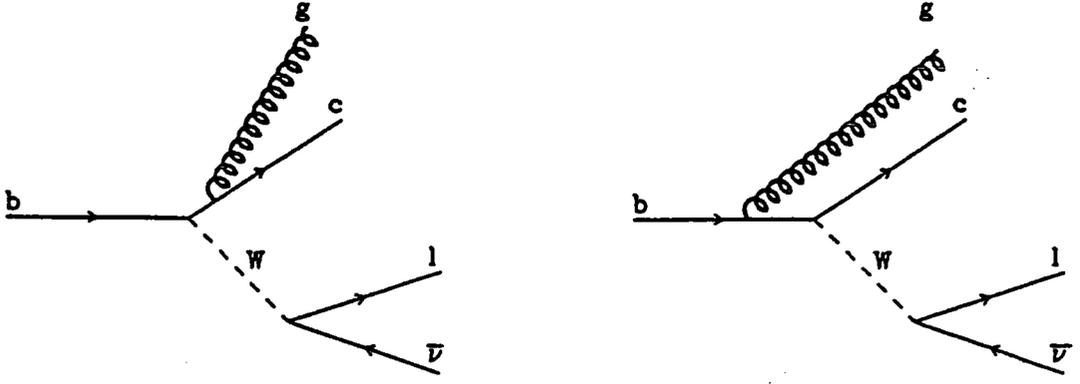$$D_1 = m_g^2 - 2p_b \cdot p_g \qquad D_2 = m_g^2 + 2p_c \cdot p_g \tag{7.12}$$

136

Figure 7.3   First order bremsstrahlung Feynman diagrams.

and

$$B_1 = (p_c \cdot p_l)[(p_\nu \cdot p_g)(p_b \cdot p_g) + 2m_b^2 p_\nu \cdot (p_g - p_b) - m_g^2(p_b \cdot p_\nu)]$$

$$\begin{aligned}
B_2 = (p_c \cdot p_l)[&2(p_\nu \cdot p_g)(p_b \cdot p_c) - 2(p_c \cdot p_\nu)(p_b \cdot p_g) \\
&+ (p_b \cdot p_\nu)(m_g^2 + 2p_g \cdot (p_c - p_b) - 4p_b \cdot p_c)] \\
&+ (p_c \cdot p_b)[-2(p_l \cdot p_g)(p_b \cdot p_\nu) + m_g^2 p_\nu \cdot p_l] \\
&+ (p_l \cdot p_b)[2(p_c \cdot p_g)(p_b \cdot p_\nu) - m_g^2 p_c \cdot p_\nu]
\end{aligned}$$

$$B_3 = (p_b \cdot p_\nu)[2(p_l \cdot p_g)(p_c \cdot p_g) - 2m_c^2 p_l \cdot (p_c + p_g) - m_g^2 p_c \cdot p_l].$$

(7.13)

The virtual term, M_1, is similarly defined, but for simplicity we do not reproduce it here. The decay rate is then given by

$$d\Gamma = \frac{1}{2m_B} \left\{ \left(|M_0|^2 + M_1 \right) d\Phi_3(b \to c l \bar{\nu}) + |M_2|^2 d\Phi_4(b \to c g l \bar{\nu}) \right\}. \qquad (7.14)$$

The three-body phase-space factor can be conveniently split into two two-body phase-space factors by

$$\begin{aligned}
d\Phi_3(b \to c l \bar{\nu}) &= d\tilde{p}_c d\tilde{p}_l d\tilde{p}_\nu (2\pi)^4 \delta^4(p_b - p_c - p_l - p_\nu) \\
&= d\tilde{p}_c d\tilde{p}_l d\tilde{p}_\nu (2\pi)^4 \delta^4(p_b - p_c - p_l - p_\nu) \\
&\qquad \times dq^2 \delta(q^2 - p_W^2) \times d^4 p_W \delta^4(p_W - p_l - p_\nu) \\
&= d\Phi_2(b \to c W^*) \frac{dq^2}{2\pi} d\Phi_2(W^* \to l \bar{\nu}),
\end{aligned} \qquad (7.15)$$

where the relations of (4.25)-(4.27) have been used for the four-momentum of the virtual W (we know that $\theta(q^0) = 1$ since the lepton and antineutrino are on-shell).

137

The four-body phase-space factor can be similarly split into three two-body phase-space factors

$$d\Phi_4(b \to cgl\bar{\nu}) = d\tilde{p}_c d\tilde{p}_g d\tilde{p}_l d\tilde{p}_\nu (2\pi)^4 \delta^4(p_b - p_c - p_g - p_l - p_\nu)$$
$$= d\Phi_2(b \to YW^*)\frac{dq^2}{2\pi}d\Phi_2(W^* \to l\bar{\nu})\frac{dm_Y^2}{2\pi}d\Phi_2(Y \to cg), \qquad (7.16)$$

where m_Y is the invariant mass of the cg system, $m_Y^2 = (p_c + p_g)^2$. Note that this mathematical splitting of the phase-space factor is possible even though the gluon can be emitted by the b quark rather than the c quark (see fig.7.3).

The virtual and bremsstrahlung terms are both infrared singular in the limit of vanishing gluon energy. In order to regulate this singularity a gluon mass has been introduced, as in ref. [9]. In the virtual term the singularity manifests itself in the form $\ln(m_g/m_c)$, while in the bremsstrahlung term it will turn out to be essentially of the form $1/(m_Y^2 - m_c^2)$ (see section 7.3.7 below). By the Kinoshita theorem [10] these two divergences cancel order by order in the limit $m_g \to 0$. Note also that in squaring the matrix elements we have dropped a term of $O(\alpha_s^2)$ coming from the square of the virtual diagram.

7.3.2 Kinematics

In order to calculate the phase-space integrals it is convenient to choose the b-quark rest-frame, in analogy with the B-meson rest-frame of section 4.2.2, with the charmed quark moving along the z-axis, and the lepton and neutrino in the x-z plane, with lepton having positive momentum in the x-direction. Thus the relevant four-momenta may be written, using (4.7)-(4.10), as

$$p_b^\mu = (m_b, 0, 0, 0)$$
$$p_Y^\mu = (E_Y, 0, 0, p_Y)$$
$$q^\mu = (q^0, 0, 0, -p_Y) \qquad (7.17)$$
$$p_l^\mu = E_l(1, \sin\psi_l, 0, \cos\psi_l),$$

where

$$2m_b q^0 = m_b^2 - m_Y^2 + q^2$$
$$p_Y = \sqrt{(q^0)^2 - q^2} \qquad (7.18)$$
$$\cos\psi_l = \frac{q^2 - 2q_0 E_l}{2p_Y E_l}.$$

138

The exclusive $\bar{B}$ decay rate was written in terms of two independent variables, q^2 and $x = p_l \cdot p_B / m_B^2$. Here we will choose q^2 and E_l, the lepton energy in the b quark rest-frame. In addition to these variables the emission of the gluon introduces three new independent variables, but of these we will retain only m_Y, and integrate over the other two, as they are unobservable, as discussed below.

7.3.3 The $b \to YW^*$ Phase-Space

In the b-quark rest-frame the $b \to YW^*$ phase-space factor can now be evaluated

$$
\begin{aligned}
d\Phi_2(b \to YW^*) &= d\tilde{p}_Y d\tilde{p}_W (2\pi)^4 \delta^4(p_b - p_Y - p_W) \\
&= \frac{1}{4\pi^2} \frac{d^3 p_Y}{2E_Y} d^4 p_W \delta(p_W^2 - q^2) \delta^4(p_b - p_Y - p_W) \\
&= \frac{1}{\pi} \frac{p_Y^2}{2E_Y} dp_Y \delta(m_b^2 + m_Y^2 - 2m_b E_Y - q^2) \\
&= \frac{p_Y}{4\pi m_b},
\end{aligned} \tag{7.19}
$$

using (4.27). Recall that $Y = c$ for the lowest order and virtual terms, while $Y = c + g$ for the bremsstrahlung term.

7.3.4 The $W^* \to l\bar{\nu}$ Phase-Space

The two-body $W^* \to l\bar{\nu}$ phase-space is also simply calculable in the b quark rest-frame, giving

$$
\begin{aligned}
d\Phi_2(W^* \to l\bar{\nu}) &= d\tilde{p}_l d\tilde{p}_\nu (2\pi)^4 \delta^4(q - p_l - p_\nu) \\
&= \frac{1}{4\pi^2} \frac{d^3 p_l}{2E_l} \delta(q^2 - (p_l + p_\nu)^2) \\
&= \frac{1}{2\pi} \frac{E_l}{2} dE_l d\cos\psi_l \delta(q^2 - 2E_l(q^0 + p_Y \cos\psi_l)) \\
&= \frac{1}{8\pi p_Y} dE_l
\end{aligned} \tag{7.20}
$$

for massless leptons.

7.3.5 The $Y \to cg$ Phase-Space

The final phase-space calculation is

$$
\begin{aligned}
d\Phi_2(Y \to cg) &= d\tilde{p}_c d\tilde{p}_g (2\pi)^4 \delta^4(p_Y - p_c - p_g) \\
&= \frac{1}{4\pi^2} d^4 p_c \delta(p_c^2 - m_c^2) d^4 p_g \delta(p_g^2 - m_g^2) \delta^4(p_Y - p_c - p_g) \qquad (7.21) \\
&= \frac{1}{4\pi^2} d^4 p_g \delta((p_Y - p_g)^2 - m_c^2) \delta(p_g^2 - m_g^2).
\end{aligned}
$$

Defining the gluon four-momentum to be

$$
p_g^\mu \equiv (E_g, p_g \sin\theta_g \cos\phi_g, p_g \sin\theta_g \sin\phi_g, p_g \cos\theta_g), \qquad (7.22)
$$

and

$$
M^2 \equiv m_Y^2 - m_c^2 + m_g^2, \qquad (7.23)
$$

we can write

$$
\begin{aligned}
d\Phi_2(Y \to cg) &= \frac{1}{4\pi^2} dE_g p_g^2 dp_g d\cos\theta_g d\phi_g \delta(E_g^2 - p_g^2 - m_g^2) \\
&\quad \times \delta(M^2 - 2(E_Y E_g - p_Y p_g \cos\theta_g)) \qquad (7.24) \\
&= \frac{1}{8\pi p_Y} dE_g \frac{d\phi_g}{2\pi}.
\end{aligned}
$$

7.3.6 Integration over the ϕ_g and E_g Degrees of Freedom

The differential decay rate may now be written in the form

$$
d\Gamma = \frac{1}{256\pi^4 m_b} \left\{ (|M_0|^2 + M_1) 2\pi \delta(m_Y^2 - m_c^2) + |M_2|^2 \frac{1}{8\pi p_Y} dE_g \frac{d\phi_g}{2\pi} \right\} dq^2 dE_l dm_Y^2.
\qquad (7.25)
$$

Since the gluon energy, E_g, and azimuthal angle, ϕ_g, are not observable we now need to integrate over them, which will leave the decay rate as a distribution in E_l, q^2 and m_Y^2. These two integrations are performed analytically, using the algebraic manipulation package FORM. The bremsstrahlung matrix element of (7.11) is a function of the momenta p_b, p_c, p_g, p_l and p_ν. Firstly, the p_c dependence is replaced

by p_Y dependence, using $p_c = p_Y - p_g$. The gluon momentum is then written in the form

$$p_g \equiv \alpha p_b + \delta p_Y + p_T, \qquad (7.26)$$

where

$$p_T \equiv p_g(0, \sin\theta_g \cos\phi_g, \sin\theta_g \sin\phi_g, 0) \qquad (7.27)$$

so that

$$p_b \cdot p_T \equiv 0 \equiv p_Y \cdot p_T. \qquad (7.28)$$

Substituting (7.26) into (7.28) we find

$$\alpha = \frac{E_Y M^2 - 2E_g m_Y^2}{2m_b p_Y^2}$$

$$\delta = \frac{2E_Y E_g - M^2}{2p_Y^2}. \qquad (7.29)$$

Thus the ϕ_g dependence only remains in p_T, which only occurs in $|M_2|^2$ as $p_T \cdot p_T$, $p_T \cdot p_l$ or $p_T \cdot p_\nu$. The first of these is actually independent of ϕ_g, since

$$m_g^2 = p_g \cdot p_g = \alpha^2 m_b^2 + 2\alpha\delta m_b E_Y + \delta^2 m_Y^2 - |p_T \cdot p_T|. \qquad (7.30)$$

Thus we need to evaluate the following integrals

$$I \equiv \int \frac{d\phi_g}{2\pi} = 1 \qquad (7.31)$$

$$I^\mu \equiv \int \frac{d\phi_g}{2\pi} p_T^\mu = 0 \qquad (7.32)$$

and

$$I^{\mu\nu} \equiv \int \frac{d\phi_g}{2\pi} p_T^\mu p_T^\nu \qquad (7.33)$$

(higher order terms do not occur). The first two integrals are both trivial, while the third is evaluated as follows: using the definition of (7.27) we have

$$I^{\mu\nu} = \frac{1}{2}|p_T \cdot p_T|\text{diag}(0,1,1,0) \qquad (7.34)$$

$$= \frac{1}{2}|p_T \cdot p_T| \left[-g^{\mu\nu} + B\frac{p_b^\mu p_b^\nu}{m_b^2} + C\frac{p_Y^\mu p_Y^\nu}{m_Y^2} + D\frac{p_b^\mu p_Y^\nu + p_Y^\mu p_b^\nu}{m_b m_Y} \right], \qquad (7.35)$$

141

for some B, C and D. On comparison of (7.35) with (7.34), using the definitions of (7.17), we find

$$B = C = -\frac{m_Y^2}{p_Y^2} \qquad D = \frac{E_Y m_Y}{p_Y^2}. \tag{7.36}$$

Finally we need to integrate over the gluon energy, for which we need to know the integration range. The maximum and minimum gluon energies occur when the c quark and gluon are moving either parallel or antiparallel, which means that

$$E_c^2 = (E_Y - E_g)^2 \qquad \text{and} \qquad p_c^2 = (p_Y \pm p_g)^2. \tag{7.37}$$

Eliminating the dependence on the charmed quark momentum yields the maximum and minimum values

$$E_g = \frac{E_Y M^2 \pm p_Y \sqrt{M^4 - 4m_Y^2 m_g^2}}{2m_Y^2}, \tag{7.38}$$

in terms of M^2 introduced in (7.23). The E_g integral is now relatively easy to do algebraically, since the numerator of $|M_2|^2$ contains only powers of E_g, while $D_2 = m_Y^2 - m_c^2$ is independent of E_g and

$$D_1 = m_g^2 - 2m_b E_g. \tag{7.39}$$

The domain of integration for the three independent variables q^2, E_l and m_Y is given, as in the exclusive case, by (4.11), subject also to

$$(m_c + m_g) \leq m_Y \leq m_b. \tag{7.40}$$

7.3.7 The Massless Gluon Limit

We now take the limit $m_g \to 0$. Both the virtual and bremsstrahlung terms, which are finite when $m_g \neq 0$, become infinite. In the virtual case the singularity manifests itself in the differential decay rate as a term proportional to $\ln(m_g/m_c)\delta(m_Y^2 - m_c^2)$. In the bremsstrahlung case the singularity also occurs at $m_Y = m_c$, but is not so simple. By considering the magnitude of the various

terms in the bremsstrahlung matrix element in the limit $m_Y = m_c + m_g$ one can set $m_g = 0$ in all but three terms, proportional to

$$\text{i)} \quad \frac{\sqrt{M^4 - 4m_Y^2 m_g^2}}{(m_Y^2 - m_c^2)^2}$$

$$\text{ii)} \quad \frac{\sqrt{M^4 - 4m_Y^2 m_g^2}}{M^4 + 4p_Y^2 m_g^2} \tag{7.41}$$

$$\text{iii)} \quad \frac{1}{(m_Y^2 - m_c^2)} \ln \left\{ \frac{E_Y M^2 + p_Y \sqrt{M^4 - 4m_Y^2 m_g^2}}{E_Y M^2 - p_Y \sqrt{M^4 - 4m_Y^2 m_g^2}} \right\}.$$

Integrating these three terms over m_Y yields a logarithmic singularity that exactly cancels the singularity in the virtual term. Since we wish to retain the m_Y dependence we cannot perform this integration, but must instead take the $m_g \to 0$ limit in the numerical calculations by choosing a sufficiently small value, so that the results are unaffected by changing it (typically this means choosing $m_g \sim 10^{-4}\, GeV$).

The lowest order total rate calculated for the free quark decay is in agreement with the analytic formula of (5.22), while the first order correction is in agreement with the calculation given in ref. [9].

7.4 Fermi Smearing

The conversion of the above free quark decay to the meson decay is carried out according to the model introduced by ACCMM [6], briefly described in section 7.1. The spectator antiquark $\bar{q}$ is treated as a particle of definite mass m_{sp}, while the b quark is taken to be off-mass-shell. In the $\overline{B}$ meson rest-frame, with z-direction chosen along the b quark direction, the four momenta are

$$p_b^\mu = (E_b, 0, 0, p)$$
$$p_{sp}^\mu = (E_{sp}, 0, 0, -p), \tag{7.42}$$

with $p_B = p_b + p_{sp}$. The invariant mass of the b quark is thus

$$m_b^2 = (p_B - p_{sp})^2 = m_B^2 + m_{sp}^2 - 2m_B \sqrt{m_{sp}^2 + p^2}. \tag{7.43}$$

The free quark total decay rate Γ depends upon the fermi-momentum p through the dependence of m_b on p. The distribution of the three-momentum p is usually

143

chosen to be gaussian

$$\phi(\mathbf{p}) = \frac{1}{(\sqrt{\pi}p_F)^3}e^{-p^2/p_F^2}, \tag{7.44}$$

which is normalised so that $\int d^3p\phi(\mathbf{p}) = 1$. In terms of $p = |\mathbf{p}|$, we can rewrite this as

$$\phi(p) = \frac{4p^2}{\sqrt{\pi}p_F^3}e^{-p^2/p_F^2}, \tag{7.45}$$

so that $\int dp\phi(p) = 1$. In fact the maximum value of p is not infinite, but is determined by the bound $m_b \geq m_c$ in (7.43), although $p_{max}^2 \gg p_F^2$ so this makes no practical difference.

Since there is no correlation between the direction of p and the orientation of the particles emitted in the quark decay, the b quark decay is isotropically distributed in the b rest-frame, which is chosen as in fig.7.4 (this is just a rotation of the frame originally chosen in section 7.3.2). Of the three angles shown, only ψ_l is determined by the decay, being given by (7.18), while the azimuthal angle ϕ_l and $\cos\theta_Y$ are uniformly distributed. The four-momenta of Y and the lepton in the b frame are

$$p_Y^\mu = (E_Y, p_Y\sin\theta_Y, 0, p_Y\cos\theta_Y)$$
$$p_l^\mu = E_l^b(1, \sin\psi_l\cos\phi_l\cos\theta_Y + \cos\psi_l\sin\theta_Y, \sin\psi_l\sin\phi_l, \tag{7.46}$$
$$- \sin\psi_l\cos\phi_l\sin\theta_Y + \cos\psi_l\cos\theta_Y),$$

where the superscript on E_l^b refers to the frame in which the energy is defined. The invariant mass of the final hadronic system is

$$m_X^2 \equiv (p_Y + p_{sp})^2 = m_Y^2 + m_{sp}^2 + 2(E_Y E_{sp} + p_Y p\cos\theta_Y). \tag{7.47}$$

Boosting to the $\overline{B}$ rest-frame the lepton energy becomes

$$E_l^B = E_l^b\gamma^b(1 + \beta^b(\cos\psi_l\cos\theta_Y - \sin\psi_l\cos\phi_l\sin\theta_Y)), \tag{7.48}$$

where

$$\gamma^b \equiv \frac{E_b}{m_b} \quad\text{and}\quad \gamma^b\beta^b \equiv \frac{p}{m_b}. \tag{7.49}$$

Finally we need to include the boost to the laboratory (or $\Upsilon(4S)$) frame. Choosing the $\overline{B}$ frame as in fig.7.5, where the lepton direction is again isotropically
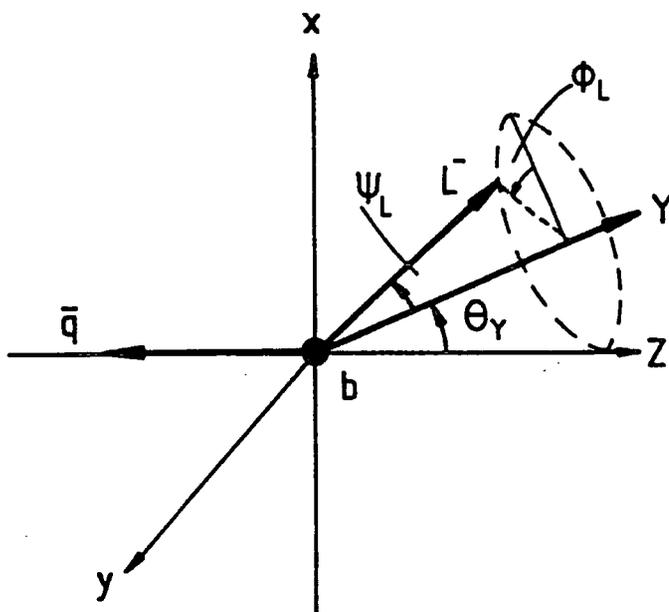
Figure 7.4 The b quark rest-frame.

distributed, the lepton energy in the laboratory frame becomes

$$E_l^\Upsilon = E_l^B \gamma^B (1 + \beta^B \cos\theta), \tag{7.50}$$

where θ is defined in the figure and

$$\gamma^B \equiv \frac{m_\Upsilon}{2m_B} \quad \text{and} \quad \gamma^B \beta^B \equiv \sqrt{\gamma^{B2} - 1}. \tag{7.51}$$

We may use (7.50) to deduce the boost formula of ref. [6], used in section 6.7, as follows: the lepton energy distribution in the laboratory frame is given by

$$\frac{d\Gamma}{dE_l^\Upsilon} = \int dE_l^B \frac{d\Gamma}{dE_l^B} \frac{d\cos\theta}{2} \delta(E_l^\Upsilon - E_l^B \gamma^B (1 + \beta^B \cos\theta))$$

$$= \frac{1}{2\gamma^B \beta^B} \int_{E_-}^{E_+} dE_l^B \frac{d\Gamma}{dE_l^B} \frac{1}{E_l^B}, \tag{7.52}$$

where $E_\pm$ occur when $\cos\theta = \mp 1$, so that

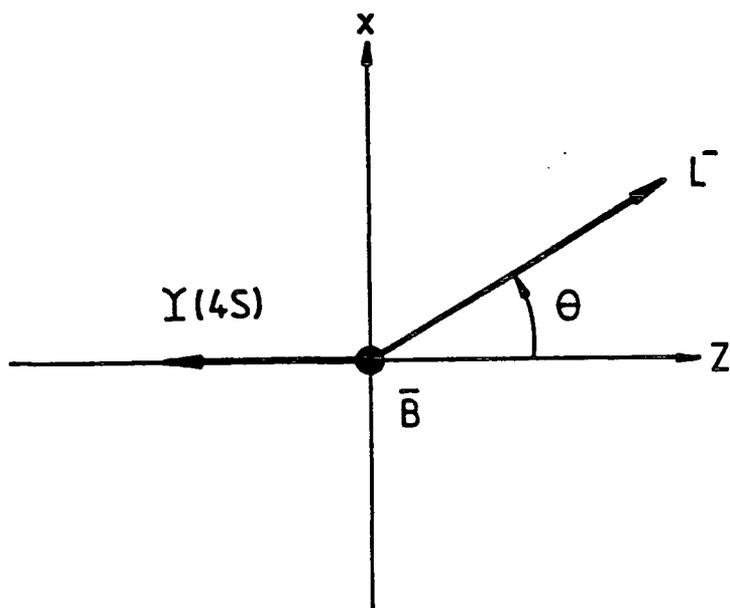$$E_\pm = \frac{E_l^\Upsilon}{\gamma^B (1 \mp \beta^B)}, \tag{7.53}$$

Figure 7.5   The $\overline{B}$ meson rest-frame.

unless E_+ exceeds the maximum possible lepton energy in the $\overline{B}$ rest-frame,

$$\text{Max}(E_l^B) = \frac{m_B^2 - m_D^2}{2m_B}, \qquad (7.54)$$

given by (4.15).

7.4.1 Numerical Calculation of Total Rate and Distributions

We are now left with integrals over E_l^b, q^2, m_Y^2, p, $\cos\theta_Y$, ϕ_l and $\cos\theta$ (the m_Y^2 integral is trivial for the lowest order and virtual terms on account of the δ-function). We require the E_l^Υ, q^2 and m_X distributions and the total rate Γ. By using the Monte-Carlo integration routine VEGAS it is easy to calculate all of these simultaneously. The program is used to calculate the total rate

$$\Gamma = \int dE_l^b dq^2 dm_Y^2 \int dp\phi(p) \frac{d\cos\theta_Y}{2} \frac{d\psi_l}{2\pi} \frac{d\cos\theta}{2} \frac{d^3\Gamma}{dE_l^b dq^2 dm_Y^2}, \qquad (7.55)$$

but, by calculating E_l^Υ, q^2 and m_X during the function evaluations and adding the function value to the appropriate 'bin', the three distributions are obtained at the same time. The three angular integrations take place over the full ranges, while the limits on E_l^b, q^2 and m_Y^2 are discussed in section 7.3.6 above.

146

7.5 Inclusive Distributions

The predictions of the above model for the total decay rate and lepton energy distribution are exactly the same as those of the ACCMM and BKP models, since those models are obtained by integrating the above model over q^2 and m_X.

The recent ARGUS analysis [3], using a fixed spectator mass $m_{sp} = 0.15\,GeV$, finds the parameters

$$p_F = (0.26 \pm 0.06)\,GeV \qquad \text{and} \qquad m_c = (1.65 \pm 0.07)\,GeV, \qquad (7.56)$$

with a strong negative correlation. For the following discussions we use the central values and 1σ-limits of this fit, but with m_{sp} chosen to satisfy the constraint (7.9). Using $\alpha_s = 0.25$, the total rates for these three sets of parameters are given in table 7.1. The effect of the first order corrections is to decrease the decay rate by just under 13% in each case.

(p_F, m_c) [GeV]	$\Gamma^{(0)}$ [$10^{-11}|V_{cb}|^2\,GeV$]	$\Gamma^{(0)} + \Gamma^{(1)}$ [$10^{-11}|V_{cb}|^2\,GeV$]
(0.02,1.72)	3.04	2.66
(0.26,1.65)	2.84	2.48
(0.32,1.58)	2.65	2.31

Table 7.1. Inclusive decay rates at lowest and first order, for the standard three sets of parameter values discussed in the text.

Fig.7.6 shows the lepton energy and invariant mass spectra predicted by the inclusive model and the BKP approximation at leading and first order, for the three sets of parameters $(p_F, m_c) = (0.20, 1.72)$, $(0.26, 1.65)$ and $(0.32, 1.58)\,GeV$. Considering first the E_l spectrum we see that the effect of the first order corrections is essentially just an overall normalisation change. This is because $G(x, \epsilon)$ of (7.4) is roughly constant, except very close to $x = x_{max}$, where there is a logarithmic singularity. The effect of this singularity is washed out by the vanishing phase-space and the fermi-smearing, as discussed in ref. [6]. The effect of increasing p_F, other than decreasing the overall normalisation, is to shift the distribution slightly towards lower energies, decreasing the slope in the region $E_l \gtrsim 1.7\,GeV$.
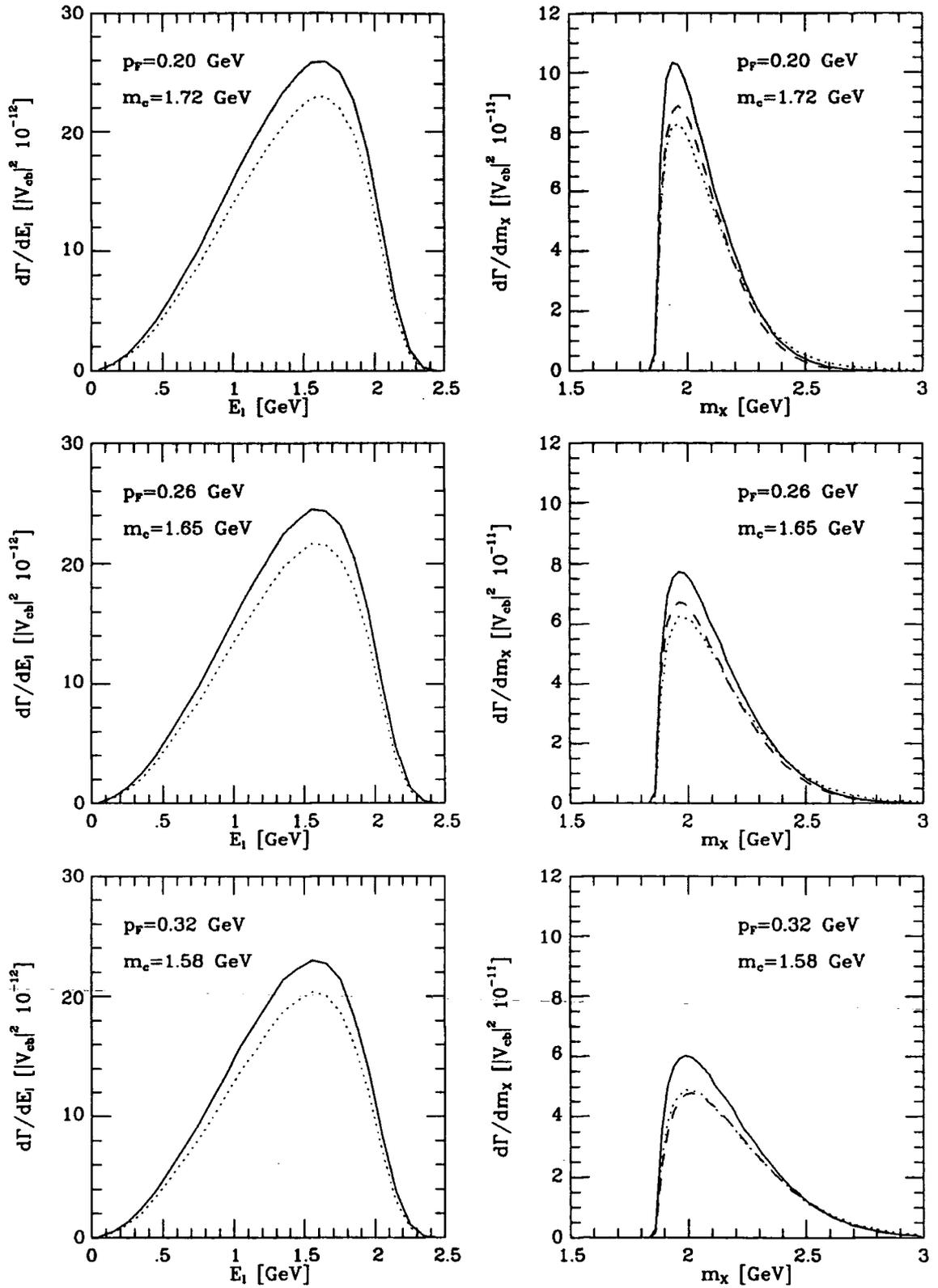
Figure 7.6   Lepton energy and invariant mass spectra predicted by the inclusive model of semileptonic $b \to c$ decays, using the models described in the text, with the three sets of parameters $(p_F, m_c) = (0.20, 1.72)$, $(0.26, 1.65)$ and $(0.32, 1.58)$ GeV. The solid and dotted lines show the lowest and first order QCD results, while the dashed line shows the prediction of Barger et al. [8] for the invariant mass spectrum.

Fig.7.6 also shows the m_X spectra for the three sets of parameters. The BKP and first order predictions are slightly different, with the predictions of the free quark model being shifted towards higher m_X, and a correspondingly suppressed peak. Given the large errors on the relative D and D^* branching fractions this would not cause a significant deviation from the BKP results, if we were to impose their mass cuts as a constraint on the above model. Looking at the m_X spectra in fig.7.6 we see that the variation in parameters has a much more significant effect than it did in the E_l spectra. The larger values of p_F push the spectrum towards the higher invariant mass region, since the initial quarks have higher relative momenta.

7.6 Analysis of the Low-Mass Region

If we wish to include the invariant mass spectrum in the fit, as BKP have attempted, then we should try to analyse how good a description of the physics such models are.

For this purpose we consider two different sets of mass cuts. The first is that used by BKP, where the spectrum is cut so that $1.87\,GeV \leq m_X \leq 1.94\,GeV$ corresponds to the D meson, while $1.94\,GeV \leq m_X \leq 2.08\,GeV$ corresponds to the D^* meson. In order to see the effect of varying the cuts, the second set uses narrower slices of the spectrum, in an attempt to model the narrow widths of the mesons. For this we use $1.87\,GeV \leq m_X \leq 1.90\,GeV$ for the D, and $1.98\,GeV \leq m_X \leq 2.04\,GeV$ for the D^*.

We now predict the E_l and q^2 spectra for the two 'mesons' in each case, with the results shown in fig.7.7. The spectra have been scaled so that the central value of the V/PS ratio (3.15), measured by ARGUS, is obeyed. The first point to note is that the variation between the results predicted by two sets of cuts is very small, so the predictions are stable to changes in the model.

However, comparing these figures with the exclusive model predictions shown in figs.5.7 and 5.8 shows considerable disagreement. This is particularly noticeable in the q^2 spectra for the $\overline{B} \rightarrow Dl\overline{\nu}$ case, where the exclusive models predict a monotonically decreasing spectrum, unlike those in fig.7.7 from the inclusive analysis. In order to reproduce the q^2 spectrum of fig.7.7 with the form-factor models we would need to dramatically alter the spatial overlap function $F(q^2)$ of (5.1). A
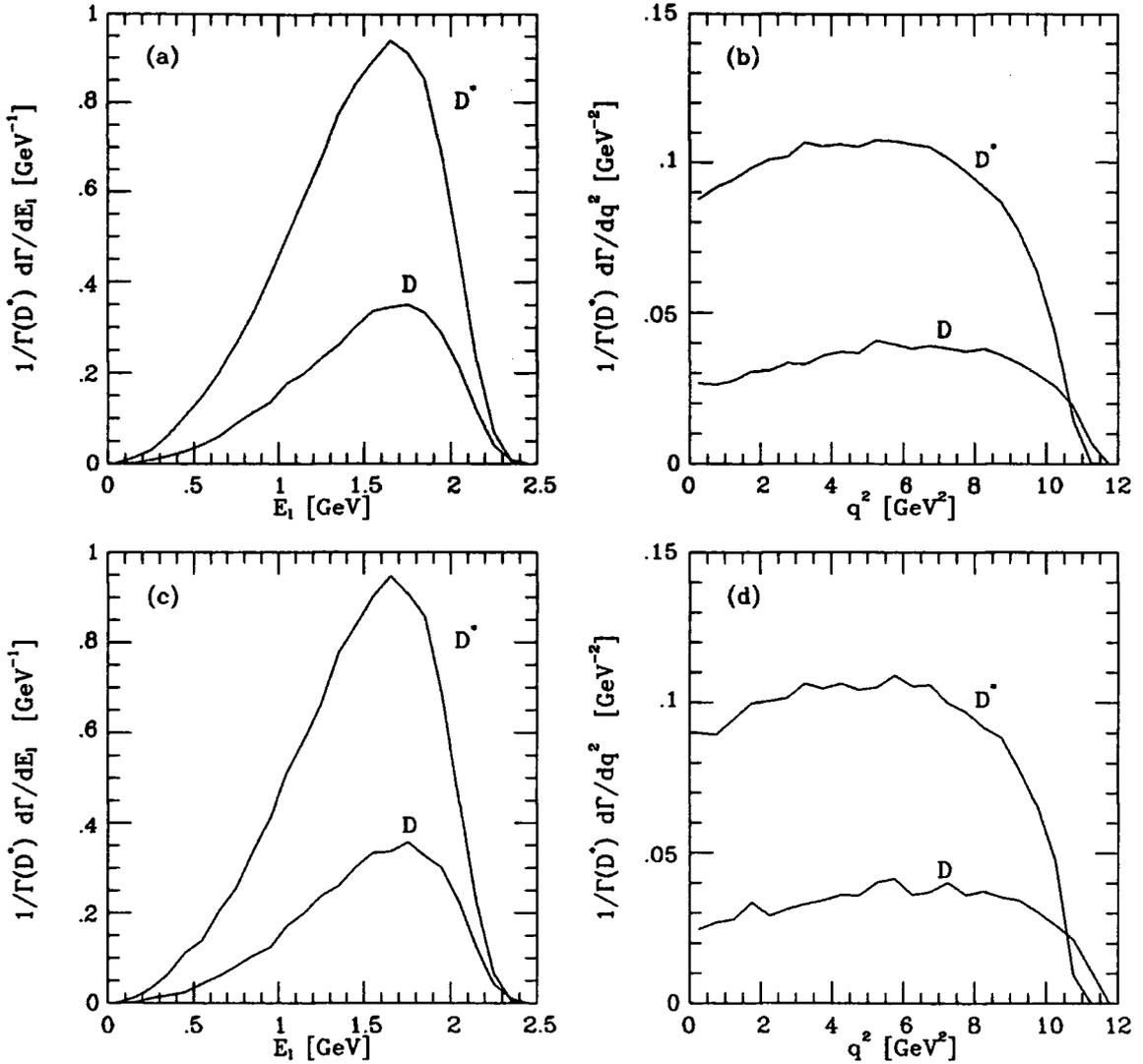
Figure 7.7 Predictions of the inclusive free quark decay for the 'D'
and 'D^*' slices of the invariant mass spectrum, as described in the text.
Figs. (a) and (B) are for the cuts recommended by Barger et al. [8],
while (c) and (d) are for the narrower 'resonance-like' cuts.

small, but important, change is also noticeable in the lepton spectra, where the
shapes are different. This can be seen most clearly in the position of the peaks.
The exclusive models predict peaks in the lepton spectrum for D and D^* decays
at roughly $(1.4 - 1.5)\,GeV$ and $(1.7 - 1.75)\,GeV$ respectively, while the spectra of
fig.7.7 peak at about $1.7\,GeV$ and $1.65\,GeV$. Assuming that the exclusive mod-
els are not dramatically wrong, this shows that we cannot model the D and D^*
resonances in this way, since the fit to the lepton spectrum will be incorrect.

The main reason for the incorrect spectra is that no attempt has been made

150

to impose the correct spin structure on the D and D^* meson slices of the m_X spectrum. The D and D^* spectra are similar in shape because they both contain contributions from similar averages over quark spins. To include the spin structure at lowest order would essentially reproduce the spectator quark (SQ) model form-factors of section 5.3.1, with the spatial overlap function $F(q^2)$ determined by the fermi smearing, as discussed in section 7.7 below. Including first order corrections to this would be very complicated.

7.7 Averaging over the Inclusive Invariant Mass Spectrum

One might regard the predictions of the inclusive model as an average over all possible final states, as is done, for instance, in the calculation of the $R_{e^+e^-}$ ratio in e_+e_- annihilation. Using this interpretation we can use the inclusive calculation to estimate the size of the QCD corrections to the exclusive models of chapter 5, to calculate the inclusive model 'prediction' for the spatial overlap function $F(q^2)$ of section 5.1, and to find a reason for the difference between exclusive and inclusive determinations of $|V_{cb}|$.

Given that the total semileptonic branching ratio is about 10%, and that the sum of the mean exclusive branching ratios to D and D^* of (6.6) is about 6.5%, we cut the above invariant mass spectrum at m_{X_0}, where

$$\frac{1}{\Gamma} \int_{m_D}^{m_{X_0}} dm_X \frac{d\Gamma}{dm_X} \approx 0.65, \tag{7.57}$$

and assume that the integral over masses below $m_{\overline{X}_0}$ approximates the sum of D and D^* resonances. The values of m_{X_0} found in the analysis below range from about 0.1 to 0.25 GeV above the D^* mass, and so are physically reasonable. The predicted q^2 spectrum is then compared with the q^2 spectrum predicted by the spectator quark (SQ) model of section 5.3.1, which has $F(q^2) = 1$ by definition, in order to extract the inclusive prediction

$$|F(q^2)|^2 \approx \frac{d\Gamma/dq^2(m_X < m_{X_0})}{d\Gamma^{SQ}/dq^2}. \tag{7.58}$$

The QCD corrections calculated above to the free quark decay would actually occur as corrections to the SQ model form-factors $f_i^{SQ}(q^2)$ of (5.20) and (5.21).

151

However, with the above averaging, the best we can achieve by this method is an estimate of the overall correction to the spectra. Since the differential decay rate is proportional to $|F(q^2)|^2$ we can absorb the effects of this correction into the spatial overlap, $F(q^2)$, changing both the q^2 dependence and the normalisation at q^2_{max}. Since the q^2 dependence will eventually be determined by experiment, it is only the correction to the normalisation that affects the determination of $|V_{cb}|$.

The graphs of fig.7.8 show the predictions for $F(q^2)$, with parameters taken from the ARGUS best-fit and 1σ limits of (7.56). For $q^2 \lesssim 8\,GeV$ the predictions are close to stright lines, while above this the$_\wedge^y$deviate considerably. This deviation is caused by the failure of the averaging over the above mass region to reproduce the correct $D + D^*$ spectrum at high values of q^2, particularly for large p_F. The problem is exacerbated by the fact that the q^2 spectum for $\overline{B} \to D^*$ decays ends about $1\,GeV$ below that for $\overline{B} \to D$ decays.

Given the problems with the high-q^2 region we extrapolate the results from lower q^2 up to $q^2_{max} \approx 11\,GeV$ (a rough average over the D and D^* enpoints). The QCD corrections at q^2_{max} and $q^2 = 0$ vary very little with the parameters used, being about 3.5% and 15% respectively. Since the determination of $|V_{cb}|$ relies on the normalisation at q^2_{max} this means the QCD corrections would increase the exclusive determination of the KM matrix element by about 3.5%, in close agreement with the analytical result of ref. [11], discussed in section 5.3.1.

It is very noticeable that the inclusive model predictions for $F(q^2)$ do not obey the requirement $F(q^2_{max}) = 1$, even after extrapolation from the lower-q^2 region, which is motivated by the belief that the $\overline{B}$, D and D^* meson wave functions are very nearly the same size. The higher the value of p_F, the lower the prediction. This could explain why the inclusive model value of $|V_{cb}|$ of (7.6) is so much higher than that determined from the exclusive models in section 6.3. Other than this normalisation the slopes of the predictions in fig.7.8 are very similar to the estimates of chapter 5, with the value at $q^2 = 0$ being about 70% of the value at q^2_{max} for all three sets of parameters.

The fraction of the total semileptonic rate made up from D and D^* decays is experimentally uncertain. Including more of the high m_X region does not affect the high-q^2 region, and just increases the predicted $F(q^2)$ at lower values. Conversely, including less of the m_X spectrum decreases $F(q^2)$ at low values of q^2.
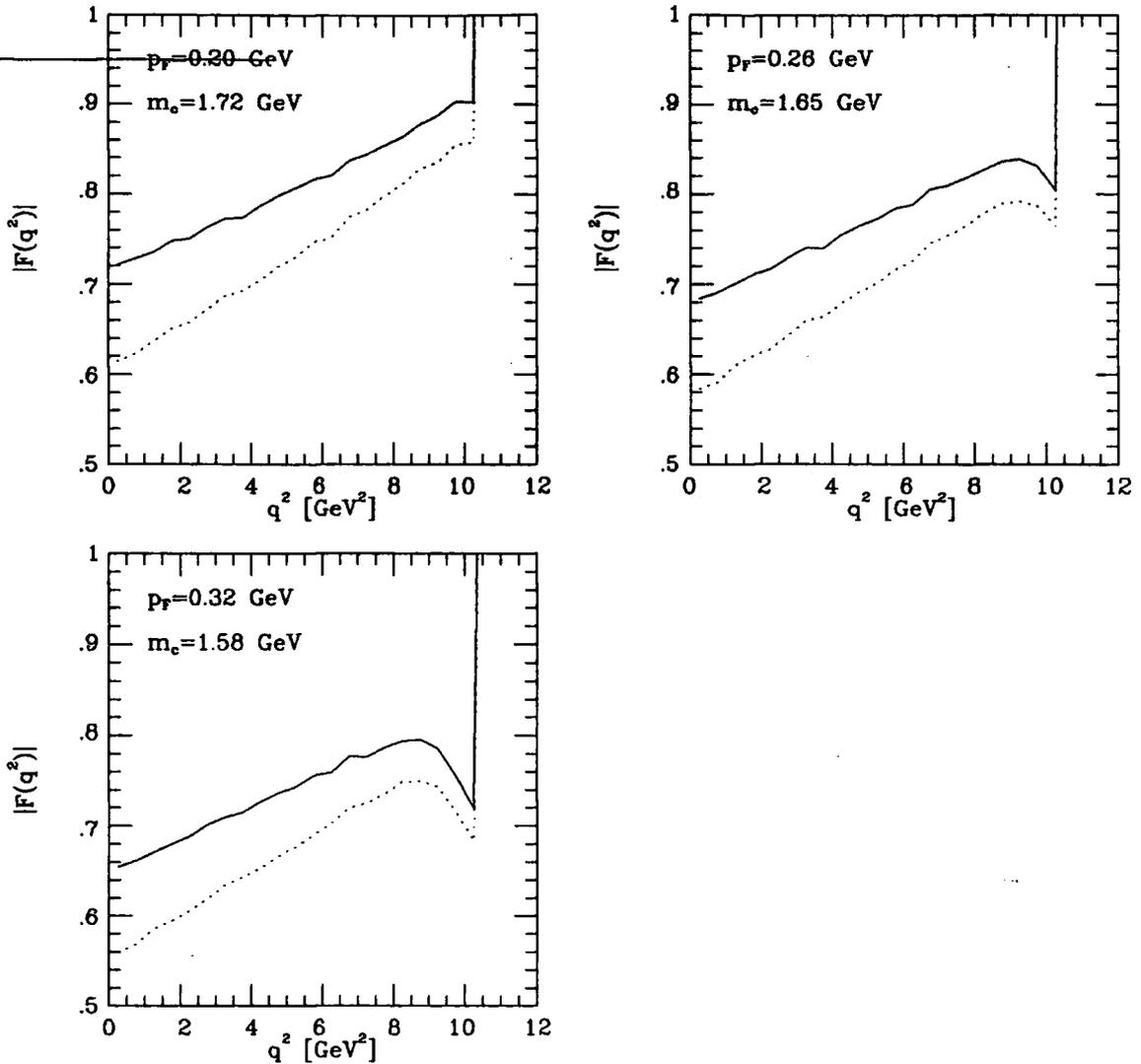
Figure 7.8 Inclusive model predictions for the spatial overlap $F(q^2)$ as defined in (7.58), for the parameter values shown. The solid and dotted lines are the lowest and first order predictions.

7.8 Inclusive $b \rightarrow u l \bar{\nu}$ Decays

The free quark decay model is expected to be more reliable for the prediction of $b \rightarrow u$ decays than for $b \rightarrow c$ decays, because the former spectrum is not expected to be quite so dominated by a few exclusive channels.

Unfortunately the above fermi-smeared free-quark model cannot be used directly for the prediction of $b \rightarrow u$ decays, due to the smallness of the u quark mass. For small but non-zero quark masses the single logarithmic singularity discussed above has a very large effect, actually making the m_X distribution negative at low

values of m_X (this is possible because we have neglected the square of the virtual diagram, since it is $O(\alpha_s^2)$). For zero quark mass the singularity can removed from the lepton spectrum by exponentiation, as discussed in ref. [6], but this is much more difficult to do for the combined E_l, q^2 and m_X distribution. Attempts by the author and Jean-René Cudell to resum multiple soft gluon emission, which should have the effect of softening, or even removing, this singularity have not been entirely successful, mainly because the energy scale of the decay is not really sufficiently large for such a perturbative calculation.

7.9 Conclusions

In this chapter we have investigated the ability of the ACCMM model to reproduce the exclusive decay spectra derived in chapters 4 to 6, in order to test the validity of its predictions for the KM matrix elements. The model is unable to produce the correct D and D^* spectra, which must have a serious effect upon the accuracy of its determination of $|V_{cb}|$. Unfortunately, the above naive discussion of the invariant mass spectrum seems to be the only test of the inclusive model, given that it is extremely difficult to measure either the q^2 or m_X spectra experimentally.

As a result we feel that exclusive decay models must eventually, after thorough testing against experimental data, give a more reliable determination of the KM matrix elements than the ACCMM inclusive decay model.

References

1. N. Isgur, D. Scora, B. Grinstein and M.B. Wise, *Phys. Rev.* **D39**, 799 (1989).

2. Y. Kubota, private communication concerning CLEO preprint, in preparation.

3. H. Albrecht et al., DESY 90-088 (July 1990).

4. H. Albrecht et al., *Phys. Lett.* **B234**, 409 (1990).

5. R. Fulton et al., *Phys. Rev. Lett.* **64**, 16 (1990).

6. G. Altarelli, N. Cabibbo, G. Corbo, L. Maiani and G. Martinelli, *Nucl. Phys.* **B208**, 365 (1982).

7. N. Cabibbo, G. Corbo and L. Maiani, *Nucl. Phys.* **B155**, 93 (1979).

8. V. Barger, C.S. Kim and R.J.N. Phillips, *Phys. Lett.* **B235**, 187 (1990).

9. A. Ali and E. Pietarinen, *Nucl. Phys.* **B154**, 519 (1979).

10. T. Kinoshita, *J. Math. Phys.* **3**, 650 (1962).

11. M.B. Voloshin and M.A. Schifman, *Sov. J. Nucl. Phys.* **45**, 292 (1987).

O! That a man might know
The end of this day's business, ere it come;
But it sufficeth that the day will end,
And then the end is known.
                    William Shakespeare, 1564-1616